

# Multiple ligand docking by Glide: implications for virtual second-site screening

Márton Vass · Ákos Tarcsay · György M. Keserü

Received: 3 December 2011 / Accepted: 1 May 2012 / Published online: 26 May 2012  
© Springer Science+Business Media B.V. 2012

**Abstract** Performance of Glide was evaluated in a sequential multiple ligand docking paradigm predicting the binding modes of 129 protein–ligand complexes crystallized with clusters of 2–6 cooperative ligands. Three sampling protocols (single precision—SP, extra precision—XP, and SP without scaling ligand atom radii—SP hard) combined with three different scoring functions (GlideScore, Emodel and Glide Energy) were tested. The effects of ligand number, docking order and druglikeness of ligands and closeness of the binding site were investigated. On average 36 % of all structures were reproduced with RMSDs lower than 2 Å. Correctly docked structures reached 50 % when docking druglike ligands into closed binding sites by the SP hard protocol. Cooperative binding to metabolic and transport proteins can dramatically alter pharmacokinetic parameters of drugs. Analyzing the cytochrome P450 subset the SP hard protocol with Emodel ranking reproduced two-thirds of the structures well. Multiple ligand binding is also exploited by the fragment linking approach in lead discovery settings. The HSP90 subset from real life fragment optimization programs revealed that Glide is able to reproduce the positions of multiple bound fragments if conserved water molecules are considered. These case studies assess the utility of Glide in sequential multiple docking applications.

**Keywords** Cooperative binding · Multiple ligand binding · Docking · Molecular modeling · Cytochrome P450 · Fragment screening

## Introduction

Cooperativity is a powerful way of Nature to accelerate or regulate specific biological processes [1]. It is encountered on virtually all levels of biochemical complexity, from metal chelation through allosteric modulation and protein folding to communication between cells. Pharmaceutically relevant examples of cooperativity include multiple ligand binding to a single (typically orthosteric) binding site. This situation is typical for proteins that belong to the intricate defense mechanism of the body facilitating the metabolism or efflux of drugs and other xenobiotics. Cytochromes P450 (CYPs) are characteristic examples of these enzymes [2]. Particularly CYP3A4, the isoform responsible for the metabolism of the majority of marketed drugs [3], is involved in cooperative binding. Other metabolic enzymes such as UDP-glucuronosyltransferases (UGTs) [4, 5] and glutathione S-transferases (GSTs) [6] are able to bind ligands cooperatively. ATP-binding cassette (ABC) efflux transporters [7–10] such as the highly promiscuous P-gp can also bind multiple ligands simultaneously. Increasing number of evidences collected in these systems by site-directed mutagenesis experiments [11–13], deuterium isotope effect experiments [14], NMR T<sub>1</sub> paramagnetic relaxation studies [15–18] and the X-ray structure determination of protein–ligand complexes [19, 20] indicate that the binding of the substrate and effector compounds takes place at orthosteric sites. Recently published structures of CYP3A4 in complex with two ketoconazole molecules [21] and that of mouse P-glycoprotein with two cyclic peptide inhibitors bound [22] provided remarkable advances in the field.

**Electronic supplementary material** The online version of this article (doi:10.1007/s10822-012-9578-6) contains supplementary material, which is available to authorized users.

M. Vass · Á. Tarcsay · G. M. Keserü (✉)  
Discovery Chemistry, Gedeon Richter Plc., P.O.B. 27, 1475  
Budapest, Hungary  
e-mail: gy.keseru@richter.hu

The other important example of multiple ligand binding is fragment based drug discovery. The linking strategy involves screening and connecting fragments bound adjacent within the binding site keeping the fragments in their original binding modes [23]. An efficient method to identify fragments suitable for linking has been described, in which a fragment hit from the primary screen is added to the protein in high concentration so that it occupies the primary binding site and a second-site screen is performed to obtain proximally bound fragments. A subnanomolar inhibitor of Bcl-X<sub>L</sub> [24] and a low micromolar inhibitor of HSP90 [25] are successful examples of this approach. A virtual analog of this procedure can be implemented by identifying first-site hits from a virtual fragment screening [26] and then docking another library into the predicted complexes of high-scoring ligands that explores further potential sites. Finding a suitable linker and finally docking the resulting compound as a whole to the receptor would then yield druglike hits.

Considering relevant applications of second site screening on both targets and anti-targets and also the increasing number of multiple ligand complexes solved in the last decade (Fig. 1) we concluded that computational prediction of cooperative binding could have significant impact on lead discovery and optimization.

To reach this goal we set out to investigate multiple ligand docking in a more general context. Traditional docking applications treat one site—one ligand interactions. Docking of multiple ligands to a single binding site has not yet been thoroughly investigated. Li et al. have recently implemented a Multiple Ligand Simultaneous Docking (MLSD) strategy into AutoDock4 using Lamarckian genetic algorithm and particle swarm optimization for the simultaneous conformational search of multiple ligands [27, 28]. However, this application has not yet been extensively tested. In this study we describe a

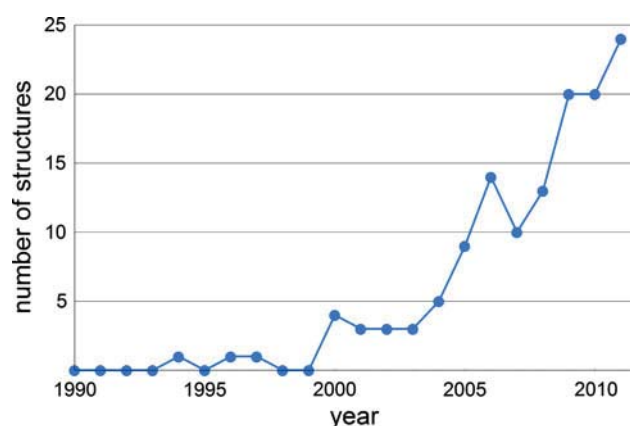


**Fig. 1** Number of X-ray crystallographic structures with multiple ligands solved per year

simple sequential docking protocol using the commercial docking software Glide for reproducing experimental binding conformations of multiple ligands. A set of 129 X-ray crystal structures was collected from the RCSB Protein Data Bank (PDB) containing at least two non-cofactor type ligands in close proximity. Ligands were docked sequentially to their respective structure in a self-docking setup and the performance of the methodology was then analyzed. Results obtained for the pharmaceutically relevant subset of cytochrome P450 enzymes and structures coming from HSP90 fragment screens were further investigated.

## Methods

### Compilation of the data set

Crystal structures of protein–ligand complexes were selected from the PDB. Initial filters included a resolution of at least 2.5 Å, protein structures excluding DNA and RNA binding, and no appearance of words associated with photosynthesis or the words MEMBRANE and IMMUNE in the HEADER section of the pdb files. The number of non-covalently bound ligands in each structure was determined excluding water, common cations and anions, common solvents and crystallization agents including PEGs, buffer constituents, lipids, disulfide bond reducing agents etc., cofactors, common carbohydrates and carbohydrate-amines (e.g. NAG), modified residues, and the unknown species (UNL and UNX). Pairwise minimal interatomic distances (MIDs) between the ligands were calculated and clusters with 2–6 ligands having an MID within 6.0 Å were identified. Structures that did not contain cations, anions and cofactors except for heme in the 6.0 Å neighborhood of such a cluster were saved. Docking calculations were performed on clusters having at least two ligand centroids within the  $14 \times 14 \times 14 \text{ \AA}^3$  cube centered on the common ligand centroid (the inner box in Glide docking). Protein binding sites were characterized using SiteMap [29] version 2.4 in single binding site region evaluation mode with a 6.0 Å buffer around the ligand cluster. Structures without a SiteMap recognized binding site were discarded. The remaining structures were finally visually inspected to eliminate cases with incorrectly defined connectivity or atom types not parametrized in the OPLS-2005 force field. This filtering of the PDB resulted in 129 structures as of 1 October 2011 (see the Supporting Information for PDB ID codes). These structures thus have good resolution and contain a cluster of at least two and at most six ligands in close proximity to each other suitable for docking. Two of these protein–ligand complexes (1e7c and 3g35) had two distinct, non-symmetry equivalent sites

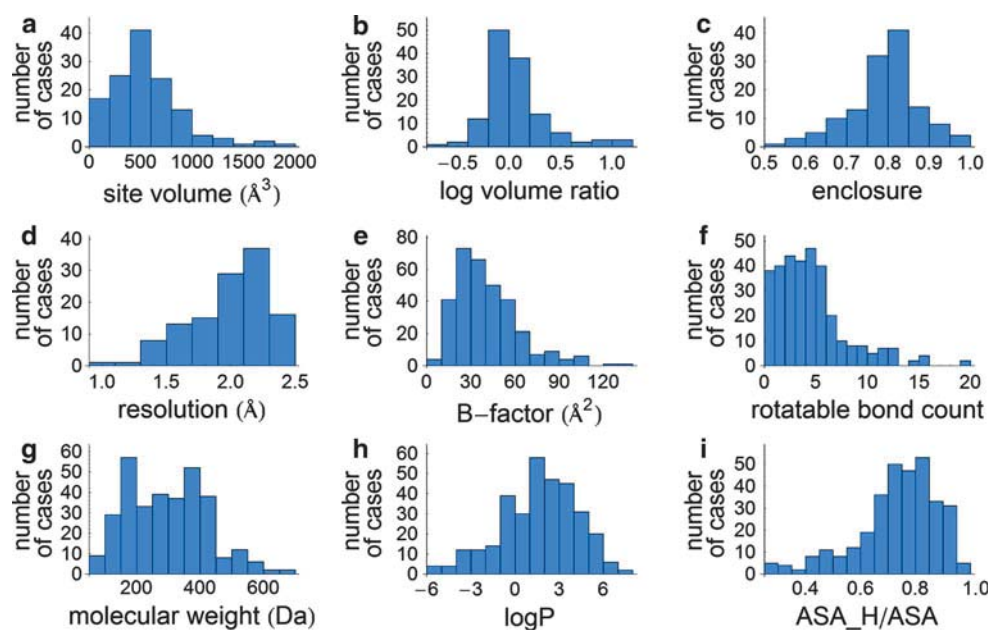
where multiple ligands were present. The docking procedure in these cases was performed for both binding sites increasing the total number of sites to 131 representing 54 targets. These sites contain a total of 294 ligands to be docked, meaning an average of 2.24 ligands per binding site. Binding sites were then classified as sites containing multiple copies of the same ligand and those containing different ligands. Since in the latter case ligands can be docked in different orders the total number of docking calculations was 324.

### Structure preparation

The most completely modeled biological assembly in the unit cell was retained from the crystal structures. If the biological assembly contained crystal mates, only chains in the vicinity of the docked ligands were added. In cases where there were more identical chains in the unit cell, the first chain containing the multiply ligated site was selected. Further phases of the work were automated using the Schrödinger Python API available in Schrödinger Suite 2010 (version 3.8). The structures were prepared for docking with the Protein Preparation Wizard [30] that includes assigning bond orders, adding hydrogens, treating metals, creating disulfide bonds, converting selenomethionines, deleting distant waters, assigning the H-bond network with water sampling and finally minimizing the structure up to 0.3 Å RMSD with the OPLS-2005 force field. All waters and ligands were then deleted from the structures before grid generation. In the second case study of HSP90 complexes structure preparation included retaining six conserved crystallographic water molecules in the structures, since these waters are known to play an

important role in HSP90 binding [31]. Retained water molecules were selected by aligning the five HSP90 structures and identifying those present in all structures. Orientation of their hydrogens and protonation states of nearby residues were automatically assigned by the Protein Preparation Wizard. They form hydrogen bonds with the Asn51, Asp93 and Trp162 side chains, backbone carbonyls of Leu48 and Gly97, backbone NH of Gly137 and with each other. They all form two or three hydrogen bonds and have a relative B-factor of 0.4–0.9. Docked ligands were prepared by converting them first to 2D structures with the ChemAxon molconvert plugin [32] and then back to 3D with the Schrödinger LigPrep [33] version 2.4 retaining the configuration of the chiral centers. This procedure eliminated the conformational bias of using experimental binding modes. Epik [34–36] version 2.1 was used to generate tautomers and protomers at  $\text{pH } 7 \pm 2$ . For proteins crystallized outside of this range we verified that LigPrep found no additional ligand protomers on the pH of crystallization. Physico-chemical properties, namely molecular weight, logP, number of H-bond donors and acceptors, number of rotatable bonds, molecular volume, hydrophobic and total accessible surface area (ASA) of the ligands were calculated with the ChemAxon cxcalc plugin [37] and their druglikeness was assessed using Lipinski's rule ( $\text{MW} \leq 500$  Da,  $\text{logP} \leq 5.0$ , hydrogen bond acceptor count  $\leq 10$ , hydrogen bond donor count  $\leq 5$ ). SiteMap was used to estimate binding site volumes and enclosure. The enclosure parameter ranges from 0.5 to 1, a higher value means a more buried site. The average value for tight-binding sites is 0.78 [38]. Figure 2 shows the distributions of crystallographic and calculated properties of binding sites and ligands considered in our dataset.

**Fig. 2** Distribution histograms of binding site (a–d) and ligand (e–i) properties calculated with SiteMap (a–c), obtained from crystallographic data (d–e) and calculated with cxcalc (f–i). Log volume ratio is the logarithm of total ligand volume divided by the site volume to base 10. ASA is the accessible surface area and ASA\_H is the hydrophobic accessible surface area



## Docking protocol

Docking was performed by Glide 5.6 [39–42] using Single Precision (SP), Extra Precision (XP) and SP hard modes. The latter represents SP calculations without scaling down the van der Waals radii of nonpolar ligand atoms (using a scaling factor of 1.0 instead of the default 0.8). A docking run for a particular structure consisted of at most as many consecutive grid generation and docking steps as the number of ligands in the docked ligand cluster. The maximum available grid size ( $36 \times 36 \times 36 \text{ \AA}^3$  outer and  $14 \times 14 \times 14 \text{ \AA}^3$  inner box) was used. The grid was always centered on the common centroid of all the heavy atoms of the ligand cluster that allowed positioning the grid in the same way in each step of a docking run. The number of poses entered to post-docking minimization and saved was set to 30, other sampling parameters were set to their default. RMSDs between docked and experimental ligand conformations were calculated for heavy atom positions.

The sequential docking protocol used in this study contains multiple grid generations depending on the number of ligands evaluated for a particular binding site. The first grid was generated for the ligand-free receptor. In the first docking step each tautomer and protomer of the first ligand was docked. If different ligands were bound, both docking permutations were evaluated. The 30 saved poses were ranked by their respective Emodel scores. If any of the top three poses of any protomer or tautomer had an RMSD less than  $2.0 \text{ \AA}$  to any of the experimental ligand conformations, that pose was selected and merged with the ligand-free starting structure (first poses had priority over second ones and second poses had priority over third ones; lower RMSDs had priority among different protomers and tautomers). If none of the top three poses had an RMSD less than  $2.0 \text{ \AA}$ , but a higher ranked pose had, then the pose

with the minimal RMSD was merged with the ligand-free starting structure, and the rank of the merged pose was recorded. If no poses with RMSD less than  $2.0 \text{ \AA}$  were found, then the docking run was terminated since no satisfactory pose was generated.

In the second step a new grid was generated for the merged structure and all protomers and tautomers of the second ligand were docked. The pose to be merged with the one-ligand containing structure was selected the same way as in the first step and its rank was recorded. If the cluster contained more than two ligands, this procedure was repeated until all ligands were docked or the run was terminated because of no satisfactory RMSDs. After the docking run the ranks of good poses were also calculated using GlideScore and Glide Energy scoring functions by reordering the 30 saved poses for all protomers and tautomers (top three poses if any had an RMSD less than  $2.0 \text{ \AA}$ , otherwise the pose with minimal RMSD). Our workflow is shown in Fig. 3.

## Data analysis

RMSD values and Emodel, GlideScore and Glide Energy ranks of the merged poses were assigned. RMSDs of the first docking steps were analyzed in order to compare sequential multiple ligand docking to single ligand docking benchmark studies. Median and mean RMSDs and standard deviations were calculated for top scoring and lowest RMSD poses. Success rates are defined as the ratio of ligands where any pose had an RMSD less than  $2.0 \text{ \AA}$ . Top pose rates were calculated as the ratio where the top pose had an RMSD less than  $2.0 \text{ \AA}$ . RMSD and rank distributions of all docking steps for the different docking modes were subjected to Kolmogorov–Smirnov statistical analysis using STATISTICA 10.

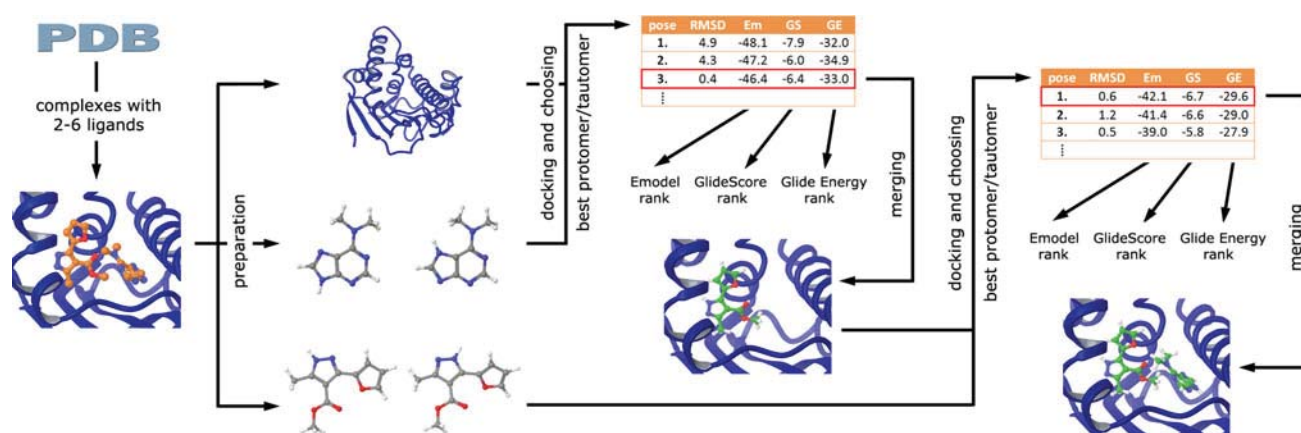


**Fig. 3** The sequential docking workflow used in this study

## Results and discussion

### Docking performance for the first ligand

Sampling efficiency of docking programs is most often assessed by RMSD values calculated between docking poses and experimental binding modes. The RMSD distribution of top scoring poses and ranks of the best poses are informative of scoring performance. Evaluating the sampling efficiency of Glide in multiple ligand docking we first calculated the median and mean RMSDs for the top scoring and the best pose of the first ligands and compared the results to those obtained in single ligand docking for 68 high resolution X-ray complexes [43] (see Table 1). We found that median and mean RMSDs of top poses were typically higher in our data set than those for single ligand docking as expected for docking ligands significantly smaller than their respective binding sites. Although XP mode is usually considered being more precise, the difference in top pose median RMSDs is smaller for the SP protocol than that for the XP (0.09 and 0.75 Å, respectively). Best pose median RMSDs were, however, somewhat smaller than those of Cross et al. (0.18 and 0.03 Å for SP and XP, respectively). This might not be specific to multiple ligand docking but might even be attributed to the difference in Glide versions. Standard deviations for the SP protocol are pretty much similar to those reported for single ligand docking, while for XP we obtained significantly

higher values (with the difference of 0.8 Å and 1.0 Å for top poses and best poses, respectively). SP and SP hard protocols performed similarly when docking the first ligand. Although the top pose rates (the percentage of top poses within 2.0 Å RMSD relative to the experimental binding mode) reported by Cross et al. were identical for SP and XP protocols (69.1 %) [43], for our dataset we found that SP based protocols outperformed the XP (top pose rates were 58.0, 51.1 and 58.0 %, for SP, XP and SP hard protocols, respectively). Other parameters such as the resolution of the X-ray structure, relative B-factors (the ligand's mean B-factor divided by the whole structure's mean B-factor) and physico-chemical descriptors of the ligands showed virtually no impact on docking accuracy (data not shown).

### Docking performance for the next ligands

Our objective in this step was the evaluation of the sequential docking methodology. To achieve this goal the number of successful docking steps (defined by any docking pose within 2.0 Å RMSD) among the 30 saved poses and the impact of the number of consecutively docked ligands was investigated. Analysis of the expectation values revealed that the successive docking of more than two ligands is highly unlikely to give reliable results (Table 2). The calculated values were 1.37, 1.03 and 1.40 for SP, XP and SP hard protocols, respectively, reflecting

**Table 1** Statistical results for docking the first ligands to multiple ligand binding sites and for single ligand docking

RMSD	This study			Cross et al. [43]		
	Median (Å)	Mean (Å)	SD (Å)	Median (Å)	Mean (Å)	SD (Å)
SP top pose	1.31	2.42	2.49	1.22	2.08	2.49
SP best pose	0.54	1.23	1.50	0.72	1.30	1.40
XP top pose	1.90	2.96	2.93	1.15	1.97	2.13
XP best pose	0.76	2.16	2.56	0.79	1.34	1.53
SP hard top pose	1.34	2.40	2.48	–	–	–
SP hard best pose	0.49	1.29	1.66	–	–	–

**Table 2** Number of successfully docked ligands (RMSD < 2.0 Å) per binding site using SP, XP and SP hard protocols as the function of the number of ligands

Number of ligands at the site	Number of sites	Number of docking runs with n successful consecutive docking steps											
		SP				XP				SP hard			
		n = 0	n = 1	n = 2	n = 3	n = 0	n = 1	n = 2	n = 3	n = 0	n = 1	n = 2	n = 3
2	110	20	28	62	–	37	31	42	–	23	25	62	–
3	13	4	2	3	4	6	4	3	0	3	1	4	5
4	6	3	1	1	1	1	2	2	1	2	1	2	1
5	1	0	0	1	0	0	1	0	0	0	0	1	0
6	1	1	0	0	0	1	0	0	0	1	0	0	0
Total	131	28	31	67	5	45	38	47	1	29	27	69	6

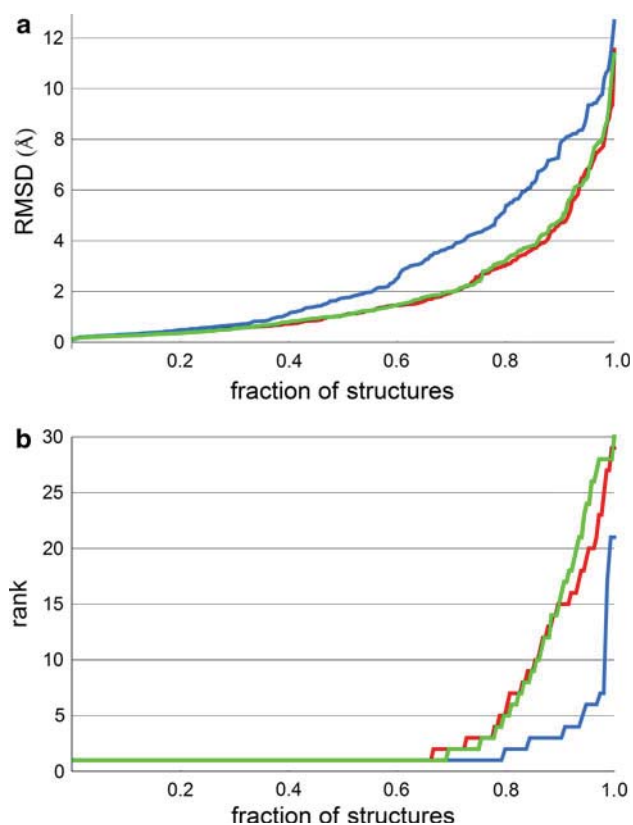


**Fig. 4** RMSD (a) and rank distributions (b) using the Emodel scoring function of all docking steps obtained by SP (red), XP (blue) and SP hard (green) protocols

that the chance to recover at least two experimental binding conformations is 55, 37 and 57 %, respectively. In conjunction to that observed for docking the first ligand, we found that SP and SP hard performed similar and much better relative to the XP protocol in multiple docking situations.

RMSD distributions for all docking steps and rank distributions for all successful (RMSD < 2.0 Å) steps were analyzed by Kolmogorov–Smirnov statistics (Fig. 4). RMSD distributions were significantly higher for the XP protocol as compared to that of SP and SP hard ( $p < 0.005$ ). Rank distributions obtained by the default Emodel scoring function showed the reverse trend; XP provided significantly lower ranks relative to the other two protocols ( $p < 0.05$ ), while SP and SP hard were similar. Rank distributions obtained by the three different scoring functions (Emodel, GlideScore and Glide Energy) showed no statistically significant differences in any of the docking protocols (SP, XP, SP hard). In successful docking steps RMSDs were usually similar or lower for XP than that of the SP. However, it was interesting to see that the higher the rank of the selected pose (typically if larger than the 6th), the more challenging successful docking was for XP. Thus, it seems that XP typically sorts out high-scoring

poses only, and is unable to score better than SP in docking multiple ligands. RMSDs of the second docking steps were somewhat higher than those of the first docking steps, however, their distributions were not significantly different from that of the first steps. Median RMSDs of second docking steps were 0.26 Å, 0.59 Å and 0.28 Å higher than first ones for SP, XP and SP hard, respectively. We found that if the first ligand was docked successfully (RMSD  $\leq$  2.0 Å), then the second docking step was also successful in 70 % of the cases. If the first RMSD was over 2.0 Å, 86 % of the second ligands also failed to dock successfully (in the SP protocol when the docking run was not terminated after an RMSD > 2.0 Å).

#### Performance on druglike ligands and closed sites

Finally, the impact of ligand and binding site properties were investigated. Considering that scoring functions were typically optimized against a set of known binders of pharmaceutical targets and decoys with drug- and lead-like features [40, 41], we expected that the multiple docking of druglike ligands would be more efficient. This hypothesis was tested by ligands which did not violate any of Lipinski's rules providing a 110 membered druglike subset. Using the SP protocol with Emodel scoring the success rate calculated in at least two consecutive and successful (RMSD < 2.0 Å) docking steps increased from 55 to 59 % (see Fig. 5, all numerical data are available in the Supporting Information). The number of cases where the selected pose was actually the top ranking pose (top pose rate) also increased from 31 to 33 %. Thus we concluded that druglike ligands performed only slightly better in multiple docking settings. XP and SP hard protocols showed similar characteristics as for the whole dataset. The success rates increased from 37–40 % to 57–61 %, respectively, while only marginal improvements were seen in top pose rates (from 25–26 % to from 34–35 %, respectively). Success rates and top pose rates obtained by all the protocols with GlideScore and Glide Energy score were slightly lower.

We also expected that docking to shallow and open binding sites would be more challenging than to the closed sites. Since in the former case ligands can exploit less binding interactions, scoring would be more difficult. Binding sites were therefore classified using their enclosure values calculated by SiteMap as 48 open and 83 closed sites. Out of the 83 closed sites 53 (64 %) provided a docking pose within 2.0 Å RMSD relative to the experimental binding conformation in at least two successive steps. Docking to 29 out of the 48 open sites (60 %), however, was unsuccessful yielding poses with RMSD larger than 2.0 Å. Finally combining the enclosure and druglike filters we investigated docking druglike ligands to

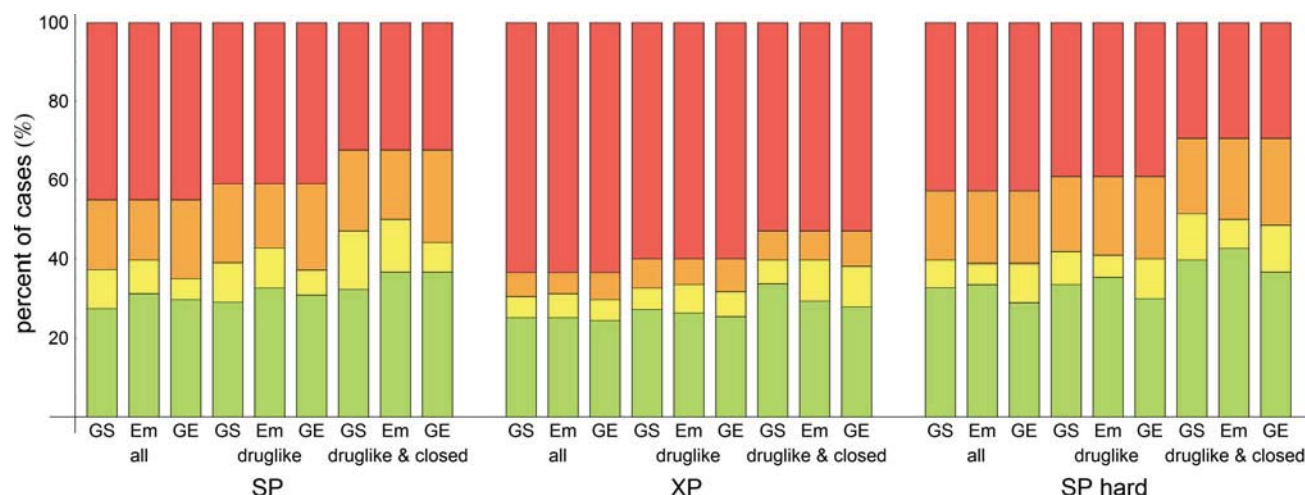


**Fig. 5** Cumulative success rates obtained in at least two successful consecutive docking steps for SP, XP and SP hard protocols combined with GlideScore, Emodel and Glide Energy scoring functions and filters (all sites, sites with druglike ligands and closed sites with druglike ligands). From *bottom to top*: fraction of cases

where both of the top ranking poses had  $\text{RMSD} < 2.0 \text{ \AA}$  (*green*), where any of the top three poses had  $\text{RMSD} < 2.0 \text{ \AA}$  (*green + yellow*), where any of the poses had  $\text{RMSD} < 2.0 \text{ \AA}$  (*green + yellow + orange*) and all structures in the subset (*green + yellow + orange + red*)

closed sites. Evaluating at least two consecutive docking steps in this subset of 68 complexes we obtained the success rates of 68, 47 and 71 % for the SP, XP and SP hard protocols with Emodel scoring, respectively. Top pose rates were 37, 29 and 43 %, respectively.

Independent analysis of each docking step required the selection of a near native binding mode for the first ligand that mimics the best case scenario in a real life screening situation. Since typically this information is not available in prospective applications the binding mode of the first ligand should be selected based on docking scores to merge with the receptor for the next round of docking. The simplest method is to merge the top pose identified by a single scoring function. Top pose rates calculated in two consecutive steps for our dataset show the usefulness of this method. Thus, using the SP hard protocol with Emodel scoring on druglike ligands and closed binding sites binding modes obtained for 43 % of the compounds are expected to be accurate. A computationally more demanding method would be to merge multiple ( $N$ ) poses of the first docked ligand with the receptor and perform the second docking step on all of the acquired complexes saving multiple ( $N$ ) poses again. However, in this method the selection of the best complex from the resulting  $N \times N$  pool is not trivial. Instead, we evaluated the performance for  $N = 3$  by considering well-docked poses among the top three binding modes. This estimates the upper limit of the performance since the second docking steps usually failed when the first merged pose had an RMSD over  $2.0 \text{ \AA}$ . Selecting the well-docked poses from a  $30 \times 30$  pool would provide significant improvement on the expense of 31 grid generation and docking steps.

#### Case study 1: Application to cooperative CYP binding

Cytochromes P450 (CYPs) are the most studied promiscuous metabolic enzymes with the ability to bind multiple ligands in their active site as demonstrated by X-ray crystallography [19, 21, 44–49]. In vitro CYP assays are generally used to predict in vivo pharmacokinetic properties and drug interaction potential of compounds. Determination of binding constants, however, is sometimes not straightforward as these assays often show non-Michaelis–Menten kinetic profiles [50] indicating the cooperative binding of substrates. There is a large body of evidence published on cooperative binding to CYP3A4 [51] and CYP2C9 [52] but similar findings have been reported for CYP2A6 [14], CYP1A2 [53] isoforms and the bacterial CYPeryF [54] as well. Heterotropic cooperativity in these isozymes may lie in the background of drug–drug interactions, though only a few studies were able to connect in vitro and in vivo observations [55–58]. Predicting drug interactions or metabolic activation by computational methods is a challenging task since metabolic enzymes usually have broad substrate specificities and their heteroactivation profile is substrate dependent. Up to now only two CYP3A4 and CYP2C9 heteroactivator pharmacophore models [59, 60] have been published and a single structure based docking method was developed to predict activators of CYP2C9-mediated flurbiprofen hydroxylation [61].

Since our data set contains seven CYP structures it was straightforward to evaluate the performance of our sequential docking protocol on this set of pharmaceutically relevant enzymes. Two further CYP structures (human CYP2C8 with two bound retinoic acids with a resolution of

2.60 Å and human CYP3A4 with two bound ketoconazole molecules with a resolution of 3.80 Å) were added to this assembly as they fulfilled all but the resolution criterion, that were set up in the compilation of our data set. The resolution of the latter is higher than typically required for docking but we used the structure since double occupancy is evident from the electron density map, however, the binding mode of the distal ligand may be ambiguous. Our final CYP dataset composed six bacterial, a rabbit and two human CYP isoforms.

Selected crystallographic properties and docking results are summarized in Table 3. It can be seen that except for the triple occupancy 3g5n structure, all other CYP sites are characterized as closed sites due to high enclosure values. Calculated site volumes confirm that bacterial CYP isoforms comprise much more compact sites, while mammalian CYPs exhibit more spacious ones that can accommodate compounds of various sizes. The ligands present in the bacterial and the rabbit 2B4 isoforms fulfill Lipinski's rule of druglikeness, while in human CYPs a logP value of 5.01 was calculated for retinoic acid and ketoconazole has a molecular weight of 531 Da, both rather close to corresponding Lipinski limits. Most B-factors of the ligands are relatively low indicating that the experimental binding modes are realistic. Based on our previous experience these observations suggested good

docking results. In fact, SP and SP hard protocols with Emodel scoring provided successful poses in all cases but one that was the third ligand in the only triple ligand complex. Again, the performance of the XP protocol was inferior; 6 of the 19 docking steps were unsuccessful. SP provided 6 of the 9 structures with good poses found among the top three poses in both steps, while XP performed similarly for only 3 complexes.

The aminophenanthrene ligand coordinating the heme iron in 1egy was docked perfectly as the top pose by both SP and SP hard protocols. The top pose of XP had the aromatic rings flipped but occupied almost the same space. The second ligand made apolar contacts with the aromatic and aliphatic side chains of the active site and its amino group was not involved in any hydrogen bonds in the crystal structure. Interestingly, Glide identified a hydrogen bond in most of the top ranked poses to the hydroxyl group of Tyr75 or to the backbone carbonyl of Phe86. As a result a flipped pose or even an irrelevant binding mode was predicted.

The proximal androstenedione in 1eup forms a hydrogen bond with both of its carbonyl groups. One of them is with Asn89 that was lost in the docking runs due to flipped asparagine side chain created by the Protein Preparation Wizard when optimizing the H-bond network. Despite this Glide identified the experimental binding mode as top.

**Table 3** Crystallographic and docking data of cytochrome P450 structures with multiple bound ligands

PDB ID	CYP isoform	res. (Å)	vol. (Å <sup>3</sup> )	encl.	Ligands	lig. ID	B-fact. (Å <sup>2</sup> )	RMSD	Em	RMSD	Em	RMSD	Em
								(Å) SP		(Å) XP		(Å) SP hard	
1egy	107	2.35	489.8	0.931	9-Aminophenanthrene	1	25.73	0.19	1	0.18	3	0.20	1
						2	35.40	0.36	3	0.32	1	0.33	2
1eup	107	2.10	615.0	0.910	Androstenedione	1	29.95	0.57	1	0.68	4	0.45	1
						2	47.27	0.73	1	0.62	1	0.93	1
2whf	130	1.58	644.8	0.759	1-(3-Methylphenyl)-1H-benzimidazol-5-amine	1	43.67	0.77	2	>2.00	-	1.97	2
						2	38.02	0.68	5	>2.00	-	1.25	1
2d0e	158	2.15	562.5	0.908	2-Hydroxynaphthoquinone	1	47.45	0.50	3	0.76	3	0.25	12
						2	71.84	0.42	1	>2.00	-	0.35	1
1t93	158	1.62	358.1	0.948	Flaviolin	1	16.50	0.48	3	0.48	4	0.45	2
						2	16.22	0.52	9	>2.00	-	0.27	8
2z3u	245	2.40	353.3	0.905	Chromopyrrolic acid	1	14.79	0.20	1	0.22	1	0.18	1
						2	33.02	0.40	1	0.40	1	0.34	1
3g5n	2B4	2.50	633.1	0.672	1-(Biphenyl-4-ylmethyl)-1H-imidazole	1	64.48	0.25	1	0.53	1	0.94	1
						2	40.36	0.48	1	>2.00	-	0.41	1
						3	73.21	>2.00	-	>2.00	-	>2.00	-
2nnh	2C8	2.60	772.1	0.869	Retinoic acid	1	57.23	0.49	1	0.39	1	0.40	1
						2	54.19	0.52	14	1.94	1	0.55	1
2v0m	3A4	3.80	1247.1	0.808	Ketoconazole	1	34.35	0.89	1	0.86	1	1.17	1
						2	71.84	1.94	2	1.20	6	1.54	30

res. = resolution, vol. = site volume calculated by SiteMap, encl. = enclosure calculated by SiteMap, lig. ID = ligand number, B-fact. = mean B-factor of the ligand, Em = rank by Emodel

Many misdocked poses featured a perpendicular orientation of the androstenedione molecule to the heme probably because of the overemphasized electrostatic interactions between the heme iron and one of the carbonyl groups. The distal ligand was well-docked with all docking protocols.

In 2whf the scoring function ranked a flipped iron coordinating pose to the top thus rendering the well-docked distal pose second. It was interesting to see that the distal ligand could penetrate deeper into the active site with its aromatic end, retaining only one of its hydrogen bonds that resulted in a high RMSD (see Fig. 6). Surprisingly no heme iron coordinating pose could be found with the XP protocol.

2d0e and 1t93 are structures of the same isoform cocrystallized with very similar ligands, thus the two binding sites are nearly identical. Flaviolin and hydroxynaphthoquinone molecules form multiple hydrogen bonds. Active site Arg288 anchors the ligands in both

experimental and docked poses in addition to aromatic stacking with the heme and each other. Interestingly this was not preserved in the top ranking poses of the first docking steps instead a binding mode with three hydrogen bonds was found for both compounds. For the second docked flaviolin molecule the stacking interaction was captured well but poses involved in more hydrogen bonds were still enforced for hydroxynaphthoquinone even at the expense of distorting the planarity of its rings.

In 2z3u the two chromopyrrolic acid residues (the natural substrate of CYPStaP) are held very firmly by multiple hydrogen bonds,  $\pi$ - $\pi$  and cation- $\pi$  interactions that were predicted successfully as the top ranked pose in all docking protocols.

3g5n was one of the cases where the inner grid box contained only two out of the three ligand centroids. Two molecules were correctly docked by SP based protocols (see Fig. 6). The semi-distal ligand forms contacts mostly

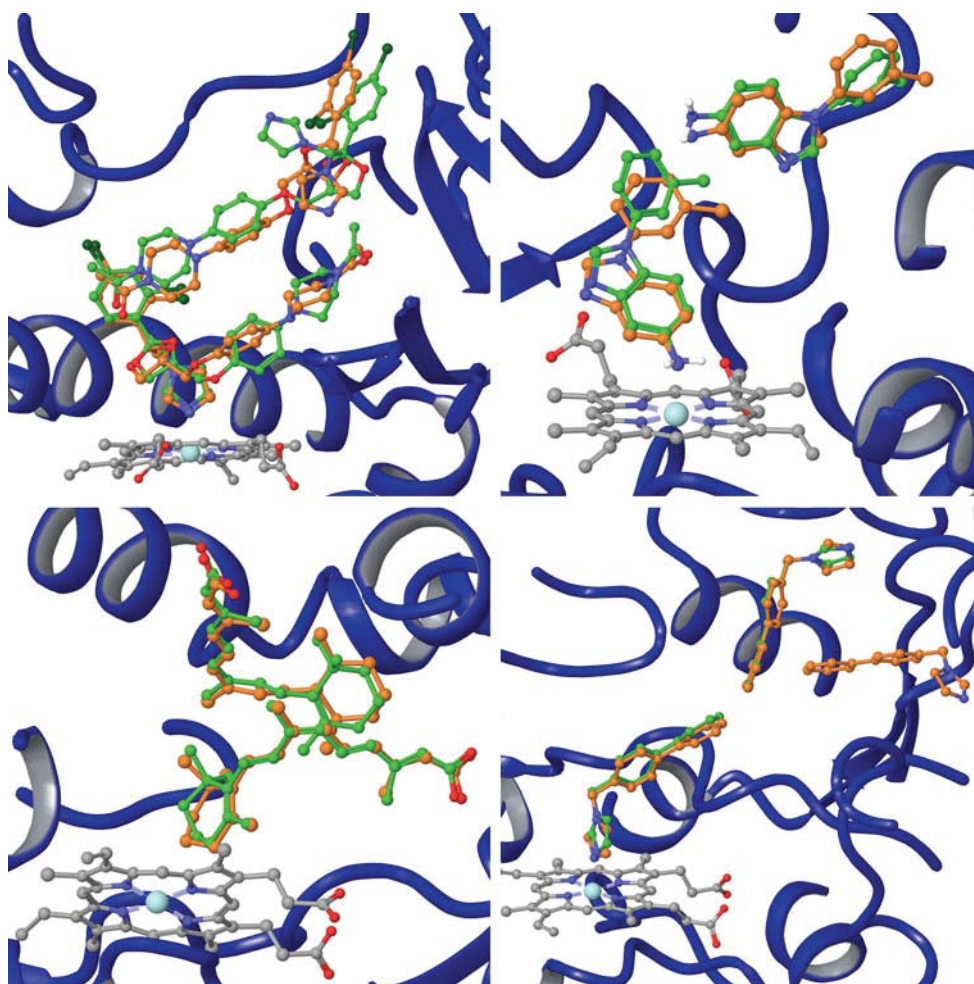


**Fig. 6** Representative binding modes found in cytochrome P450 complexes with multiple ligands by the SP protocol and Emodel scoring. *Top left* 2v0m, *top right* 2whf, *bottom left* 2nnh, *bottom right* 3g5n. Heme carbon, docked ligand carbon, docked ligand polar

hydrogen, co-crystallized ligand carbon, oxygen, nitrogen, chlorine and iron atoms are colored grey, green, white, orange, red, blue, dark green and cyan, respectively

with aromatic and aliphatic side chains that were correctly identified in the first docking step. Its imidazole part is encased in a polar environment but is not involved in specific interactions. The iron coordinating binding mode was found second by the SP protocols, but XP missed the iron coordinating pose again. The binding conformation of the third ligand, which is partially exposed to the solvent with its imidazole ring, could not be reproduced by either of the protocols. Instead poses exhibiting aromatic stacking with the iron coordinating ligand and involved in a hydrogen bond with the amide hydrogen of Gly99 were obtained.

The retinoic acid molecules in 2nnh are both involved in two strong hydrogen bonds with the backbone amides of Gly98 and Ser100 for the proximal and with Asn204 and Arg241 for the distal ligand. These interactions were recovered in all docked poses that resulted in good ranks in the first docking step. On the other hand, however, the ring of the distal ligand was flipped in many poses in the second docking step that was responsible for RMSDs greater than 2.0 Å, though the binding motif is essentially the same (see Fig. 6).

The binding mode of the proximal ketoconazole molecule in 2v0m was remarkably well reproduced with all docking protocols. The acetyl piperazine moiety of the distal ligand was positioned well in the second step; however, the dichlorophenyl and imidazole rings were typically misdocked that increased the RMSDs significantly (see Fig. 6). The chlorine atom of the distal ligand forms interactions with the backbone amide of Leu216 and the aromatic ring of Phe213 while its imidazole ring faces a polar environment in the crystal structure. These interactions were replaced by a hydrogen bond between the backbone of Asp217 and the rotated imidazole ring in many of the docked poses resulting high ranks in the second step. It should be noted, however, that the electron density at the head region of the distal ligand was poorly defined [21] and the experimental binding mode might also be questionable.

#### Case study 2: Application to virtual fragment screening against HSP90

One of the most important drug discovery applications of multiple ligand docking would be fragment based hit identification. Our approach provides the virtual equivalent of experimental second site screening in order to find fragments suitable for linking. Demonstrating this capability we picked up five complexes of the heat shock protein 90- $\alpha$  (HSP90) from our dataset that were obtained in fragment based discovery programs [25, 31, 62, 63]. Each of these complexes contains two different fragments mostly with low B-factors and fulfilling Lipinski's criteria

by definition. The binding site of the protein is quite small and closed as indicated by the corresponding enclosure values. These features implicated successful docking but high RMSDs and ranks were obtained. With the exception of the 2xdu complex, protocols were able to reproduce experimental binding modes, but poses within 2.0 Å RMSD were typically not ranked into the top three poses (the average rank was 8.3). However, structural waters are known to play an important role in ligand binding to HSP90 [31]. Visual inspection indeed revealed that top ranked high RMSD poses overlap with conserved crystal water molecules that were omitted by the Protein Preparation Wizard in our original protocol.

The total of six conserved water molecules were identified that form hydrogen bonds with the Asn51, Asp93 and Trp162 side chains, backbone carbonyls of Leu48 and Gly97, backbone NH of Gly137 and with each other as described in the methods section. Repeating the docking runs with the six conserved waters included yielded top ranked poses with RMSDs less than 2.0 Å for all of the docking steps in the SP protocol, and most of the docking steps in the XP and SP hard runs. Selected crystallographic properties and docking results of this protocol are summarized in Table 4. The binding site volumes calculated with SiteMap decreased by 60–110 Å<sup>3</sup> while enclosure values did not change significantly. The better ranks of the well-docked poses, however, are probably not only the results of the decreased site volumes and different binding site shapes. Instead without waters included, docked fragments interact with the same side chains of the receptor that form hydrogen bonds in the water mediated complex. Docking the phenylaminofuranone first to 2qfo without waters the top pose forms direct hydrogen bonds with Asp93 and Asn51 taking the place of the pyrimidinamine moiety. In 3hz1 and 2yej top poses of all ligands form direct hydrogen bonds with the carbonyl of Leu103 without waters while in the crystal structures the pyrazole ring forms a water mediated bridge with the same amino acid. In top poses identified in 2yei direct hydrogen bonds to Leu103 and Trp162 were found without considering structural waters. Thus, the region around the Leu103 carbonyl group is a docking hot spot of HSP90. Examples of docking results are shown in Fig. 7. In this system the SP protocol with Emodel ranking proved to be the best in binding mode reproduction but even the XP and SP hard protocols failed at the ranking of only one well-docked pose.

#### Conclusions

The objective of this work was to evaluate the performance of a simple sequential docking methodology in reproducing

**Table 4** Crystallographic and docking data of HSP90 complexes with multiple fragments bound

PDB ID	res. (Å)	vol. (Å <sup>3</sup> )	vol. with waters (Å <sup>3</sup> )	encl.	lig ID	B-fact. (Å <sup>2</sup> )	RMSD (Å) SP	Em	RMSD (Å) XP	Em	RMSD (Å) SP hard	Em
2qfo	1.68	388.3	324.5	0.761	1	15.95	0.38	1	0.38	1	0.43	1
					2	17.41	0.16	1	0.16	1	0.26	1
3hz1	2.30	476.1	364.6	0.795	1	25.84	0.46	1	1.10	1	0.29	1
					2	18.53	0.47	1	1.25	1	0.38	1
2xdu	1.74	411.9	350.9	0.811	1	24.60	0.21	1	0.21	1	0.20	1
					2	33.47	0.29	1	0.30	1	0.24	1
2yei	2.20	418.8	362.2	0.800	1	47.47	1.04	1	0.28	1	1.14	3
					2	42.31	0.90	1	1.13	1	0.95	1
2yej	2.20	447.3	346.8	0.779	1	53.74	1.02	1	1.02	1	1.04	1
					2	82.07	0.42	1	0.40	2	0.25	1

Conserved waters were included in all docking runs. res. = resolution, vol. = site volume calculated by SiteMap, encl. = enclosure calculated by SiteMap, lig. ID = ligand number, B-fact. = mean B-factor of the ligand, Em = rank by Emodel

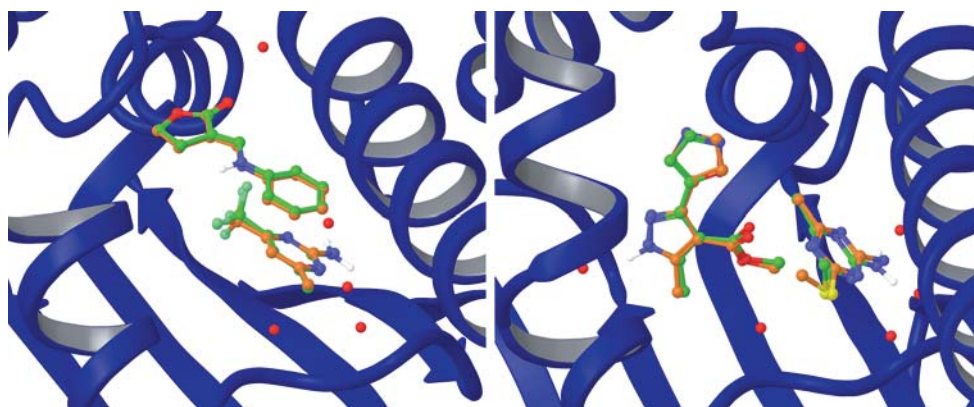


**Fig. 7** Representative binding modes of ligands in HSP90 complexes obtained with the SP protocol using Emodel scoring with conserved waters included. *Left* 2qfo, *right* 2yej. Docked ligand carbon, docked ligand polar hydrogen, co-crystallized ligand carbon, oxygen,

nitrogen, sulfur and fluorine atoms are colored green, white, orange, red, blue, yellow and turquoise respectively. Only the oxygen atoms of waters are shown

experimental binding modes of ligands in higher stoichiometry protein–ligand complexes. This phenomenon has relevance to the linking strategy of fragment evolution in fragment based drug discovery and to the study of drug–drug interactions, which are frequently mediated by metabolic enzymes or transporters that can bind multiple ligands in their active site. The performance of Glide in docking multiple ligands to their native binding sites was evaluated on a set of 129 protein–ligand complexes from the PDB. Three different docking protocols were tested: default single (SP) and extra precision (XP), and single precision without scaling down the van der Waals radii of nonpolar ligand atoms (SP hard). Each of the protocols was used in conjunction with three scoring functions: GlideScore, Emodel and Glide Energy.

It was seen that docking to multiply ligated binding sites is more difficult than single ligand docking indicated by higher top pose RMSDs and lower success rates for all

protocols. Docking of the second ligand fails with a chance of 86 % if the RMSD of the first docked ligand is over 2.0 Å, thus a well-docked first ligand is a prerequisite to dock the second ligand successfully. Docking more than two ligands with such a sequential protocol seems to be even more challenging. SP and SP hard protocols did not provide significant difference in RMSD and rank distributions. In contrast, XP yielded significantly lower success rates and lower ranks. This indicates that the sampling algorithm in XP usually doesn't find different poses than that of the SP protocol. More likely it is able to separate reasonable poses from false solutions but it often rejects good poses as well. Though excessive differences between the performances of the different scoring functions were not discovered, Emodel gave somewhat higher ratios of top ranked well-docked poses in the SP and SP hard protocols than the two other functions. For the XP protocol, however, GlideScore provided the highest success rates.

The fractions of structures with at least two well-docked ligands ranked among the top three poses, which is a preferred scenario when docking compounds with unknown binding modes, were 40 % for the SP protocol, 31 % for the XP protocol and 39 % for the SP hard protocol with Emodel scoring. Specific subsets of the structures were examined to find criteria for a higher success rate of the methodology. Success rates increased both for the subset of closed sites with enclosure values greater than 0.78, and for sites containing only Lipinski compliant ligands. Sites fulfilling both criteria provided ratios of 50, 40 and 50 % using SP, XP and SP hard protocols with Emodel scoring, respectively. The highest ratios of successful docking runs are encountered with the SP hard protocol. On the other hand, the fact that XP gave the lowest ratios and it rarely produced well-docked poses when SP did not find one either, is likely the consequence of its sampling algorithm, which uses specific parts of the ligand from the SP poses as starting cores [42], thus not being able to sample substantially different binding modes from those found by SP.

Further sources of high RMSDs in docking multiple ligands may be the reward and penalty terms of the scoring functions for filling hydrophobic pockets by hydrophobic groups, or inadequate solvation of groups forming hydrogen bonds. During the first docking step the ligand may partially occupy the space or even important interaction points needed for the binding of the other ligand(s), because those contacts are scored more favorable than the ones formed in the multiply ligated structure. The most common errors in the docking runs identified by inspection of the top poses and experimental binding conformations conform to this hypothesis. In many cases the first docked pose either occupied such specific interaction points of the other ligand, or if it was mostly lipophilic—it appeared to maximize its apolar contact surface with the binding site. A special case of the latter was when two planar ligands were aligned parallel in the X-ray structure (e.g. in 1eb9, 2cbt, 2vq5, 3e85, 3etg and 3g35), and the docked poses were also parallel to each other but different to the experimental binding modes, the two ligands together filling essentially the same space. Either way, the second ligand was partially excluded from the place it should have been docked into, which resulted in misdocked poses and high RMSDs in the docking steps after the first one. A possible remedy for this problem would be to allow the previously docked ligands to move when docking a new one, which would mean a special induced fit approach considering translations and rotations of ligands. Furthermore a ligand might need to hop from one interaction point to another, involving greater displacement, or passing through a higher energy barrier than is usually allowed. Attempts were made to refine misdocked poses of two docked ligands simultaneously using low-mode conformational sampling including

rotations and translations of the ligands in the binding site. However, this method did not provide significantly lower RMSDs on a small subset of our data set.

In the cytochromes P450 case study we investigated 9 complexes in total. SP and the SP hard protocols were able to find well-docked poses for all the ligand pairs with generally low ranks. Two-thirds of the docking steps provided well-docked top ranked poses in the SP hard protocol. These results are especially encouraging as binding modes in the human 2B4, 2C8 and 3A4 isoforms were reproduced well by the default SP protocol. Thus, it seems that this important family of enzymes is a promising target for multiple ligand docking. Misdocked poses could be mainly related to scoring problems. They most often arose from enforcing hydrogen bonds not present in the experimental structures or inaccurate scoring of interactions with the heme iron.

Results omitting conserved crystal waters were less than promising for HSP90 complexes, but their inclusion yielded excellent docking results. Two top ranked well-docked poses were obtained for all complexes with all protocols. The binding motifs of the fragments in these structures usually comprise only one specific interaction. Misdocked poses obtained with the water-free structures arose when the sterically feasible alternative position of the fragment was stabilized by a hydrogen bond formed with a residue originally involved in a hydrogen bond with a water molecule.

In summary, the performance of Glide was investigated on 129 multiple ligand bound protein complexes in a sequential docking setup with three different protocols and three different scoring functions. On average 36 % of the whole set of structures with at least two well-docked ligands ranked among the top three poses were obtained. The introduction of the druglikeness filter for ligands and closeness filter for binding sites resulted in higher performance, and the ratio of well-reproduced structures increased to 50% for the SP hard protocol. XP was found to provide lower success rates but with a higher probability of the top scoring poses being well-docked. Three ligands could be docked in only a few cases. Two pharmaceutically relevant subsets, that of cytochromes P450 and HSP90 complexes from fragment screens, were examined in more detail. In these cases higher success rates were observed than in the druglike and closed site subset. These results show the limitations of large-scale screening applications in the sequential docking of multiple ligands but indicate their utility in screening against drug interactions and in virtual fragment screening. Further efforts with induced fit protocols, however, seem to be validated to provide more precise binding mode information for the increasing number of cooperative binding events.

**Acknowledgments** The authors thank Dóra K. Menyhárd for critically reading the manuscript.

## References

- Whitty A (2008) Cooperativity and biological complexity. *Nat Chem Biol* 4:435–439
- Denisov IG, Frank DJ, Sligar SG (2009) Cooperative properties of cytochromes P450. *Pharmacol Ther* 124:151–167
- Guengerich FP (2008) Cytochrome P450 and chemical toxicology. *Chem Res Toxicol* 21:70–83
- Wong H, Tong V, Riggs KW, Rurak DW, Abbott FS, Kumar S (2007) Kinetics of valproic acid glucuronidation: evidence for in vivo autoactivation. *Drug Metab Dispos* 35:1380–1386
- Uchaipichat V, Galetin A, Houston JB, Mackenzie PI, Williams JA, Miners JO (2008) Kinetic modeling of the interactions between 4-methylumbelliferone, 1-naphthol, and zidovudine glucuronidation by UDP-glucuronosyltransferase 2B7 (UGT2B7) provides evidence for multiple substrate binding and effector sites. *Mol Pharmacol* 74:1152–1162
- Caccuri AM, Antonini G, Ascenzi P, Nicotra M, Nuccetelli M, Mazzetti AP, Federici G, Lo Bello M, Ricci G (1999) Temperature adaptation of glutathione S-transferase P1-1. A case for homotropic regulation of substrate binding. *J Biol Chem* 274:19276–19280
- Martin C, Berridge G, Higgins CF, Mistry P, Charlton P, Callaghan R (2000) Communication between multiple drug binding sites on P-glycoprotein. *Mol Pharmacol* 58:624–632
- Kondratov RV, Komarov PG, Becker Y, Ewenson A, Gudkov AV (2001) Small molecules that dramatically alter multidrug resistance phenotype by modulating the substrate specificity of P-glycoprotein. *Proc Natl Acad Sci USA* 98:14078–14083
- Higgins CF (2007) Multiple molecular mechanisms for multidrug resistance transporters. *Nature* 446:749–757
- Storz K, Möllmann L, Jacobs A, Baumert D, Wiese M (2009) Activators of P-glycoprotein: structure-activity relationships and investigation of their mode of action. *Chem Med Chem* 4:1897–1911
- Harlow GR, Halpert JR (1998) Analysis of human cytochrome P450 3A4 cooperativity: construction and characterization of a site-directed mutant that displays hyperbolic steroid hydroxylation kinetics. *Proc Natl Acad Sci USA* 95:6636–6641
- Domanski TL, He YA, Khan KK, Roussel F, Wang Q, Halpert JR (2001) Phenylalanine and tryptophan scanning mutagenesis of CYP3A4 substrate recognition site residues and effect on substrate oxidation and cooperativity. *Biochemistry* 40:10150–10160
- Khan KK, He YQ, Domanski TL, Halpert JR (2002) Midazolam oxidation by cytochrome P450 3A4 and active-site mutants: an evaluation of multiple binding sites and of the metabolic pathway that leads to enzyme inactivation. *Mol Pharmacol* 61:495–506
- Harrelson JP, Atkins WM, Nelson SD (2008) Multiple-ligand binding in CYP2A6: probing mechanisms of cytochrome P450 cooperativity by assessing substrate dynamics. *Biochemistry* 47:2978–2988
- Hummel MA, Gannett PM, Aguilar JS, Tracy TS (2004) Effector-mediated alteration of substrate orientation in cytochrome P450 2C9. *Biochemistry* 43:7207–7214
- Roberts AG, Díaz MD, Lampe JN, Shireman LM, Grinstead JS, Dabrowski MJ, Pearson JT, Bowman MK, Atkins WM, Campbell AP (2006) NMR studies of ligand binding to P450eryF provides insight into the mechanism of cooperativity. *Biochemistry* 45:1673–1684
- Cameron MD, Wen B, Allen KE, Roberts AG, Schuman JT, Campbell AP, Kunze KL, Nelson SD (2005) Cooperative binding of midazolam with testosterone and alpha-naphthoflavone within the CYP3A4 active site: a NMR T1 paramagnetic relaxation study. *Biochemistry* 44:14143–14151
- Cameron MD, Wen B, Roberts AG, Atkins WM, Campbell AP, Nelson SD (2007) Cooperative binding of acetaminophen and caffeine within the P450 3A4 active site. *Chem Res Toxicol* 20:1434–1441
- Schoch GA, Yano JK, Sansen S, Dansette PM, Stout CD, Johnson EF (2008) Determinants of cytochrome P450 2C8 substrate binding: structures of complexes with montelukast, troglitazone, felodipine, and 9-cis-retinoic acid. *J Biol Chem* 283:17227–17237
- Schumacher MA, Miller MC, Brennan RG (2004) Structural mechanism of the simultaneous binding of two drugs to a multidrug-binding protein. *EMBO J* 23:2923–2930
- Ekroos M, Sjögren T (2006) Structural basis for ligand promiscuity in cytochrome P450 3A4. *Proc Natl Acad Sci USA* 103:13682–13687
- Aller S, Yu J, Ward A, Weng Y, Chittaboina S, Zhuo R, Harrell PM, Trinh YT, Zhang Q, Urbatsch IL, Chang G (2009) Structure of P-glycoprotein reveals a molecular basis for poly-specific drug binding. *Science* 323:1718–1722
- Congreve M, Chessari G, Tisi D, Woodhead AJ (2008) Recent developments in fragment-based drug discovery. *J Med Chem* 51:3661–3680
- Petros AM, Dinges J, Augeri DJ, Baumeister SA, Betebenner DA, Bures MG, Elmore SW, Hajduk PJ, Joseph MK, Landis SK, Nettesheim DG, Rosenberg SH, Shen W, Thomas S, Wang X, Zanze I, Zhang H, Fesik SW (2006) Discovery of a potent inhibitor of the antiapoptotic protein Bcl-xL from NMR and parallel synthesis. *J Med Chem* 49:656–663
- Huth JR, Park C, Petros AM, Kunzer AR, Wendt MD, Wang X, Lynch CL, Mack JC, Swift KM, Judge RA, Chen J, Richardson PL, Jin S, Tahir SK, Matayoshi ED, Dorwin SA, Lador US, Severin JM, Walter KA, Bartley DM, Fesik SW, Elmore SW, Hajduk PJ (2007) Discovery and design of novel HSP90 inhibitors using multiple fragment-based design strategies. *Chem Biol Drug Des* 70:1–12
- Sandor M, Kiss R, Keseru GM (2010) Virtual fragment docking by Glide: a validation study on 190 protein-fragment complexes. *J Chem Inf Model* 50:1165–1172
- Li H, Li C (2010) Multiple ligand simultaneous docking: orchestrated dancing of ligands in binding sites of protein. *J Comput Chem* 31:2014–2022
- Li H, Liu A, Zhao Z, Xu Y, Lin J, Jou D, Li C (2011) Fragment-based drug design and drug repositioning using multiple ligand simultaneous docking (MLSD): identifying celecoxib and template compounds as novel inhibitors of signal transducer and activator of transcription 3 (STAT3). *J Med Chem* 54:5592–5596
- SiteMap, version 2.4, Schrödinger, LLC, New York, NY, 2010
- Schrödinger Suite 2010 Protein Preparation Wizard; Epik version 2.1, Schrödinger, LLC, New York, NY, 2010; Impact version 5.6, Schrödinger, LLC, New York, NY, 2010; Prime version 2.2, Schrödinger, LLC, New York, NY, 2010
- Roughley SD, Hubbard RE (2011) How well can fragments explore accessed chemical space? A case study from heat shock protein 90. *J Med Chem* 54:3989–4005
- Molecule File Converter, version 5.4.1.1, © 1999–2011 ChemAxon Ltd
- LigPrep, version 2.4, Schrödinger, LLC, New York, NY, 2010
- Epik, version 2.1, Schrödinger, LLC, New York, NY, 2010
- Shelley JC, Cholletti A, Frye LL, Greenwood JR, Timlin MR, Uchiyama M (2007) Epik: a software program for pKa prediction and protonation state generation for druglike molecules. *J Comput Aided Mol Des* 21:681–691
- Greenwood JR, Calkins D, Sullivan AP, Shelley JC (2010) Towards the comprehensive, rapid, and accurate prediction of the favorable tautomeric states of drug-like molecules in aqueous solution. *J Comput Aided Mol Des* 24:591–604

37. Calculator, version 5.4.1.1, © 1998–2011 ChemAxon Ltd
38. SiteMap 2.4 User Manual, <http://www.schrodinger.com/support/docs/18/20/>
39. Glide, version 5.6, Schrödinger, LLC, New York, NY, 2010
40. Friesner RA, Banks JL, Murphy RB, Halgren TA, Klicic JJ, Mainz DT, Repasky MP, Knoll EH, Shelley M, Perry JK, Shaw DE, Francis P, Shenkin PS (2004) Glide: a new approach for rapid, accurate docking and scoring. 1. Method and assessment of docking accuracy. *J Med Chem* 47:1739–1749
41. Halgren TA, Murphy RB, Friesner RA, Beard HS, Frye LL, Pollard WT, Banks JL (2004) Glide: a new approach for rapid, accurate docking and scoring. 2. Enrichment factors in database screening. *J Med Chem* 47:1750–1759
42. Friesner RA, Murphy RB, Repasky MP, Frye LL, Greenwood JR, Halgren TA, Sanschagrin PC, Mainz DT (2006) Extra precision Glide: docking and scoring incorporating a model of hydrophobic enclosure for protein-ligand complexes. *J Med Chem* 49:6177–6196
43. Cross JB, Thompson DC, Rai BK, Baber JC, Fan KY, Hu Y, Humblet C (2009) Comparison of several molecular docking programs: pose prediction and virtual screening accuracy. *J Chem Inf Model* 49:1455–1474
44. Cupp-Vickery J, Anderson R, Hatziris Z (2000) Crystal structures of ligand complexes of P450eryF exhibiting homotropic cooperativity. *Proc Natl Acad Sci USA* 97:3050–3055
45. Podust LM, Ouellet H, von Kries JP, de Montellano PR (2009) Interaction of *Mycobacterium tuberculosis* CYP130 with heterocyclic arylamines. *J Biol Chem* 284:25211–25219
46. Zhao B, Guengerich FP, Voehler M, Waterman MR (2005) Role of active site water molecules and substrate hydroxyl groups in oxygen activation by cytochrome P450 158A2: a new mechanism of proton transfer. *J Biol Chem* 280:42188–42197
47. Zhao B, Guengerich FP, Bellamine A, Lamb DC, Izumikawa M, Lei L, Podust LM, Sundaramoorthy M, Kalaitzis JA, Reddy LM, Kelly SL, Moore BS, Stec D, Voehler M, Falck JR, Shimada T, Waterman MR (2005) Binding of two flavin substrate molecules, oxidative coupling, and crystal structure of *Streptomyces coelicolor* A3(2) cytochrome P450 158A2. *J Biol Chem* 280:11599–11607
48. Makino M, Sugimoto H, Shiro Y, Asamizu S, Onaka H, Nagano S (2007) Crystal structures and catalytic mechanism of cytochrome P450 StP that produces the indolocarbazole skeleton. *Proc Natl Acad Sci USA* 104:11591–11596
49. Gay SC, Sun L, Maekawa K, Halpert JR, Stout CD (2009) Crystal structures of cytochrome P450 2B4 in complex with the inhibitor 1-biphenyl-4-methyl-1H-imidazole: ligand induced structural response through  $\alpha$ -helical repositioning. *Biochemistry* 48:4762–4771
50. Atkins WM (2005) Non-Michaelis-Menten kinetics in cytochrome P450-catalyzed reactions. *Annu Rev Pharmacol Toxicol* 45:291–310
51. Houston JB, Galetin A (2005) Modelling atypical CYP3A4 kinetics: principles and pragmatism. *Arch Biochem Biophys* 433:351–360
52. Zhou SF, Zhou ZW, Yang LP, Cai JP (2009) Substrates, inducers, inhibitors and structure-activity relationships of human cytochrome P450 2C9 and implications in drug development. *Curr Med Chem* 16:3480–3675
53. Sohl CD, Isin EM, Eoff RL, Marsch GA, Stec DF, Guengerich FP (2008) Cooperativity in oxidation reactions catalyzed by cytochrome P450 1A2: highly cooperative pyrene hydroxylation and multiphasic kinetics of ligand binding. *J Biol Chem* 283:7293–7308
54. Khan KK, Liu H, Halpert JR (2003) Homotropic versus heterotropic cooperativity of cytochrome P450eryF: a substrate oxidation and spectral titration study. *Drug Metab Dispos* 31:356–359
55. Lasker JM, Huang MT, Conney AH (1984) In vitro and in vivo activation of oxidative drug metabolism by flavonoids. *J Pharmacol Exp Ther* 229:162–170
56. Tang W, Stearns RA, Kwei GY, Iliff SA, Miller RR, Egan MA, Yu NX, Dean DC, Kumar S, Shou M, Lin JH, Baillie TA (1999) Interaction of diclofenac and quinidine in monkeys: stimulation of diclofenac metabolism. *J Pharmacol Exp Ther* 291:1068–1074
57. Hutzler JM, Frye RF, Korzekwa KR, Branch RA, Huang SM, Tracy TS (2001) Minimal in vivo activation of CYP2C9-mediated flurbiprofen metabolism by dapson. *Eur J Pharm Sci* 14:47–52
58. Egnell AC, Houston B, Boyer S (2003) In vivo CYP3A4 heteroactivation is a possible mechanism for the drug interaction between felbamate and carbamazepine. *J Pharmacol Exp Ther* 305:1251–1262
59. Egnell AC, Eriksson C, Albertson N, Houston B, Boyer S (2003) Generation and evaluation of a CYP2C9 heteroactivation pharmacophore. *J Pharmacol Exp Ther* 307:878–887
60. Egnell AC, Houston JB, Boyer CS (2005) Predictive models of CYP3A4 Heteroactivation: in vitro-in vivo scaling and pharmacophore modeling. *J Pharmacol Exp Ther* 312:926–937
61. Locuson CW, Gannett PM, Ayscue R, Tracy TS (2007) Use of simple docking methods to screen a virtual library for heteroactivators of cytochrome P450 2C9. *J Med Chem* 50:1158–1165
62. Barker JJ, Barker O, Courtney SM, Gardiner M, Hesterkamp T, Ichihara O, Mather O, Montalbetti CA, Muller A, Varasi M, Whittaker M, Yarnold CJ (2010) Discovery of a novel Hsp90 inhibitor by fragment linking. *Chem Med Chem* 5:1697–1700
63. Murray CW, Carr MG, Callaghan O, Chessari G, Congreve M, Cowan S, Coyle JE, Downham R, Figueroa E, Frederickson M, Graham B, McMenamin R, O'Brien MA, Patel S, Phillips TR, Williams G, Woodhead AJ, Woolford AJ (2010) Fragment based drug discovery applied to Hsp90. Discovery of two lead series with high ligand efficiency. *J Med Chem* 53:5942–5955

Cite this: DOI: 10.1039/c2md20267k

www.rsc.org/medchemcomm

CONCISE ARTICLE

## Fragments to link. A multiple docking strategy for second site binders†

Márton Vass and György M. Keserű\*

Received 7th September 2012, Accepted 22nd October 2012

DOI: 10.1039/c2md20267k

Fragment based drug discovery employs growing and linking strategies for optimization. Here we report the binding mode prediction of multiple fragments bound to a single target using a sequential docking methodology employing Glide to support the identification and linking of fragment hits. Sampling and scoring accuracy for the first and second site binders in self- and cross-docking situations is assessed.

Fragment-based drug discovery (FBDD) has recently been proved to have significant utility in early phase drug research. Fragments are polar compounds of low molecular weight (100–250 Da) and of low complexity that are able to make optimal interactions with the protein target.<sup>1</sup> Screening of such compounds has advantages over traditional hit finding approaches, since much fewer of them need to be tested and hits with higher ligand efficiencies can be found. However, due to their low affinities they are typically identified by sensitive biophysical screening methods, such as X-ray crystallography,<sup>2</sup> nuclear magnetic resonance (NMR),<sup>3</sup> surface plasmon resonance (SPR),<sup>4</sup> *etc.* FBDD has already provided the market with an approved drug<sup>5</sup> and several others in clinical development, demonstrating the potential of fragment hits to be quickly developed into leads and drug candidates. The two main strategies of fragment hit elaboration are growing and linking.<sup>6</sup> In the first one a single fragment is decorated with additional functionalities, while in the second two (or more) fragments need to be identified that bind to the target simultaneously and in close proximity. The latter approach seems to be the more challenging, as fewer successful examples are reported in the literature.<sup>7</sup> Such fragment pairs may be identified by co-crystallization of ternary complexes usually from fragment cocktails. However, extensive care must be taken in the structure determination of cocktail screening hits as shown by Mark *et al.*<sup>8</sup> Other biophysical methods are also used for the identification of second-site binding fragments, such as the method termed SAR by NMR<sup>9</sup> or the exploitation of interligand nuclear Overhauser effects (ILOEs).<sup>10</sup> Due to the heavy instrumentation, throughput limitations (usually a few hundred by X-ray crystallography and a few thousand with NMR or SPR screening), experimental artefacts and the synthetic challenges in hit elaboration,

computational methods supporting both the hit identification and elaboration<sup>11</sup> would be useful. Virtual fragment screening has been shown to have potential in FBDD<sup>12,13</sup> and there are numerous examples of successful structure based fragment optimizations.<sup>14</sup> However, *in silico* support for second-site screening and fragment linking has not been excessively studied.

We recently reported a computational methodology for predicting cooperative binding modes of drug-like ligands on a set of 129 ternary or higher order complexes from the PDB.<sup>15</sup> The methodology consisted of the sequential docking of the ligands using Glide and merging of low-RMSD docked poses with the protein structure. The docking workflow provided promising results for these complexes, 180 out of the 294 poses were predicted successfully. Encouraged by this finding, we intended to investigate the performance of the reported methodology on ternary protein-fragment complexes to provide a docking-based computational tool for identifying suitable starting points for the fragment linking approach. To this end, the literature was searched for successful examples of the linking strategy and ternary fragment complexes with structures available in the RCSB Protein Data Bank (PDB). In line with the finding of our previous work – that sequential docking of more than two ligands is significantly less reliable – examples where more than two fragments were linked were not pursued. Finally 32 synthetically linked or tethered (linked *in situ* using disulfide bonds<sup>16</sup>) examples representing 18 targets were collected; of which one was an NMR structure. For eight examples the linked compounds were not synthesized, only the ternary complex is available. Additionally three examples were included where the hit elaboration strategy was actually growing, but a well-defined second fragment was attached through a linker. Two examples are from ligand deconstruction experiments where the deconstructed fragments were shown to bind the target in a similar fashion as in the linked ligand. X-ray structures of either the two fragments (for 14 structures) or the linked compound (for 18 structures) complexed with its target were retrieved, whichever was available. Ternary complexes were prepared using the standard workflow described in ref. 15, while linked ligands were first split at the linker, free valences were capped with hydrogens

Discovery Chemistry, Gedeon Richter Plc. Gyömrői út 19-21, H-1103 Budapest, Hungary. E-mail: gy.keseru@richter.hu; Fax: +36 1-432-6002; Tel: +36 1-431-4605

† Electronic supplementary information (ESI) available: Details of the PDB structures, structures of the docked ligands and numeric docking results. See DOI: 10.1039/c2md20267k

and then submitted to the preparation workflow. The docking workflow was identical to that used in ref. 15, only the updated Schrödinger Suite 2011 (LigPrep 2.5 and Epik 2.2 for ligand preparation and Single Precision (SP) Glide version 5.7 for docking) was used. Due to the presence of metalloproteins in the dataset, Epik was set to generate additional metal binding states during ligand preparation. Fragments were docked in the order of their binding, where such information was available, *i.e.* the first-site binders were docked first and second-site binders after. Where this information was not available (2c8w, 3img, 3le8, 4a7i, 4dm3), the fragment accommodated deeper in the binding cleft was docked first. This consideration is based on the finding of our previous work that the reverse order docking provided similar or poorer results. Docking results are reported as the heavy atom graph RMSDs (considering symmetry) of the first and second ligands compared to their experimental binding modes, and the ranks by the Emodel scoring function of the ligand poses merged with the protein structure from among the top 30 saved poses. In the case of the 1nny structure it was noted that the naphthyl ring of the first fragment was flipped compared to the single fragment bound structure 1no6, thus the RMSD in this case was calculated to the latter binding mode after fitting the two protein chains onto each other.

**Docking results** are shown in Fig. 1. Details of the PDB structures, structures of the docked ligands and numeric docking results are given in the ESI.† The structures have reasonably good resolution ranging from 0.95 to 2.60 Å, only two having resolution over 2.5 Å, the cutoff used in our previous work. Targets among others include proteases, kinases, phosphatases and metalloproteins, and are implicated in the pathomechanisms of cancer, diabetes, Alzheimer's disease, *etc.* As can be seen, the default sampling of Glide SP was sufficient in all of the examples: a pose was always found with RMSD < 2.0 Å to the experimental binding conformation among the top 30 saved poses. Furthermore, in 49 out of the 64 docking steps (77%) a pose with RMSD < 1.0 Å, and in 39 cases (59%) a pose with RMSD < 0.5 Å were found, the distribution of whose did not depend on whether the first or the second docking steps are in question. This result is especially important, since the accurate prediction of the binding poses is a precondition for the successful structure based design

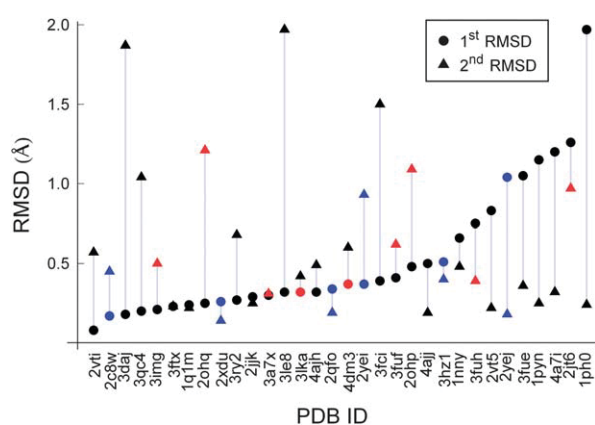


**Fig. 1** Multiple fragment docking results obtained by sequential Glide docking. Plot markers are colored red for docking steps with scoring errors (Emodel rank > 1) and blue for complexes where structural waters were included in grid generation.

of appropriate linkers. The linker length is approximately 1.3 Å for a methylene group in the extended conformation, and even if both of the predicted binding modes have only a 0.5 Å uncertainty, the sum of the errors can be in the distance range of an extra linker atom. Hence, the generally low average error of Glide posing is encouraging for *in silico* FBDD. There are reports in the literature stating that conventional docking scores underperform for fragments, however, studies of Sándor *et al.*<sup>17</sup> and Verdonk *et al.*<sup>18</sup> revealed no significant difference in docking performance between fragments and drug-like molecules with success rates ranging from 50% to 90%. Similarly, in our case the overall scoring was satisfactory, though in a few cases Glide had difficulty in identifying the experimental binding conformation from among the 30 saved poses. Considering the first docking stage only 2 fragments were not ranked top out of the 32 examples (6%). In the second docking step, the rate was somewhat higher, and in 7 cases (22%) was the Emodel scoring function unable to score the experimental binding mode as top. We hypothesize that this lower success rate in the second docking step can originate from two factors. One is the inaccuracy of the prediction of the first fragment's binding mode, which can in turn enlarge the error in the second docking step if the first docked fragment partially overlaps with the experimental binding conformation of the second. Such an effect was seen for the sequential docking of drug-like ligands previously, though it is not evident for the present dataset (see Fig. 1). Another possible reason is that only the first-site fragments can exploit the specific interactions of the protein hot-spot, while the second site is usually less attractive, and identifying the correct binding mode at these sites is intrinsically more difficult. The latter hypothesis is exemplified by 3 out of the 7 scoring errors, where the top poses had extra or alternative H-bonds compared to the experimental binding modes.<sup>19</sup>

*Heat shock protein 90-alpha (HSP90)* structures from the previous work were evaluated again using the newer versions of the software. Though significantly more accurate than before, docking to these structures without waters was still unsuccessful in the sense that poses within 2.0 Å RMSD to the experimental binding modes had an average rank of 6.4. Also, for the thrombin structure 2c8w the RMSD of the first docked ligand was 5.04 Å and thus the docking workflow was terminated. Only when structural waters were retained could a top ranked solution be found. For these six structures the docking results with waters are indicated in Fig. 1.

*Protein tyrosine phosphatase 1B (PTP1B)* has been a difficult target pursued in the research for type II diabetes and obesity therapeutics. Since its catalytic site is identical to that of T-cell protein tyrosine phosphatase, achieving selectivity is a very challenging task. Moreover, PTP1B inhibitors tend to be large and highly charged with low membrane permeability. NMR-based second-site screening and linking of fragments was able to successfully overcome these obstacles and provided selective inhibitors with lower charge density.<sup>20–23</sup> Thus the docking results for these fragments were particularly interesting. In the four crystal structures of PTP1B the first-site fragments are *N,N*-diaryloxamic acids, phenoxymalonic acid and an isoxazole carboxylic acid anchored by Arg221, Gln266 and backbone NHs. Second-site fragments include a naphthoic acid and methyl salicylate based fragments interacting with Tyr20, Arg24, Arg254

and Gln262. The evolution from triacidic antagonists to mono-acidic ones markedly improved their druglikeness. In the case of this target both binding sites seem to encompass specific interaction points. Docking results confirm this finding as low RMSD top ranked poses were obtained for all 8 fragments. However, the RMSD close to 2.0 Å for the *N,N*-diaryloxamic acid in the 1ph0 structure is a consequence of the misplacement of its non-substituted phenyl ring, while the specific interactions could be predicted successfully. Similarly in the case of the 1nny structure the naphthyl ring of the first-site ligand was flipped in the top ranked poses compared to the experimental one (having an RMSD of 1.65 Å), and only after checking the other structures deposited together with 1nny did we notice that this flip was also seen experimentally. The RMSD calculated to the original binding mode in 1no6 was 0.66 Å. Fig. 2 shows the top ranked binding modes compared to the 1nny and 1no6 experimental structures. Thus docking actually drew our attention to a phenomenon that otherwise might have had been overlooked.

*High-throughput X-ray crystallography* may be prone to experimental errors as shown by Mark *et al.* in a recent article, where they examined the validity of phenylethanolamine *N*-methyltransferase (PNMT) complexes acquired by fragment cocktail screening.<sup>8</sup> For one cocktail they found that the modeled 6-chlorooxindole binding mode was not stable in a molecular dynamics (MD) simulation. Instead, re-refinement of the electron density and subsequent MD confirmation revealed that two other fragments of the cocktail were bound. In fact, resorcinol and imidazole bind together to PNMT forming specific interactions with Tyr35, Lys57 and Glu219, instead of only  $\pi$ -stacking interactions for 6-chlorooxindole. Glide was able to identify the binding modes of the two ligands with RMSDs of 0.37 and 0.61 Å. However, the experimental resorcinol binding mode was recovered only as the 5<sup>th</sup> in the Emodel rank order. Top poses formed H-bonds with the same amino acid side chains, but the aromatic ring was flipped (Fig. 3). The imidazole binding mode was reproduced as a top ranked pose. Docking of

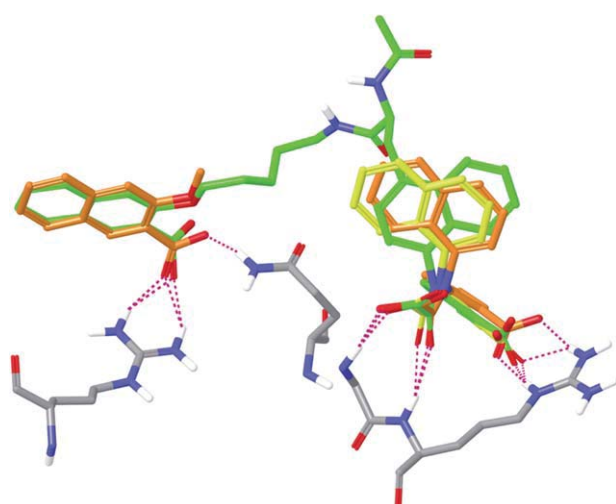


**Fig. 2** Top ranked docked binding conformations of the linked fragments (orange) overlaid with the experimental binding conformation of the linked compound from 1nny (green) and the first-site fragment binding conformation from 1no6 (yellow). Key interacting residues from 1nny are shown in gray and H-bonds in magenta.

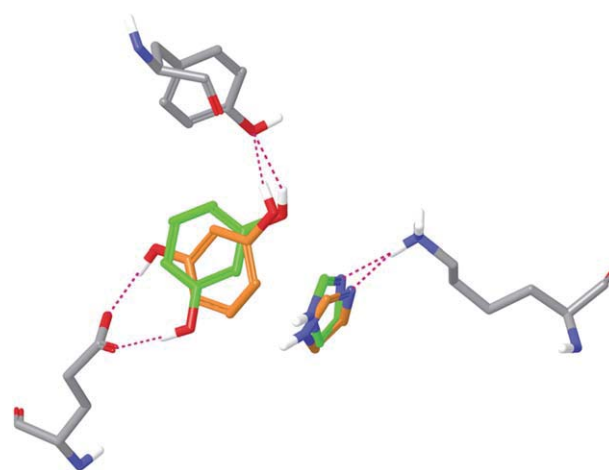


**Fig. 3** Top ranked docked binding conformations of the cocktail fragments (orange) overlaid with their experimental binding conformations from 4dm3 (green). Key interacting residues from 4dm3 are shown in gray and H-bonds in magenta.

6-chlorooxindole to the alternatively modeled structure 3kpy provided RMSDs of 2.02–4.75 Å and various different binding modes. These findings implicate that docking could aid high-throughput X-ray crystallography in identifying multiple fragment binding from cocktails.

*Cross-docking simulations* were performed in order to assess the robustness of the sequential docking methodology with respect to small deviations in binding site geometry. Our dataset contained two structures of *M. tuberculosis* pantothenate synthetase, lactate dehydrogenase A, fructose-1,6-bisphosphatase 1, and beta-secretase 1, four structures of protein tyrosine phosphatase 1B and leukotriene A4 hydrolase and five structures of the heat shock protein 90-alpha, which afforded altogether 52 cross-docking cases. Structures of the same protein were aligned using the Protein Structure Alignment tool in Maestro and the docking methodology was repeated for all combinations of protein–ligand pairs. The RMSD was calculated between the docked poses and the experimental binding conformations of the aligned pairs. Docking performance for the first fragments was only slightly poorer compared to self-docking cases (shown in Fig. 4, numeric docking results are given in the ESI†): there were two unsuccessful docking runs, where no pose with RMSD < 2.0 Å could be found, but for 41 out of the 52 docking steps (79%) a pose with RMSD < 1.0 Å, and in 23 cases (44%) a pose with RMSD < 0.5 Å were found. Scoring failed for 6 out of the 50 successful docking steps (12%). Docking of the second fragments in cross-docking situations proved to be more challenging: there were 13 unsuccessful docking runs (25%) and for 24 out of the 52 docking steps (46%) a pose with RMSD < 1.0 Å, and for 12 cases (23%) a pose with RMSD < 0.5 Å were found. A near-native second-site binding pose was ranked top in 21 out of the 52 cases (40%). While for most structures of the same proteins the binding sites were very similar, there were two problematic cases, which produced most of the posing and scoring errors. The 1qlm structure of PTP1B represents a closed Pro180–Gly183 loop, while the other three complexes have an open loop. Also the key interacting residue Arg221 adopts a different rotamer, which precludes well-docked poses for oxamic acid and malonic acid

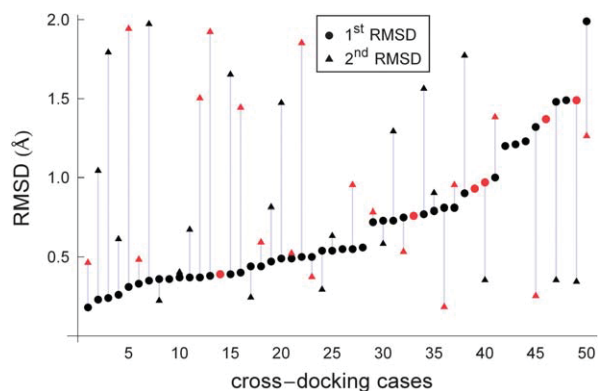


**Fig. 4** Multiple fragment docking results obtained in cross-docking experiments. Plot markers are colored red for docking steps with scoring errors (Emodel rank > 1).

ligands. The 2qfo structure of HSP90 similarly shows a closed Asp102-Gly114 stretch, while this sequence is helical in the other complexes. Thus docking of the 2qfo second-site fragment to the other structures and docking the other second-site ligands to the 2qfo structure both failed.

Though docking of fragment sized ligands has been considered more challenging than docking of drug-like compounds, it was found that in a simple sequential docking protocol Glide was able to correctly predict the binding modes of multiple fragments from successful fragment linking examples and ternary protein-fragment complexes. Cross-docking experiments also provided reasonably high success rates, though proteins with mobile structural elements near the binding site impose a greater challenge for docking. Sampling on this dataset was found to be sufficient; however, cross-docking data suggest some opportunities to improve the scoring functions further. This methodology could be useful in generating promising starting points for fragment linking and supports the identification of suitable linking strategies in fragment based drug design. Furthermore, in combination with high-throughput X-ray crystallography, it might prevent the misinterpretation of diffraction data. These preliminary results suggest virtual second-site screening as a promising strategy; however, comparison of real life screening programs and computational results would be beneficial to explore its full potential in drug discovery settings.

## Acknowledgements

The authors thank Ákos Tarcsay for valuable discussions.

## Notes and references

- G. G. Ferenczy and G. M. Keserü, *J. Chem. Inf. Model.*, 2012, **52**, 1039.
- M. J. Hartshorn, C. W. Murray, A. Cleasby, M. Frederickson, I. J. Tickle and H. Jhoti, *J. Med. Chem.*, 2005, **48**, 403.
- E. R. Zartler and H. Mo, *Curr. Top. Med. Chem.*, 2007, **7**, 1592.
- T. Neumann, H. D. Junker, K. Schmidt and R. Sekul, *Curr. Top. Med. Chem.*, 2007, **7**, 1630.
- J. Tsai, J. T. Lee, W. Wang, J. Zhang, H. Cho, S. Mamo, R. Bremer, S. Gillette, J. Kong, N. K. Haass, K. Sproesser, L. Li, K. S. Smalley, D. Fong, Y. L. Zhu, A. Marimuthu, H. Nguyen, B. Lam, J. Liu, I. Cheung, J. Rice, Y. Suzuki, C. Luu, C. Settachatgul, R. Shellooe, J. Cantwell, S. H. Kim, J. Schlessinger, K. Y. Zhang, B. L. West, B. Powell, G. Habets, C. Zhang, P. N. Ibrahim, P. Hirsh, D. R. Artis, M. Herlyn and G. Bollag, *Proc. Natl. Acad. Sci. U. S. A.*, 2008, **105**, 3041.
- A. W. Hung, H. L. Silvestre, S. Wen, A. Ciulli, T. L. Blundell and C. Abell, *Angew. Chem., Int. Ed.*, 2009, **48**, 8452.
- O. Ichihara, J. Barker, R. J. Law and M. Whittaker, *Mol. Inf.*, 2011, **30**, 298.
- P. C. Nair, A. K. Malde, N. Drinkwater and A. E. Mark, *ACS Med. Chem. Lett.*, 2012, **3**, 322.
- S. B. Shuker, P. J. Hajduk, R. P. Meadows and S. W. Fesik, *Science*, 1996, **274**, 1531.
- P. Sledz, H. L. Silvestre, A. W. Hung, A. Ciulli, T. L. Blundell and C. Abell, *J. Am. Chem. Soc.*, 2010, **132**, 4544.
- D. C. Thompson, R. A. Denny, R. Nilakantan, C. Humblet, D. Joseph-McCarthy and E. Feyfant, *J. Comput.-Aided Mol. Des.*, 2008, **22**, 761.
- S. Kawatkar, H. Wang, R. Czerminski and D. Joseph-McCarthy, *J. Comput.-Aided Mol. Des.*, 2009, **23**, 527.
- G. F. Ruda, G. Campbell, V. P. Alibu, M. P. Barrett, R. Brenk and I. H. Gilbert, *Bioorg. Med. Chem.*, 2010, **18**, 5056.
- C. W. Murray and T. L. Blundell, *Curr. Opin. Struct. Biol.*, 2010, **20**, 497.
- M. Vass, A. Tarcsay and G. M. Keserü, *J. Comput.-Aided Mol. Des.*, 2012, **26**, 821.
- D. A. Erlanson, J. A. Wells and A. C. Braisted, *Annu. Rev. Biophys. Biomol. Struct.*, 2004, **33**, 199.
- M. Sándor, R. Kiss and G. M. Keserü, *J. Chem. Inf. Model.*, 2010, **50**, 1165.
- M. L. Verdonk, I. Giangreco, R. J. Hall, O. Korb, P. N. Mortenson and C. W. Murray, *J. Med. Chem.*, 2011, **54**, 5422.
- In 2ohp the indole fragment formed an H-bond to the Phe108 backbone carbonyl instead of the Gly230 backbone carbonyl. In 2ohq the methoxybiphenyl moiety was flipped to form an H-bond with Tyr71. In 3img the carboxyl group of benzofurane-2-carboxylic acid was accommodated in the place of the sulfate ion between His44, Lys160 and Ser197, which belongs to the hot spot of the protein, since in 3le8 the carboxyl group of the indolylic acid also resides there.
- B. G. Szczepankiewicz, G. Liu, P. J. Hajduk, C. Abad-Zapatero, Z. Pei, Z. Xin, T. H. Lubben, J. M. Trevillyan, M. A. Stashko, S. J. Ballaron, H. Liang, F. Huang, C. W. Hutchins, S. W. Fesik and M. R. Jirousek, *J. Am. Chem. Soc.*, 2003, **125**, 4087.
- G. Liu, Z. Xin, H. Liang, C. Abad-Zapatero, P. J. Hajduk, D. A. Janowick, B. G. Szczepankiewicz, Z. Pei, C. W. Hutchins, S. J. Ballaron, M. A. Stashko, T. H. Lubben, C. E. Berg, C. M. Rondinone, J. M. Trevillyan and M. R. Jirousek, *J. Med. Chem.*, 2003, **46**, 3437.
- Z. Pei, X. Li, G. Liu, C. Abad-Zapatero, T. Lubben, T. Zhang, S. J. Ballaron, C. W. Hutchins, J. M. Trevillyan and M. R. Jirousek, *Bioorg. Med. Chem. Lett.*, 2003, **13**, 3129.
- G. Liu, Z. Xin, Z. Pei, P. J. Hajduk, C. Abad-Zapatero, C. W. Hutchins, H. Zhao, T. H. Lubben, S. J. Ballaron, D. L. Haasch, W. Kaszubska, C. M. Rondinone, J. M. Trevillyan and M. R. Jirousek, *J. Med. Chem.*, 2003, **46**, 4232.

# The Impact of Molecular Dynamics Sampling on the Performance of Virtual Screening against GPCRs

Ákos Tarcsay,<sup>†</sup> Gábor Paragi,<sup>‡,||</sup> Márton Vass,<sup>†</sup> Balázs Jójárt,<sup>§</sup> Ferenc Bogár,<sup>‡</sup> and György M. Keserű<sup>\*,†,⊥</sup>

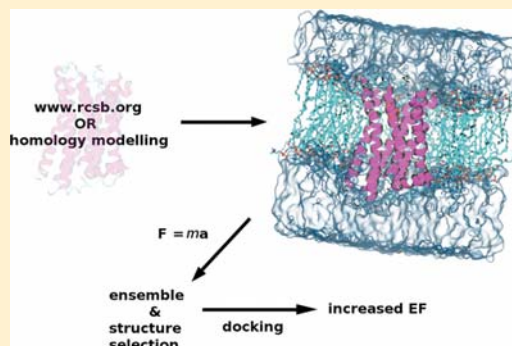
<sup>†</sup>Discovery Chemistry, Gedeon Richter plc., 19-21 Gyömrői út, H-1103 Budapest, Hungary

<sup>‡</sup>MTA-SZTE Supramolecular and Nanostructured Materials Research Group, Hungarian Academy of Sciences, University of Szeged, Dóm tér 8, H-6720, Szeged, Hungary

<sup>§</sup>Department of Chemical Informatics, Faculty of Education, University of Szeged, Boldogasszony sgt. 6, Szeged H-6725, Hungary

## Supporting Information

**ABSTRACT:** The formation of ligand–protein complexes requires simultaneous adaptation of the binding partners. In structure based virtual screening, high throughput docking approaches typically consider the ligand flexibility, but the conformational freedom of the protein is usually taken into account in a limited way. The goal of this study is to elaborate a methodology for incorporating protein flexibility to improve the virtual screening enrichments on GPCRs. Explicit-solvated molecular dynamics simulations (MD) were carried out in lipid bilayers to generate an ensemble of protein conformations for the X-ray structures and homology models of both aminergic and peptidergic GPCRs including the chemokine CXCR<sub>4</sub>, dopamine D<sub>3</sub>, histamine H<sub>4</sub>, and serotonin 5HT<sub>6</sub> *holo* receptor complexes. The quality of the receptor models was assessed by enrichment studies to compare X-ray structures, homology models, and snapshots from the MD trajectory. According to our results, selected frames from the MD trajectory can outperform X-ray structures and homology models in terms of enrichment factor and AUC values. Significant changes were observed considering EF1% values: comparing the original CXCR<sub>4</sub>, D<sub>3</sub>, and H<sub>4</sub> targets and the additional 5HT<sub>6</sub> initial models to that of the best MD frame resulted in 0 to 6.7, 0.32 to 3.5 (10×), 13.3 to 26.7 (2×), and 0 to 14.1 improvements, respectively. It is worth noting that rank-average based ensemble evaluation calculated for different ensemble sizes could not improve the results further. We propose here that MD simulation can capture protein conformations representing the key interacting points of the receptor but less biased toward one specific chemotype. These conformations are useful for the identification of a “consensus” binding site with improved performance in virtual screening.



## INTRODUCTION

The success of structure based virtual screening essentially depends on the accurate modeling of the physiologically relevant protein conformation.<sup>1–3</sup> If the appropriate conformation of the ligand–protein complex is not available for some reason, the usually applied rigid protein approach prevents either enhanced sampling of ligand conformations or the use of physically meaningful scoring functions that result in unacceptable ranking. Correspondingly, ignoring the intrinsic mobility of proteins can have a detrimental effect on the performance of virtual screening and also on structure based optimization of hits that are otherwise integral components of drug discovery programs in pharmaceutical research. Beyond the principle that proteins are not static objects—as they are typically captured with X-ray crystallography—spontaneous occurrence of discrete global fluctuations and the preset conformational equilibrium between functional states influencing ligand binding characteristics is well established.<sup>4</sup> According to the hypothesis of conformational selection, receptors alternate prior to ligand binding between *apo* and ligand-specific *holo* conformations.

Protein flexibility can incorporate small or large scale movements and are classified into three categories: side-chain, backbone, and domain level movements.<sup>5</sup> A wide variety of implementations<sup>2,3</sup> have been developed to model different ranges of protein flexibility such as (i) soft potentials to avoid the penalty of small steric clashes mainly for mimicking subtle side-chain movements, (ii) rotamer exploration, for higher-order side-chain movements, (iii) docking into multiple protein conformations, generally referred to as ensemble docking, (iv) hybrid methods, that incorporate backbone and side-chain movements (for example Induced Fit (IFD)<sup>6</sup> from Schrödinger or IFREDA<sup>7</sup>), and (v) postdocking pose refinement with molecular dynamics simulation.<sup>2,3</sup>

Among the possible implementations, ensemble docking represents a balanced approach in terms of costs and benefits.<sup>1,3,8–10</sup> Docking calculations are typically fast and can be run in batch parallelization that enables the use of an ensemble of protein structures. Regarding the protein

**Received:** February 5, 2013

**Published:** October 13, 2013

conformations, crystallization of multiple ligand–protein complexes or *apo* structures as well as models built on NMR constraints are possible experimental sources to seed ensemble docking.<sup>3</sup> Although there have been several improvements in both crystallization technologies and protein crystallography, membrane proteins typically represent great challenges for experimental structure elucidation. Consequently, several key pharmaceutical targets possess only one resolved structure or can only be accessed as a comparative model.

Several computational methods are available to generate ensemble templates such as molecular dynamics simulations,<sup>11</sup> Monte Carlo conformational search, elastic network model simulations, or normal-mode analysis.<sup>1–3,12,13</sup> A fascinating proof of concept study regarding the applicability of molecular dynamics simulations of ligand–protein complex formation was recently published by Shaw and co-workers.<sup>14</sup> Atomistic prediction of the ligand–protein complex formation by molecular dynamics simulations of Src kinase with dasatinib<sup>14</sup> and  $\beta$ 2 adrenergic receptor with its ligands<sup>15</sup> provided the experimentally observed binding modes. Furthermore, the activation mechanism of  $\beta$ 2 adrenergic receptor was studied by molecular dynamics simulation of the active conformation that spontaneously transferred to the inactive crystallographically observed conformation.<sup>16</sup> Gloriam and co-workers simulated the transition of the inactive 5HT<sub>2A</sub> homology model to the active state by steered molecular dynamics simulation and selected active receptor conformations for virtual screening.<sup>17</sup> Moreover, molecular dynamics simulations were exploited in the case of successful homology model-based virtual screening on a glucagon receptor (GLR), a family B GPCR.<sup>18</sup> Therefore, it is widely accepted that generation of protein conformations by the analysis of molecular dynamics trajectories reflects the physiological conditions and provides relevant seed conformations for ensemble docking. The recent advances in experimental elucidation of GPCR structures prompted us to develop a docking methodology that incorporates protein flexibility.

We have selected targets representing both aminergic and peptidergic GPCR subfamilies, namely dopamine D<sub>3</sub> and chemokine CXCR<sub>4</sub> receptors possessing X-ray structure as well as homology models. We were interested in the performance of our methodology in a more general context, where no X-ray structure is available; this was exemplified by the comparative model of histamine H<sub>4</sub> receptor that was also included among the targets. All-atom, explicit solvated MD simulations of the membrane embedded receptors were carried out to obtain different receptor conformations for docking. Initial X-ray structure, homology model, single structures from the trajectory, and the various ensembles have been compared by retrospective virtual screening using the recently published GDD ligand collection.<sup>19</sup> The homology model of a serotonergic target (5HT<sub>6</sub>) has been developed in our laboratories during the preparation of the manuscript. Similar evaluation of the 5HT<sub>6</sub> receptor model provided a further example of the utility of homology model based conformational ensembles in virtual screening.

## MATERIALS AND METHODS

**Receptor structures.** Four systems were subjected to molecular dynamics simulation: (i) human dopamine D<sub>3</sub> receptor (hD3) with eticlopride (ETQ) (PDB ID: 3pbl<sup>20</sup>), (ii) human CXCR<sub>4</sub> chemokine receptor (CXCR<sub>4</sub>) complexed with IT1t (ITD) (PDB ID: 3odu<sup>21</sup>), (iii) human histamine H<sub>4</sub>

(hH<sub>4</sub>) receptor with JNJ7777120 (JNJ) compound and 5HT<sub>6</sub> with ligand SB-742457 (SB). The initial structures of the hH<sub>4</sub>–JNJ and 5HT<sub>6</sub>–SB complexes were prepared by homology modeling, while in the two other cases the crystal structures were applied.

**Homology Modeling of the Human Histamine H<sub>4</sub> Receptor.** The initial homology model of the human histamine H<sub>4</sub> receptor was constructed with Prime 3.0<sup>22</sup> using the 3.1 Å resolution X-ray structure of the human histamine H<sub>1</sub> receptor (PDB code: 3RZE) and the sequence alignment in the Supporting Information. The N- and C-terminal peptides as well as the ICL3 were not modeled. The conformation of the F144–N147 sequence in TM4 was adjusted to resemble that of G162–S165 from the 2.4 Å resolution X-ray structure of the human  $\beta$ 2-adrenergic receptor (PDB code: 2RH1). JNJ7777120 was first manually docked into the receptor in the binding mode described previously<sup>23</sup> and subjected to minimization of the 5 Å environment of the ligand with H bonds between the protonated amine and D94 and the indole NH and E182 as constraints using the default settings in MacroModel 9.9.<sup>24</sup> Then, JNJ7777120 was redocked into the minimized structure using Induced Fit Docking<sup>6,25</sup> in the Schrödinger Suite 2011 with the default settings and the same two H bonds as constraints in both docking stages. Finally, the whole structure was subjected to the Impref minimization step in the Protein Preparation Wizard.<sup>26</sup>

**Homology Modeling of the Human 5HT<sub>6</sub> Receptor.** The initial homology model of the human serotonin receptor 6 was built with Prime 3.0<sup>22</sup> using the 2.7 Å resolution X-ray structure of the human serotonin receptor 2B (PDB code: 4IB4<sup>28</sup>) and the sequence alignment in the Supporting Information. The N- and C-terminal peptides as well as the ICL3 were not modeled. All the extracellular loops were refined by Prime Loop Refinement<sup>22</sup> using extended sampling. The SB-742457 ligand was docked to the binding site using Induced Fit Docking (IFD<sup>6,25</sup>). The binding site was defined using the coordinates of the original ergotamine ligand of the template. The best IFDScore complex was visually inspected and was accepted for enrichment study and MD simulation.

**Molecular Dynamics Simulations.** The protein–ligand complexes were immersed into a POPC membrane bilayer<sup>29</sup> where the number of the lipid molecules was 99. For the protein atoms ff99SB<sup>30</sup>, for ligand and lipid molecules GAFF<sup>31</sup> force field parameters were assigned. The system was solvated by water molecules described by the TIP3P<sup>32</sup> potential. JNJ had partial charges published in ref 32; for ETQ, ITD, and SB-742457 the charges were calculated according to the *resp* protocol.<sup>33</sup> For ETQ, ITD, and SB-742457, conformational analysis (gas phase and MMFF94x force field<sup>34</sup>) was performed using the Molecular Operating Environment.<sup>35</sup> During partial charge calculations of the ligands, diverse conformations were selected and subjected to *ab initio* geometry optimizations at the HF/6-31G\* level of theory using the Gaussian 09 software.<sup>36</sup> The molecular electrostatic potential was calculated at the same level of theory, and atom centered charges were calculated by means of the *resp* module of AmberTools1.5.<sup>37</sup> An appropriate number of Na<sup>+</sup> cations and Cl<sup>−</sup> anions (25/34, 34/43, 25/30, and 25/40 for hD3-ETQ, CXCR<sub>4</sub>-ITD, hH<sub>4</sub>-JNJ, and 5HT<sub>6</sub>-SB-742457, respectively) were added in order to neutralize the system and mimic the ionic strength inside the cell. The force field parameters for these ions were taken from Joung and Cheatham.<sup>38,39</sup>

The molecular dynamics simulations were conducted with the NAMD 2.7 software<sup>40</sup> using the following protocol in order to equilibrate the membrane/water environment around the GPCR–ligand complexes:

- (1) minimization (3200 steps) with restrained protein–ligand atoms (force constant was set to 10 kcal/mol Å<sup>2</sup>)
- (2) minimization (3200 steps) without restraints
- (3) heating in *Np<sub>z</sub>γT* ensemble from  $T_i = 10$  K to  $T_f = 310$  K (in 10 steps with  $\Delta T = 30$  K and  $\Delta t = 4$  ps) with restrained protein–ligand atoms (force constant was set to 10 kcal/mol Å<sup>2</sup>)
- (4) 1-ns-long MD simulation in *Np<sub>z</sub>γT* ensemble ( $p_z = 1$  atm,  $\gamma = 60$  dyn/cm,  $T = 310$  K, restrained protein–ligand atoms (10 kcal/mol Å<sup>2</sup>))
- (5) removing of the restraints in 10 steps with 100 ps duration of each, with linear scaling of the force constant from 1.0 to 0.0 (*Np<sub>z</sub>γT* ensemble,  $p_z = 1$  atm,  $\gamma = 60$  dyn/cm, and  $T = 310$  K).

After this equilibration for the hD<sub>3</sub>-ETQ, CXCR<sub>4</sub>-ITD, and SHT<sub>6</sub>-SB-742457 systems, 20-ns-long simulations were conducted, which was followed by five independent (using different initial velocities), 5-ns-long MD simulations in the *Np<sub>z</sub>γT* ensemble ( $p_z = 1$  atm,  $\gamma = 60$  dyn/cm, and  $T = 310$  K). For the hH<sub>4</sub>-JNJ system, distance restraints were applied between the Asp<sup>94</sup>-JNJ and Glu<sup>182</sup>-JNJ parallel with removing the positional restraints (step 5) because without these restraints these interactions were disrupted. Thereafter, 20-ns-long unbiased dynamics were conducted as described previously.

During the calculations, the Noosé–Hoover Langevin piston method<sup>41,42</sup> was used; the cutoff was set to 10 Å, and a 2/2/4 fs multistepping scheme was applied. Long range electrostatic interactions were calculated via the particle mesh Ewald method,<sup>43</sup> and the grid spacing was set to 1 Å.

**Interacting Residues.** In the present study, our goal was to identify the characteristically different binding environments of the ligands of the investigated GPCRs. Therefore, we identified those residues which have considerable interaction with the ligand during the MD simulation. The identification process was as follows. For each trajectory point, we selected those residues whose side-chain occurs in the 5 Å environment of the ligand. Then, the number of occurrences was counted along the MD trajectory for selected residues and summed up providing the cumulative occurrences. The residues were sorted according to their contribution to the cumulative occurrences (the number of occurrences of a residue divided by the cumulative occurrences multiplied by 100, in %). Starting from the top ranked residue, we summed up the contributions until reaching the value of 90%. Those residues were defined as interacting ones for a receptor which contributed to this sum. The advantage of the definition is that residues occurring only a few times in the 5 Å environment of the ligand were omitted.

**Receptor Model Generation for Docking.** For docking calculations, two ensembles of receptor models were generated from the MD trajectories. On one hand, structures were systematically extracted from the trajectory at the end of every nanosecond. On the other hand, receptor conformations were clustered along every individual MD trajectory, and a representative structure (model) was selected for each cluster. The former method provides around 30 models for each GPCR, while in the second case the freely adjustable parameter of the cluster selection was tuned accordingly to obtain approximately the same number of models as in the first case.

**Clustering.** Calculations were carried out with the ptraj program from the AmberTools<sup>37</sup> package. First, the structures were superimposed based on the side-chain heavy atoms of the interacting residues to the initial geometry of the trajectory concerned. Next, the “average linkage” algorithm was applied to generate clusters and representatives in each case. Clustering was based on the mass-weighted RMSD distance matrix of the same atoms as used for superposition. The number of clusters was controlled by using criteria for critical distances ( $\epsilon$ ), which was the same for all trajectories of a certain GPCR.

**Docking.** In the case of the H<sub>4</sub>, D<sub>3</sub>, and SHT<sub>6</sub> targets, the GDD ligand set was used.<sup>19</sup> Since a ligand set for CXCR<sub>4</sub> was not available in GDD, we reproduced the same ligand selection method as described by Cavasotto and Gatica.<sup>19</sup> CXCR<sub>4</sub> actives were retrieved from the Thomson Integrity<sup>44</sup> database, while the ZINC database<sup>45</sup> was used to find decoys. Finally, altogether 30 active and 1170 inactive ligands were collected. These ligands are available from the authors.

Schrödinger Suite 2012 was used for protein and ligand preparation as well as for docking. Receptor structures were prepared by the Protein Preparation Wizard,<sup>26</sup> including Impref minimization. Ligands were prepared by LigPrep.<sup>46</sup> Major tautomer and protomer states were generated by the Epik module at pH 7.4. Grids were centered on the centroid of the interacting residues. The size of the grid box was defined by the maximal ligand size of 25 Å. The dimension of the inner box—where the midpoint of the ligand must be located—was set to 14 Å along the three coordinate axes.

Docking calculations were performed by Glide<sup>47,48</sup> using the single precision (SP) calculation method. The default values were applied for the docking parameters except for the maximum number of minimization steps, which was set to 400. As a brief verification of the docking protocol, the original ligands were redocked into the crystal structure. These dockings provided 0.3 and 0.8 Å RMSD values considering the heavy atoms of the ligands for the D<sub>3</sub> (3PBL) and the CXCR<sub>4</sub> (3ODU) crystal models, respectively.

The performance of virtual screening was assessed by enrichment factor (EF<sub>x</sub>%), ROC, and AUC. The enrichment factor was defined as  $EF_x\% = (n_{actx\%}/n_{allx\%})/(n_{act}/n_{all})$ , where  $n_{actx\%}$  is the number of active ligands in the top  $x\%$ ,  $n_{allx\%}$  is the number of ranked ligands in the top  $x\%$ ,  $n_{act}$  is the number of all actives, and  $n_{all}$  is the total number of ligands. ROC is the plot of actives percentage versus decoys percentage in the ranked list, while AUC is the area under the ROC curve.

## RESULTS AND DISCUSSION

GPCRs adopt multiple conformations ranging from the fully inactive to the active state that has crucial functional relevance from a pharmacological point of view, since partial, full, and inverse agonists or neutral antagonists have different therapeutic effects. Moreover, high affinity compounds of different chemotypes may show similar functional efficacy, suggesting that a functional state can also cover multiple protein conformations in terms of the extracellular binding pocket. The scope of this study is to investigate the potential of using multiple receptor conformations for structure based drug design purposes; therefore receptor conformations selected from MD trajectories were generated. The quality and the potential applicability of receptor conformations had been assessed by retrospective enrichment studies. The key goal was to compare high quality models that represent an optimized ligand–protein conformation (X-ray or comparative model) to

Table 1. Main Features of the Receptor Models Used in Our Study

target	receptor models					
	homology model	X-ray	MD details			
			system (ligand)	total length (ns)	number of frames <i>cluster</i>	number of frames <i>systematic</i>
CXCR <sub>4</sub>	VU-MedChem <sup>51</sup>	3ODU	3ODU (ITD)	20 + 5 × 5 (45)	32	30
D <sub>3</sub>	PompeuFabra <sup>51</sup>	3PBL	3PBL (Eticlopride)	20 + 5 × 5 (45)	30	30
H <sub>4</sub>	this study		homology model (JNJ777120)	20	28	21
SHT6	this study		homology model (SB-742457)	20 + 5 × 5 (45)	28	30

multiple MD frames that exhibit broader conformational variability. Three prototypic targets were investigated: CXCR<sub>4</sub>, D<sub>3</sub>, and H<sub>4</sub>. CXCR<sub>4</sub> is a peptidergic GPCR with a large, open binding site, while D<sub>3</sub> and H<sub>4</sub> are aminergic receptors representing more closed binding pockets. Among them, D<sub>3</sub> and CXCR<sub>4</sub> have small-molecule bound X-ray structures. Both CXCR<sub>4</sub> and D<sub>3</sub> were assessed in the GPCR Dock 2010 competition; therefore the best models of the modeling community are available, and the models are entirely unbiased, since they were built before the structures were disclosed.<sup>51</sup> The third target is the H<sub>4</sub> receptor, with no reported X-ray structure. In this case, a close homologue, the H<sub>1</sub> receptor–ligand complex, is available,<sup>52</sup> which was used as a template to build a comparative model. Explicit-solvent molecular dynamics simulations of the *holo* receptors were carried out using the X-ray structures (CXCR<sub>4</sub> and D<sub>3</sub>) or in the case of H<sub>4</sub>, our homology model on a nanosecond time scale. *Holo* complexes were used instead of *apo* forms to prevent the collapse of the binding pocket and to preserve the steric availability of the interaction pattern of the ligand. Binding-site RMSD-based clustering and systematic sampling were used to generate approximately 30–30 receptor conformations for each target. In the case of MD, single receptor as well as ensemble evaluations were carried out. Protein flexibility was measured in terms of per residue RMSD values compared to the initial structure and presented as Supporting Information.

During the preparation of the manuscript, novel serotonin receptor structures had been published: the human SHT<sub>1B</sub> (4IAR<sup>28</sup>) and SHT<sub>2B</sub> (4IB4<sup>28</sup>). In order to provide further confirmation of our concept, we decided to evaluate an additional aminergic target from the serotonin family based on the most recent structural information. Accordingly, the SHT<sub>6</sub> homology model was built using the SHT<sub>2B</sub> crystal structure (4IB4<sup>28</sup>) as a template (having ~35% sequence identity at TM domains compared to SHT<sub>6</sub>), and the previously described protocol (20 ns equilibration and five independent 5 ns runs, interacting residues selected by their cumulative occurrences) was applied in order to test the performance of the MD-based protein conformational sampling and frame selection protocol. The SB-742457 ligand ( $K_i$  of 0.25 nM at SHT<sub>6</sub>)<sup>53</sup> that is currently in clinical trials was docked to the binding site of the obtained homology model using the Induced Fit Docking method. This initial model was compared to the receptor models yielded by MD simulations by retrospective enrichment study using the GDD SHT<sub>6</sub> ligand set.

It should be noted that quality assessment of the different docking algorithms or the ligand sets is out of the scope of this paper. The Glide docking engine was used that has been evaluated on drug-like and fragment-sized compounds in self- and cross-docking scenarios and provided high quality results.<sup>54–57</sup> Therefore, we focused only on the preparation

of the receptor models, from a methodological aspect. The models are summarized in Table 1.

**The Impact of the Structure Source.** Our primary objective was to survey the source of receptor models. The quality of receptor models had been assessed by retrospective enrichment studies that measure the feasibility of models to select active compounds from decoys. Enrichment factor, receiver operating characteristic (ROC), and area under the ROC curve (AUC) values were calculated. Our aim was to investigate whether the X-ray structure is the paramount representation of the protein conformation and the MD simulation only perturbs the protein framework and reduces its validity, or if we could find a single conformation among the MD ensemble that can outperform the experimental structure. The second objective was to assess the quality of homology models, since most of the pharmaceutically relevant GPCRs have not been crystallized to date. The H<sub>4</sub> target was selected as a real-life scenario, where no X-ray structure is available; thus the MD simulation is based on the homology model. During this specific assessment, the best snapshot (highest enrichment factor EF) was selected from the MD simulations regardless of whether it was found with clustering or systematic sampling. The EF and AUC results are presented in Figure 1 and in the Supporting Information.

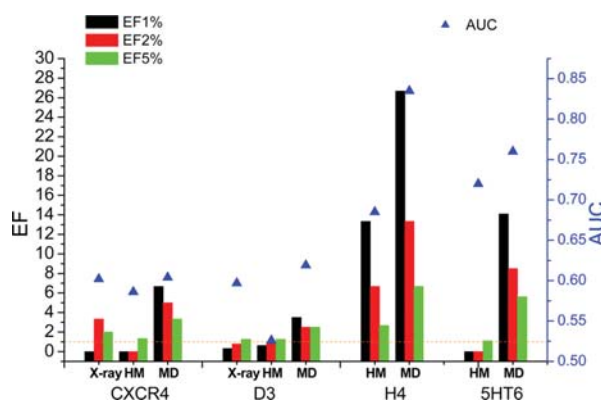


**Figure 1.** Enrichment factors (colored bars) and AUC values (blue triangles) for the CXCR<sub>4</sub>, D<sub>3</sub>, H<sub>4</sub>, and SHT<sub>6</sub> targets obtained with X-ray, homology model (HM), and the best molecular dynamics frame (MD). The orange dotted line represents EF = 1. It should be noted that the y axis starts from EF = -1 in order to enable the representation of EF = 0 bars.

In the case of CXCR<sub>4</sub>, the homology model and the X-ray structure did not result in significant enrichment. The EF1% was equal to zero (the random case produces EF1% = 1); in contrast the best MD snapshot resulted in EF1% = 6.7. Considering the aminergic D<sub>3</sub> receptor, the EF1% of the homology model and the X-ray was 0.63 and 0.32, respectively.

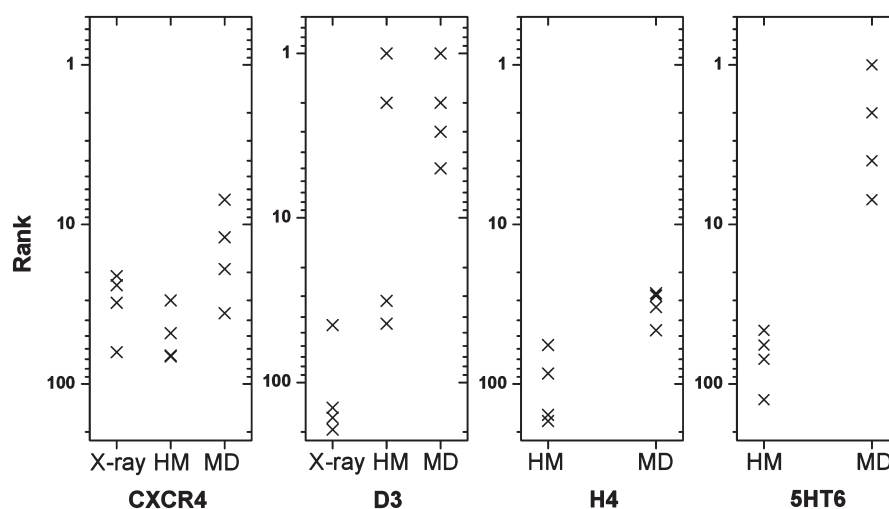


**Figure 2.** The ranks of the top four actives for the CXCR<sub>4</sub>, D<sub>3</sub>, H<sub>4</sub>, and 5HT<sub>6</sub> targets obtained with X-ray, homology model (HM) and the best molecular dynamics frame (MD).

In contrast, the best snapshot from the MD trajectory resulted in EF1% = 3.5. The H<sub>4</sub> homology model and the best MD frame yielded 13.3 and 26.7 EF1% values, respectively. In the case of the 5HT<sub>6</sub> target, the homology model and the best MD frame resulted in zero and 14.1 EF1% values, respectively. The AUC values were found to be 0.72 and 0.76 for the homology model and the best MD frame, respectively. In line with the previous results, the homology model was significantly outperformed by the best MD receptor model. It is interesting to note that the MD-based docking ranked three actives among the top five compounds and five actives among the top 10; thus the performance of the MD-optimized structure was found to be very promising for prospective screening. The results of the enrichment studies of all the MD frames for the four targets and the population of clusters are presented in the Supporting Information

The results of the enrichment studies (depicted in Figure 1) can be summarized by stating that the best single structure form of the MD simulation was superior to the initial model, regardless of the target and the evaluation method (EF or AUC). This observation suggests that during the MD simulations, a “consensus” binding pocket is formed that is able to outperform the homology model or experimentally observed conformation of the protein in terms of enrichment factor. We suggest that during MD simulation of the protein–ligand complex various low-energy protein conformations are sampled, and this ensemble contains such conformations that are not entirely refined around the original ligand, but they correctly represent the interaction pattern of the binding site. Such a protein conformation is not committed to the original ligand and therefore can host and score multiple diverse active chemotypes. This hypothesis is exemplified with the four top-ranked actives in Figure 2. The top ranked active compound in case of the X-ray or homology model structures has approximately the same rank as the MD frame, but the MD frame can host multiple active compounds with similar low ranks unlike X-ray or homology models. Our hypothesis is in line with the theory of the consensus binding site refinement protocol (cIFD) that has been recently published.<sup>58</sup> In the case of the cIFD method, the binding site is refined around multiple active compounds simultaneously by using Locally Enhanced

Sampling (LES) to preform a specific binding pocket that can host diverse actives, without steric clashes. According to our results, similar “multipotent” binding sites can be captured during MD simulation of the ligand–protein complex.

Next, we tested the robustness of the enrichment study to challenge the consensus binding site hypothesis. Because of the large number of MD frames that were included in the enrichment study, chance correlation might have occurred. In rare cases, a good enrichment might be obtained simply due to occasional scoring of some active compounds, but the whole model is not able to accommodate the actives better than inactives on average. In order to carry out statistical evaluation, the original ligand set was divided into small random subsets containing one third of the actives and one third of the decoys, and these subsets were generated 10 times for each target. During this approach, we simulated 10 enrichment studies using reduced ligand sets. However, these sets are not independent from the original; thus we consider these statistical results to be approximate. The enrichment of these small subsets was calculated, and the 10 EF1%, EF2%, EF5%, and AUC values were compared with two sample *t* tests among the homology models, X-ray structures, and best MD models. We found that the difference between homology models and X-ray structures compared to the best MD snapshots was significant ( $p < 0.05$ , MD was superior) for the D<sub>3</sub>, H<sub>4</sub>, and 5HT<sub>6</sub> cases using either EF or AUC values (Supporting Information Table). In the case of CXCR<sub>4</sub>, the difference between the homology model and the MD frame was significant ( $p < 0.05$ ). Comparison of the X-ray structure and the MD frame in the case of CXCR<sub>4</sub> revealed that the difference is not significant for EF1%, EF2%, EF5%, and AUC.

Considering another aspect and assessing the applicability of comparative modeling on GPCRs, our results suggest that in the case of CXCR<sub>4</sub> and D<sub>3</sub>, neither the X-ray nor the state of the art homology model yielded acceptable enrichment. In the cases of H<sub>4</sub> and 5HT<sub>6</sub>, where close X-ray structures were used as a template, significant enrichments were observed. The H<sub>4</sub> and 5HT<sub>6</sub> homology model-based MD simulations resulted in a similar outcome to that of the D<sub>3</sub> and CXCR<sub>4</sub> cases—the MD ensemble comprised a protein model with the utmost EF—that

underlines the usefulness of comparative modeling and subsequent MD simulation on GPCRs.

It should be noted that a characteristic difference was observed between the investigated targets in terms of the overall enrichment: CXCR<sub>4</sub> and D<sub>3</sub> were similar to each other, but H<sub>4</sub> and 5HT<sub>6</sub> were different. X-ray and homology models of CXCR<sub>4</sub> and D<sub>3</sub> resulted in lower enrichments than those of the random sampling (EF1% < 1), while the MD frames were somewhat better. Planesas recently published virtual screening results using Glide with a different ligand set from that of the present study for CXCR<sub>4</sub> and achieved similar results, EF1% = 2.8 and EF5% = 4.6.<sup>59</sup> Cavasotto and Gatica carried out an enrichment study on D<sub>3</sub> using the same ligand set and obtained EF2% = 0.3, which is also similar to our results.<sup>19</sup> Therefore, CXCR<sub>4</sub> and D<sub>3</sub> might be considered as challenging targets from a structure based virtual screening aspect. In contrast, both the homology model and the MD model of H<sub>4</sub> yielded promising EF and AUC values. This finding is in line with the literature data; the H<sub>4</sub> receptor can be considered as a more tractable target yielding promising enrichments.<sup>60,61</sup> 5HT<sub>6</sub> shows a somewhat different picture. Although, the EF value of its homology model is very poor, similarly to CXCR<sub>4</sub> and D<sub>3</sub>, the best MD model performs considerably better.

**Impact of the Binding Site Character.** In order to assess the relationship between the binding site properties and enrichment values, SiteMap<sup>62</sup> descriptors were generated for all the MD frames for CXCR<sub>4</sub>, D<sub>3</sub>, and H<sub>4</sub> targets. In the case of CXCR<sub>4</sub> and D<sub>3</sub>, we did not find significant correlation between the binding site properties and the generally low enrichment factors (Supporting Information Table). In the case of H<sub>4</sub>, the *exposure*, *size*, *contact*, and *philic* properties (definitions are given in the Supporting Information Table) had significant correlation with EF1%, EF2%, and EF5%. The *exposure* that measures how opened the binding site is showed the highest linear correlation (0.53, 0.48, and 0.59 for EF1%, EF2%, and EF5%, respectively). Overall, the SiteMap parameters were not in a strong relationship with the enrichment values, although in the case of H<sub>4</sub> the *exposure* might be indicative. Thorough testing of this relationship is out of the scope of this paper.

**The Impact of the Frame Selection Method.** Next, we compared the two frame selection methods, namely, clustering by the binding site RMSD and the systematic sampling approaches. These collections were compared with two sample *t* tests to assess the general differences (Supporting Information Tables). No statistical difference was observed in the case of CXCR<sub>4</sub> and 5HT<sub>6</sub>. With regard to the D<sub>3</sub> target, the difference was significant for EF1%. In this case, we found the clustering method slightly better, although the EF values are unacceptable (EF1% < 1). Considering EF2% and EF5% values calculated for H<sub>4</sub>, systematic sampling performed better with statistical significance. Comparing only the best structures and using EF1% for evaluation, CXCR<sub>4</sub> enrichment values were identical (both EF1% = 6.7); for D<sub>3</sub>, the clustering outperformed the systematic sampling (EF1% values were 3.5 and 2.5, respectively), and for H<sub>4</sub> and 5HT<sub>6</sub>, the systematic sampling surpassed the clustering (EF1% values were 27.7 and 13.3 for H<sub>4</sub> and 14.1 and 8.4 for 5HT<sub>6</sub>, respectively). Overall, clustering and systematic frame selections showed similar performance. This observation might be due to the fact that the systematic approach covered the most populated clusters, and the best frames were selected from those. The limited internal diversity of the clusters resulted in the centroid selection having a similar

performance to the approximately random selection of the representatives provided by the systematic approach.

**The Impact of MD Ensembles.** Finally, we used the discrete protein conformations collected from MD simulations by systematic and cluster-based sampling to assess their usefulness in ensemble docking. The histogram of enrichment factors achieved at single structure evaluation revealed that for two of the targets, multiple conformations had similar high EF values among the best structures, implicating that the combination of these rankings might be beneficial (Supporting Information Table). Based on literature data, ensemble docking has typically better performance using a few carefully selected protein conformations rather than including each and every structure available.<sup>1,63–65</sup> Therefore, average ranks of the ligands were calculated for all the possible receptor combinations to an ensemble size up to 6. The number of enumerated ensembles is shown in Figure 3.

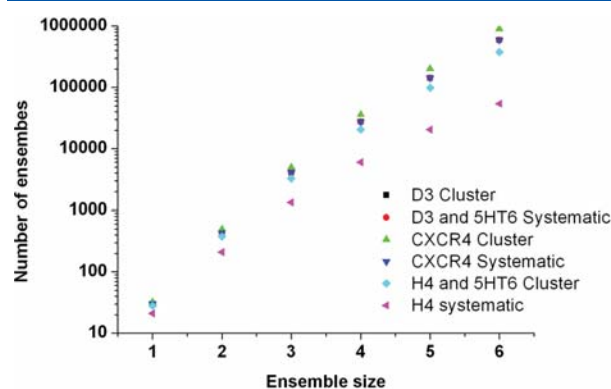


Figure 3. Number of calculated ensembles as a function of the ensemble size.

In the case of CXCR<sub>4</sub>, the EF1% was better for ensemble evaluation compared to single receptor evaluation for cluster-based frame selection, but for the AUC values, no significant improvement was observed (Figure 4). Considering the D<sub>3</sub> and H<sub>4</sub> targets, the single structure enrichments could not be outperformed by ensemble evaluation. EF values obtained for 5HT<sub>6</sub> suggest some limited improvement achieved by rank-average ensemble evaluation. Overall, no serious difference was observed between cluster-based and systematic MD frame selection, similarly to our previous analyses.

In summary, the rank average-based ensemble evaluation did not have an unambiguous positive effect on enrichment; however, in the cases of CXCR<sub>4</sub> and 5HT<sub>6</sub>, positive effects were observed considering the enrichment factor values.

**Application Domain of the Proposed Methodology.** Finally, we discuss the application domain of the MD-based receptor generation method proposed here to be adapted for other systems. The consensus receptor models that resulted in increased enrichment in this study had been captured by membrane-embedded MD simulations of the receptor–ligand complex. Therefore, the accuracy of the initial receptor–ligand complex has a fundamental impact on the outcome, since—in accordance with our hypothesis—during the MD simulations the binding site preserves its ligand interaction pattern; meanwhile it is equilibrated close to the energy minimum. Concurrently, several protein conformations are generated that are less biased toward the original bound ligand but projects its

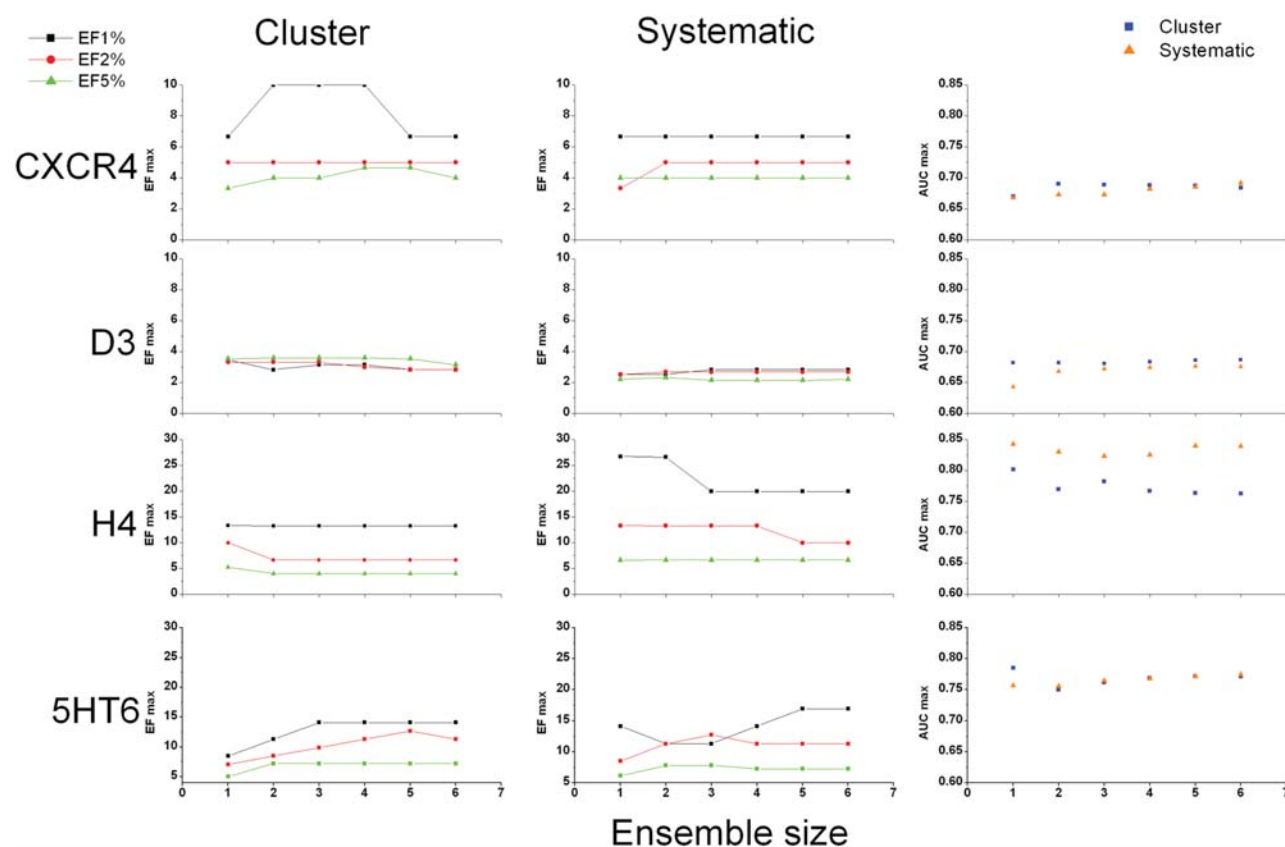


Figure 4. Best enrichment factors (EFs) and AUC values for a given ensemble size for ensemble evaluation based on rank average.

interaction surface properly. We therefore suggest using this methodology on high-quality X-ray structures (holo-form) and on those homology models that have accurately modeled complex conformation.

The GPCR Dock 2010 assessment highlighted that modeling of the D<sub>3</sub> receptor having 41% sequence identity with the transmembrane (TM) domain of the template  $\beta$ 1AR satisfied the accurate modeling criteria (ligand RMSD is 0.96 Å and 58% of the contacts are reproduced).<sup>51</sup> In contrast, the best model of the CXCR<sub>4</sub>-IT1t complex (target-template sequence identity in the TM domain is 25.5%) has a ligand RMSD of 4.88 Å, and only 36% of the contacts could be predicted correctly. In the latter case, the time scale of the MD simulations we applied here cannot ensure that the complexes find their equilibrium conformations (the backbone RMSD for the second extracellular loop of CXCR<sub>4</sub>-IT1t complex was 7.42 Å for the best model). It should be noted that Shaw and co-workers have shown that homology models—in most cases—drift away from the native structure during extra long (100  $\mu$ s) MD simulations.<sup>66</sup> In the present study, these considerations were used selecting the histamine H<sub>4</sub> as a modeling target, since the histamine H<sub>1</sub> receptor satisfied the sequence identity (~40%) for homology modeling.

Self-docking into X-ray structures and systematically built GPCR homology models yielded similar results. Aminergic GPCRs could be successfully modeled, but homology models for peptidergic GPCRs did not result in acceptable binding poses.<sup>67</sup> In addition, peptidergic GPCRs represent a higher level of complexity for structure-based virtual screening, as it is exemplified by hit rates for aminergic homology models

compared to the peptidergic ones.<sup>68</sup> Our experience suggests that experimental data (X-ray or NMR) or high-quality homology models are preferred for sampling protein conformations for virtual screening applications. The protocol, however, is not recommended for more complex homology modeling cases such as peptidergic GPCRs with low quality templates.

The GPCR Dock 2010 assessment also emphasized the utility of biochemical and ligand pharmacophore information for the accomplishment of the best models. Thereby targets without known ligands (orphan receptors), or without biochemical characterization such as site directed mutagenesis, possess difficulties similar to the prediction of the correct holo complex.

In theory, the proposed methodology is not biased toward antagonist ligands and can be adapted for agonist structures as well. Because of the complexity of the functional responses of GPCRs, the level of protein flexibility incorporated in this study does not cover changes related to the activation process. Given the limited understanding of GPCR structure and function relationships to date,<sup>27,69</sup> we assume that structure based virtual screening can recognize ligands with high affinity to the receptor structure that should be validated first in a binding assay *in vitro*.

The MD simulation increases the CPU time (in our case, 4 ns/day simulation time could be achieved on 32 CPUs) resulting in the total 45 ns simulation requiring at least 10 days. According to our methodology, 20–30 receptor structures must be tested in enrichment studies that also consume computational resources. However, the computational costs of

the retrospective enrichment studies for 20–30 test conformations are still acceptable—orders of magnitude lower compared to prospective screening—considering that typically millions of compounds are virtually screened during the prospective campaigns. Although the available computational resources increased significantly during the past decade, and the MD simulations as well as the docking studies are highly parallelized, careful design of simulations still remains a principal requirement. The cost and benefit ratio should be evaluated thoroughly, but according to our study, the changes of EF1% values are encouraging: for the CXCR<sub>4</sub>, D<sub>3</sub>, and H<sub>4</sub> and the additional 5HT<sub>6</sub> cases, the initial model compared to the best, single MD frame resulted in 0 to 6.7, 0.32 to 3.5 (10×), 13.3 to 26.7 (2×), and 0 to 14.1 improvements, respectively. This enhancement can be exploited in prospective virtual screening; therefore docking into one appropriately selected consensus receptor can replace a large number of ensemble calculations. The positive results of the very recent example, 5HT<sub>6</sub>, highlight the applicability of the proposed methodology in a real-life drug discovery scenario: a convincing improvement in virtual screening performance could also be achieved on a target with no experimental structure.

## CONCLUSIONS

The increasing role of structure based virtual screening in hit and lead discovery demands the identification of best practices for the construction of receptor models. Accordingly, the main objective of this study was to assess the potential of single structure models and the ranking based ensemble validation to guide the selection of receptor conformations for virtual hit finding. Explicit solvent membrane dynamics simulations of four protein–ligand complexes from the GPCR family (CXCR<sub>4</sub>, D<sub>3</sub>, H<sub>4</sub>, and 5HT<sub>6</sub>) were carried out to generate discrete protein conformations representing the intrinsic flexibility of the binding site. RMSD-based clustering and systematic frame selection were utilized to obtain representative conformations, and these structures were compared to X-ray structures and homology models.

According to the enrichment studies, the best single snapshots from the MD trajectory considerably outperformed the X-ray as well as the homology models. Regarding the frame selection methods, similar performance was observed. We conclude that both methods produced improved enrichments compared to the X-ray and homology model, while the ranking-based ensemble evaluation could not further increase the performance. The H<sub>4</sub> and 5HT<sub>6</sub> cases highlighted the usefulness of homology models for MD-based receptor conformer generation, although the proposed methodology requires high quality initial protein–ligand complexes. It should also be noted that the ensemble evaluation could not outperform the best single structure at least for our selection of targets, indicating that screening on a selected single structure has an advantage over ensemble docking regarding the costs and benefits. Our results suggest that the MD simulations induce protein conformational movements that do not disrupt the accessibility of the key interacting residues. However, the formation of such binding sites that are no longer biased for the original ligand could be captured. These consensus binding pockets can host multiple diverse active ligands that accomplish the original pharmacophore pattern. On the bases of this observation, we encourage the use of MD simulation to explore the conformational space of the initial GPCR–ligand complex to create an ensemble of possible

models and test their performance to find the best model for prospective screening.

## ASSOCIATED CONTENT

### Supporting Information

Sequence alignments, per residue RMSD values, full data of enrichment factors, AUC values, details of SiteMap descriptors, and ligand Tanimoto values. This material is available free of charge via the Internet at <http://pubs.acs.org>.

## AUTHOR INFORMATION

### Corresponding Author

\*Phone: +361-438-1155. Fax: +361-438-1143. E-mail: [gy.keseru@ttk.mta.hu](mailto:gy.keseru@ttk.mta.hu).

### Present Addresses

<sup>||</sup>Department of Theoretical Chemistry, VU University Amsterdam, De Boelelaan 1083, NL-1081 HV Amsterdam, The Netherlands

<sup>⊥</sup>Research Centre for Natural Sciences, Hungarian Academy of Sciences, 59-67 Pusztaszeri út, H-1025 Budapest, Hungary

### Funding

### Notes

The authors declare no competing financial interest.

## ACKNOWLEDGMENTS

This work was supported by COST Action CM1207, TÁMOP-4.2.2.C-11/1/KONV-2012-0010, and TÁMOP-4.2.2.A-11/1/KONV-2012-0047 grants.

## ABBREVIATIONS

5HT<sub>6</sub>, serotonin receptor type 6; AUC, area under the curve; CXCR<sub>4</sub>, chemokine receptor type 4; D<sub>3</sub>, dopamine receptor type 3; EF, enrichment factor; GPCR, G-protein coupled receptor; H<sub>4</sub>, histamine receptor type 4; MD, molecular dynamics; ROC, receiver operator characteristic

## REFERENCES

- (1) Totrov, M.; Abagyan, R. Flexible ligand docking to multiple receptor conformations: a practical alternative. *Curr. Opin. Struct. Biol.* **2008**, *18*, 178–184.
- (2) B-Rao, C.; Subramanian, J.; Sharma, S. D. Managing protein flexibility in docking and its applications. *Drug Discovery Today* **2009**, *14*, 394–400.
- (3) Cozzini, P.; Kellogg, G. E.; Spyrakakis, F.; Abraham, D. J.; Costantino, G.; Emerson, A.; Fanelli, F.; Gohlke, H.; Kuhn, L. A.; Morris, G. M.; Orozco, M.; Pertinhez, T. A.; Rizzi, M.; Sotriiffer, C. A. Target flexibility: an emerging consideration in drug discovery and design. *J. Med. Chem.* **2008**, *51*, 6237–6255.
- (4) Changeux, J. P.; Edelstein, S. Conformational selection or induced fit? 50 years of debate resolved. *F1000 Biol. Rep.* **2011**, *3*, 19.
- (5) Teague, S. J. Implications of protein flexibility for drug discovery. *Nat. Rev. Drug Discovery* **2003**, *2*, 527–541.
- (6) Sherman, W.; Day, T.; Jacobson, M. P.; Friesner, R. A.; Farid, R. Novel Procedure for Modeling Ligand/Receptor Induced Fit Effects. *J. Med. Chem.* **2006**, *49*, 534–553.
- (7) Cavasotto, C. N.; Abagyan, R. A. Protein flexibility in ligand docking and virtual screening to protein kinases. *J. Mol. Biol.* **2004**, *337*, 209–225.
- (8) Bottegoni, G.; Rocchia, W.; Rueda, M.; Abagyan, R.; Cavalli, A. Systematic exploitation of multiple receptor conformations for virtual ligand screening. *PLoS One* **2011**, *6*, e18845.
- (9) Korb, O.; McCabe, P.; Cole, J. The ensemble performance index: an improved measure for assessing ensemble pose prediction performance. *J. Chem. Inf. Model.* **2011**, *51*, 2915–2919.

- (10) Wada, M.; Kanamori, E.; Nakamura, H.; Fukunishi, Y. Selection of in silico drug screening results for G-protein-coupled receptors by using universal active probes. *J. Chem. Inf. Model.* **2011**, *51*, 2398–2407.
- (11) Osguthorpe, D. J.; Sherman, W.; Hagler, A. T. Exploring protein flexibility: incorporating structural ensembles from crystal structures and simulation into virtual screening protocols. *J. Phys. Chem. B* **2012**, *116*, 6952–6959.
- (12) Cavasotto, C. N.; Kovacs, J. A.; Abagyan, R. A. Representing receptor flexibility in ligand docking through relevant normal modes. *J. Am. Chem. Soc.* **2005**, *127*, 9632–9640.
- (13) Rueda, M.; Bottegoni, G.; Abagyan, R. Consistent improvement of cross-docking results using binding site ensembles generated with elastic network normal modes. *J. Chem. Inf. Model.* **2009**, *49*, 716–725.
- (14) Shan, Y.; Kim, E. T.; Eastwood, M. P.; Dror, R. O.; Seeliger, M. A.; Shaw, D. E. How does a drug molecule find its target binding site? *J. Am. Chem. Soc.* **2011**, *133*, 9181–9183.
- (15) Dror, R. O.; Pan, A. C.; Arlow, D. H.; Borhani, D. W.; Maragakis, P.; Shan, Y.; Xu, H.; Shaw, D. E. Pathway and mechanism of drug binding to G-protein-coupled receptors. *Proc. Natl. Acad. Sci. U. S. A.* **2011**, *108*, 13118–13123.
- (16) Dror, R. O.; Arlow, D. H.; Maragakis, P.; Mildorf, T. J.; Pan, A. C.; Xu, H.; Borhani, D. W.; Shaw, D. E. Activation mechanism of the  $\beta_2$ -adrenergic receptor. *Proc. Natl. Acad. Sci. U. S. A.* **2011**, *108*, 18684–18689.
- (17) Isberg, V.; Balle, T.; Sander, T.; Jørgensen, F. S.; Gloriam, D. E. G protein- and agonist-bound serotonin 5-HT<sub>2A</sub> receptor model activated by steered molecular dynamics simulations. *J. Chem. Inf. Model.* **2011**, *51*, 315–25.
- (18) de Graaf, C.; Rein, C.; Piwnica, D.; Giordanetto, F.; Rognan, D. Structure-based discovery of allosteric modulators of two related class B G-protein-coupled receptors. *ChemMedChem.* **2011**, *6*, 2159–69.
- (19) Gatica, E. A.; Cavasotto, C. N. Ligand and decoy sets for docking to G protein-coupled receptors. *J. Chem. Inf. Model.* **2012**, *52*, 1–6.
- (20) Chien, E. Y.; Liu, W.; Zhao, Q.; Katritch, V.; Han, G. W.; Hanson, M. A.; Shi, L.; Newman, A. H.; Javitch, J. A.; Cherezov, V.; Stevens, R. C. Structure of the human dopamine D<sub>3</sub> receptor in complex with a D<sub>2</sub>/D<sub>3</sub> selective antagonist. *Science* **2010**, *330*, 1091–1095.
- (21) Wu, B.; Chien, E. Y.; Mol, C. D.; Fenalti, G.; Liu, W.; Katritch, V.; Abagyan, R.; Brooun, A.; Wells, P.; Bi, F. C.; Hamel, D. J.; Kuhn, P.; Handel, T. M.; Cherezov, V.; Stevens, R. C. Structures of the CXCR4 chemokine GPCR with small-molecule and cyclic peptide antagonists. *Science* **2010**, *330*, 1066–1071.
- (22) *Prime*, version 3.0; Schrödinger, LLC: New York, 2011.
- (23) Lim, H. D.; de Graaf, C.; Jiang, W.; Sadek, P.; McGovern, P. M.; Istyastono, E. P.; Bakker, R. A.; de Esch, I. J.; Thurmond, R. L.; Leurs, R. Molecular determinants of ligand binding to H<sub>4</sub>R species variants. *Mol. Pharmacol.* **2010**, *77*, 734–743.
- (24) *MacroModel*, version 9.9; Schrödinger, LLC: New York, 2011.
- (25) Sherman, W.; Beard, H. S.; Farid, R. Use of an Induced Fit Receptor Structure in Virtual Screening. *Chem. Biol. Drug Des.* **2006**, *67*, 83.
- (26) *Schrödinger Suite 2011*, Epik version 2.2; Schrödinger, LLC: New York, 2011; Impact version 5.7; Schrödinger, LLC: New York, 2011; Prime version 2.3; Schrödinger, LLC: New York, 2011.
- (27) Jójárt, B.; Martinek, T. A. Performance of the General Amber Force Field in Modeling Aqueous POPC Membrane Bilayers. *J. Comput. Chem.* **2007**, *28*, 2051–2058.
- (28) Wang, C.; Jiang, Y.; Ma, J.; Wu, H.; Wacker, D.; Katritch, V.; Han, G. W.; Liu, W.; Huang, X. P.; Vardy, E.; McCorvy, J. D.; Gao, X.; Zhou, X. E.; Melcher, K.; Zhang, C.; Bai, F.; Yang, H.; Yang, L.; Jiang, H.; Roth, B. L.; Cherezov, V.; Stevens, R. C.; Xu, H. E. Structural basis for molecular recognition at serotonin receptors. *Science* **2013**, *340*, 610–619.
- (29) Hornak, V.; Abel, R.; Okur, A.; Strockbine, B.; Roitberg, A.; Simmerling, C. Comparison of multiple Amber force fields and development of improved. *Proteins* **2006**, *65*, 712–725.
- (30) Wang, J.; Wolf, R. M.; Caldwell, J. W.; Kollman, P. A.; Case, D. A. Development and testing of a general Amber force field. *J. Comput. Chem.* **2004**, *25*, 1157–1174.
- (31) Jørgensen, W. L.; Chandrasekhar, J.; Madura, J. D.; Impey, R. W.; Klein, M. L. Comparison of simple potential functions for simulating liquid water. *J. Chem. Phys.* **1983**, *79*, 926–935.
- (32) Jójárt, B.; Kiss, R.; Viskolcz, B.; Keserű, G. M. Theoretical Investigation of the Activation Mechanism of the Human Histamine H<sub>4</sub> Receptor – An Explicit Membrane Molecular Dynamics Simulation Study. *J. Chem. Inf. Model.* **2008**, *48*, 1199–1210.
- (33) Bayly, C. I.; Cieplak, P.; Cornell, W. D.; Kollman, P. A. A well behaved electrostatic potential based method using charge restraints for deriving atomic charges: the RESP model. *J. Phys. Chem.* **1993**, *102*, 3787–3793.
- (34) Halgren, T. A. Merck molecular force field. I. Basis, form, scope, parameterization, and performance of MMFF94. *J. Comput. Chem.* **1996**, *17*, 490–519.
- (35) *Molecular Operating Environment (MOE)*, 2010.09; Chemical Computing Group, Inc.: Montreal, Quebec, Canada, 2005.
- (36) Frisch, M. J.; Trucks, G. W.; Schlegel, H. B.; Scuseria, G. E.; Robb, M. A.; Cheeseman, J. R.; Scalmani, G.; Barone, V.; Mennucci, B.; Petersson, G. A.; Nakatsuji, H.; Caricato, M.; Li, X.; Hratchian, H. P.; Izmaylov, A. F.; Bloino, J.; Zheng, G.; Sonnenberg, J. L.; Hada, M.; Ehara, M.; Toyota, K.; Fukuda, R.; Hasegawa, J.; Ishida, M.; Nakajima, T.; Honda, Y.; Kitao, O.; Nakai, H.; Vreven, T.; Montgomery, J. A., Jr.; Peralta, J. E.; Ogliaro, F.; Bearpark, M.; Heyd, J. J.; Brothers, E.; Kudin, K. N.; Staroverov, V. N.; Kobayashi, R.; Normand, J.; Raghavachari, K.; Rendell, A.; Burant, J. C.; Iyengar, S. S.; Tomasi, J.; Cossi, M.; Rega, N.; Millam, J. M.; Klene, M.; Knox, J. E.; Cross, J. B.; Bakken, V.; Adamo, C.; Jaramillo, J.; Gomperts, R.; Stratmann, R. E.; Yazyev, O.; Austin, A. J.; Cammi, R.; Pomelli, C.; Ochterski, J. W.; Martin, R. L.; Morokuma, K.; Zakrzewski, V. G.; Voth, G. A.; Salvador, P.; Dannenberg, J. J.; Dapprich, S.; Daniels, A. D.; Farkas, Ö.; Foresman, J. B.; Ortiz, J. V.; Cioslowski, J.; Fox, D. J. *Gaussian 09*, revision A1; Gaussian, Inc.: Wallingford CT, 2009.
- (37) Case, D. A.; Cheatham, T. E.; Darden, T., III; Gohlke, H.; Luo, R.; Merz, K. M.; Onufriev, A., Jr.; Simmerling, C.; Wang, B.; Woods, R. The Amber biomolecular simulation programs. *J. Comput. Chem.* **2005**, *26*, 1668–1688.3.
- (38) Joung, S.; Cheatham, T. E. Determination of alkali and halide monovalent ion parameters for use in explicitly solvated biomolecular simulations. *J. Phys. Chem. B* **2008**, *112*, 9020–9041.
- (39) Joung, I. S.; Cheatham, T. E. Molecular dynamics simulations of the dynamic and energetic properties of alkali and halide ions using water-model-specific ion parameters. *J. Phys. Chem. B* **2009**, *113*, 13279–13290.
- (40) Phillips, J. C.; Braun, R.; Wang, W.; Gumbart, J.; Tajkhorshid, E.; Villa, E.; Chipot, C.; Skeel, R. D.; Kale, L.; Schulten, K. Scalable molecular dynamics with NAMD. *J. Comput. Chem.* **2005**, *26*, 1781–1802.
- (41) Martyna, G. J.; Tobias, D. J.; Klein, M. L. Constant pressure molecular dynamics algorithms. *J. Chem. Phys.* **1994**, *101*, 4177–4189.
- (42) Feller, S. E.; Zhang, Y.; Pastor, R. W.; Brooks, B. R. Constant pressure molecular dynamics simulation: The Langevin piston method. *J. Chem. Phys.* **1995**, *103*, 4613–4621.
- (43) Darden, T.; York, D.; Pedersen, L. Particle mesh Ewald: An Nlog(N) method for Ewald sums in large systems. *J. Chem. Phys.* **1993**, *98*, 10089.
- (44) Thomson Integrity database. <http://integrity.thomson-pharma.com/integrity/xmlxsl/> (accessed 2011).
- (45) Zinc database. <http://zinc.docking.org/> (accessed, 2011).
- (46) *LigPrep*, version 2.5; Schrödinger, LLC: New York, 2011.
- (47) *Glide*, version 5.8; Schrödinger, LLC: New York, 2012.
- (48) Friesner, R. A.; Banks, J. L.; Murphy, R. B.; Halgren, T. A.; Klicic, J. J.; Mainz, D. T.; Repasky, M. P.; Knoll, E. H.; Shaw, D. E.; Shelley, M.; Perry, J. K.; Francis, P.; Shenkin, P. S. Glide: A New Approach for Rapid, Accurate Docking and Scoring. 1. Method and Assessment of Docking Accuracy. *J. Med. Chem.* **2004**, *47*, 1739–1749.

- (49) Halgren, T. A.; Murphy, R. B.; Friesner, R. A.; Beard, H. S.; Frye, L. L.; Pollard, W. T.; Banks, J. L. Glide: A New Approach for Rapid, Accurate Docking and Scoring. 2. Enrichment Factors in Database Screening. *J. Med. Chem.* **2004**, *47*, 1750–1759.
- (50) Friesner, R. A.; Murphy, R. B.; Repasky, M. P.; Frye, L. L.; Greenwood, J. R.; Halgren, T. A.; Sanschagrin, P. C.; Mainz, D. T. Extra Precision Glide: Docking and Scoring Incorporating a Model of Hydrophobic Enclosure for Protein-Ligand Complexes. *J. Med. Chem.* **2006**, *49*, 6177–6196.
- (51) Kufareva, I.; Rueda, M.; Katritch, V.; Stevens, R. C.; Abagyan, R. GPCR Dock 2010 participants Status of GPCR modeling and docking as reflected by community-wide GPCR Dock 2010 assessment. *Structure* **2011**, *19*, 1108–1126.
- (52) Shimamura, T.; Shiroishi, M.; Weyand, S.; Tsujimoto, H.; Winter, G.; Katritch, V.; Abagyan, R.; Cherezov, V.; Liu, W.; Han, G. W.; Kobayashi, T.; Stevens, R. C.; Iwata, S. Structure of the human histamine H1 receptor complex with doxepin. *Nature* **2011**, *475*, 65–70.
- (53) Upton, N.; Chuang, T. T.; Hunter, A. J.; Virley, D. J. 5-HT<sub>6</sub> receptor antagonists as novel cognitive enhancing agents for Alzheimer's disease. *Neurotherapeutics*. **2008**, *5*, 458–69.
- (54) Sándor, M.; Kiss, R.; Keserű, G. M. Virtual fragment docking by Glide: a validation study on 190 protein-fragment complexes. *J. Chem. Inf. Model.* **2010**, *50*, 1165–72.
- (55) McGann, M. FRED pose prediction and virtual screening accuracy. *J. Chem. Inf. Model.* **2011**, *51*, 578–96.
- (56) Cross, J. B.; Thompson, D. C.; Rai, B. K.; Baber, J. C.; Fan, K. Y.; Hu, Y.; Humblet, C. Comparison of several molecular docking programs: pose prediction and virtual screening accuracy. *J. Chem. Inf. Model.* **2009**, *49*, 1455–1474.
- (57) Repasky, M. P.; Murphy, R. B.; Banks, J. L.; Greenwood, J. R.; Tubert-Brohman, I.; Bhat, S.; Friesner, R. A. Docking performance of the glide program as evaluated on the Astex and DUD datasets: a complete set of glide SP results and selected results for a new scoring function integrating WaterMap and glide. *J. Comput.-Aided Mol. Des.* **2012**, *26*, 787–799.
- (58) Kalid, O.; Toledo Warshaviak, D.; Shechter, S.; Sherman, W.; Shacham, S. Consensus Induced Fit Docking (ciFD): methodology, validation, and application to the discovery of novel Crm1 inhibitors. *J. Comput.-Aided Mol. Des.* **2012**, *26*, 1217–1228.
- (59) Planesas, J. M.; Pérez-Nuño, V. I.; Borrell, J. I.; Teixidó, J. Impact of the CXCR4 structure on docking-based virtual screening of HIV entry inhibitors. *J. Mol. Graphics Model.* **2012**, *38*, 123–36.
- (60) Kiss, R.; Noszál, B.; Rácz, A.; Falus, A.; Eros, D.; Keserű, G. M. Binding mode analysis and enrichment studies on homology models of the human histamine H4 receptor. *Eur. J. Med. Chem.* **2008**, *43*, 1059–1070.
- (61) Kiss, R.; Kiss, B.; Könczöl, A.; Szalai, F.; Jelinek, I.; László, V.; Noszál, B.; Falus, A.; Keserű, G. M. Discovery of novel human histamine H4 receptor ligands by large-scale structure-based virtual screening. *J. Med. Chem.* **2008**, *51*, 3145–3153.
- (62) *SiteMap*, version 2.5; Schrödinger, LLC: New York, 2011.
- (63) Rueda, M.; Bottegoni, G.; Abagyan, R. Recipes for the selection of experimental protein conformations for virtual screening. *J. Chem. Inf. Model.* **2010**, *50*, 186–193.
- (64) Korb, O.; Olsson, T. S.; Bowden, S. J.; Hall, R. J.; Verdonk, M. L.; Liebeschuetz, J. W.; Cole, J. C. Potential and limitations of ensemble docking. *J. Chem. Inf. Model.* **2012**, *52*, 1262–1274.
- (65) Xu, M.; Lill, M. A. Utilizing experimental data for reducing ensemble size in flexible-protein docking. *J. Chem. Inf. Model.* **2012**, *52*, 187–198.
- (66) Raval, A.; Piana, S.; Eastwood, M. P.; Dror, R. O.; Shaw, D. E. Refinement of protein structure homology models via long, all-atom molecular dynamics simulations. *Proteins* **2012**, *80*, 2071–9.
- (67) Beuming, T.; Sherman, W. Current assessment of docking into GPCR crystal structures and homology models: successes, challenges, and guidelines. *J. Chem. Inf. Model.* **2012**, *52*, 3263–3277.
- (68) de Graaf, C.; Kooistra, A. J.; Vischer, H. F.; Katritch, V.; Kuijter, M.; Shiroishi, M.; Iwata, S.; Shimamura, T.; Stevens, R. C.; de Esch, I. J.; Leurs, R. Crystal structure-based virtual screening for fragment-like ligands of the human histamine H(1) receptor. *J. Med. Chem.* **2011**, *54*, 8195–206.
- (69) Wacker, D.; Wang, C.; Katritch, V.; Han, G. W.; Huang, X. P.; Vardy, E.; McCorvy, J. D.; Jiang, Y.; Chu, M.; Siu, F. Y.; Liu, W.; Xu, H. E.; Cherezov, V.; Roth, B. L.; Stevens, R. C. Structural features for functional selectivity at serotonin receptors. *Science* **2013**, *340*, 615–619.



Contents lists available at ScienceDirect

## European Journal of Medicinal Chemistry

journal homepage: <http://www.elsevier.com/locate/ejmech>

Original article

## Virtual fragment screening on GPCRs: A case study on dopamine D3 and histamine H4 receptors

Márton Vass<sup>a</sup>, Éva Schmidt<sup>a</sup>, Ferenc Horti<sup>a</sup>, György M. Keserű<sup>b,\*</sup><sup>a</sup> Gedeon Richter Plc, H-1475, P.O.B. 27, Budapest, Hungary<sup>b</sup> Research Centre for Natural Sciences of the Hungarian Academy of Sciences, H-1525, P.O.B. 17, Budapest, Hungary

## ARTICLE INFO

## Article history:

Received 9 October 2013  
 Received in revised form  
 11 February 2014  
 Accepted 13 February 2014  
 Available online 15 February 2014

## Keywords:

Fragment screening  
 Fragment docking  
 Virtual screening  
 Ensemble docking  
 G protein-coupled receptors  
 Dopamine D3 receptor  
 Histamine H4 receptor

## ABSTRACT

Prospective structure based virtual fragment screening methodologies on two GPCR targets namely the dopamine D3 and the histamine H4 receptors with a library of 12,905 fragments were evaluated. Fragments were docked to the X-ray structure and the homology model of the D3 and H4 receptors, respectively. Representative receptor conformations for ensemble docking were obtained from molecular dynamics trajectories. *In vitro* confirmed hit rates ranged from 16% to 32%. Hits had high ligand efficiency (LE) values in the range of 0.31–0.74 and also acceptable lipophilic efficiency. The X-ray structure, the homology model and structural ensembles were all found suitable for docking based virtual screening of fragments against these GPCRs. However, there was little overlap among different hit sets and methodologies were thus complementary to each other.

© 2014 Elsevier Masson SAS. All rights reserved.

## 1. Introduction

Fragment-based lead discovery (FBLD) has become a feasible alternative to traditional lead finding approaches in drug discovery employed both by industry and academic groups [1]. It has been demonstrated that starting from polar, low molecular weight – typically <250 Da or less than 20 heavy atoms – compounds, leads and drugs with better physico-chemical properties can be achieved [2] even for difficult targets [3]. This view is supported by the increasing number of drug candidates recently entering clinical trials and one already approved drug originating from a fragment hit [4]. Since weakly binding fragments require sensitive, but typically lower throughput biophysical detection methodologies (such as SPR, NMR, XRD, MS), and also because fragments are usually optimized using structural information, there is an ongoing interest in computational methodologies capable of predicting fragment

binding and providing reliable binding modes for them. Molecular docking is an *in silico* tool aiming to predict the binding mode and binding free energy of druglike molecules. It has been shown that various docking programs have similar performance in pose prediction for fragments (especially for fragments of high ligand efficiency) and druglike molecules [5–7], since fragments usually exploit the specific interactions available at protein hot spots [8]. In virtual screening setups, where the objective is the ranking of fragments by binding free energy, the modest enrichment of actives [9,10] shall be improved using more accurate binding free energy functions. One of these methods is the computationally intensive MM-PBSA rescoring method that was used to improve enrichments [11,12]. It has also been suggested that incorporating receptor flexibility in docking (not only in the rescoring phase) might be beneficial for virtual screening enrichments. Various protocols have been published taking into account different ranges of protein flexibility [13]. The simplest approach is the use soft potentials to account for small side-chain movements. Larger movements might be considered using side chain rotamer libraries. Docking into appropriately selected multiple protein conformations (ensemble docking) is a parallelizable and resource effective way of handling the flexibility of the entire protein. The most computationally intensive methods attempt the simultaneous conformational sampling of the receptor and the ligand, such as Schrödinger's Induced

**Abbreviations:** GPCR, G protein-coupled receptor; FBLD, fragment-based lead discovery; LE, ligand efficiency; LELP, ligand-efficiency-dependent lipophilicity; MD, molecular dynamics; IFD, induced fit docking; POPC, 1-palmitoyl-2-oleoylphosphatidylcholine; RMSD, root-mean-square deviation; SP, single precision.

\* Corresponding author.

E-mail addresses: [keseru.gyorgy@ttk.mta.hu](mailto:keseru.gyorgy@ttk.mta.hu), [gy.keseru@ttk.mta.hu](mailto:gy.keseru@ttk.mta.hu) (G. M. Keserű).

<http://dx.doi.org/10.1016/j.ejmech.2014.02.034>

0223-5234/© 2014 Elsevier Masson SAS. All rights reserved.

Fit Docking (IFD) [14] application, or running molecular dynamics (MD) simulation on each individual protein-fragment complex. Different receptor conformations for ensemble docking can be obtained from multiple crystal structures or NMR structures if such data is available. However, structural studies on membrane proteins, such as G protein-coupled receptors (GPCRs) typically represent great challenges. Despite recent progress in GPCR crystallization still only a small percentage of structures have been unveiled. In such a case homology modeling may be used to obtain an atomistic model of the receptor. Structurally diverse receptor models can be obtained using different GPCR template structures during homology modeling. Diverse conformations may also be sampled by MD simulation, Monte Carlo or low-mode conformational search starting from a single homology model [15,16]. De Graaf et al. used a homology model of the histamine H3 receptor and subsequent MD sampling to provide the conformations used for retrospective and prospective virtual fragment screening [17]. In the present study we performed prospective virtual fragment screening on the available dopamine D3 receptor crystal structure and a homology model of the histamine H4 receptor based on the recently solved histamine H1 receptor crystal structure. Snapshots from all-atom membrane-embedded MD simulations were also used for ensemble virtual screening of the same fragment library. Screening performance of the different protocols was compared analyzing hit rates and hit compounds obtained by docking to the single structure and the conformational ensembles.

## 2. Computational methods

### 2.1. Homology modeling and crystal structure preparation

The construction of the histamine H4 receptor homology model was described previously [18]. Briefly, the H4 amino acid sequence from the UniProt server (<http://www.uniprot.org/>) was aligned to the sequence of the template, the 3.1 Å resolution X-ray structure of the human histamine H1 receptor (PDB code: 3RZE) using Prime 3.0 [19]. The kink in helix TM4 was modeled based on the human  $\beta$ -adrenergic receptor (PDB code: 2RH1). The JNJ7777120 ligand was first manually docked into the receptor, and then the 5 Å environment of the ligand was subjected to minimization with two H-bond constraints using MacroModel 9.9 [20]. JNJ7777120 was redocked into the minimized structure using IFD [14,21] in the Schrödinger Suite 2011. Finally the whole structure was subjected to Impref restrained minimization in the Protein Preparation Wizard [22]. Chain A of the dopamine D3 crystal structure (PDB code: 3PBL) was subjected to the Protein Preparation Wizard workflow with default settings, that included assigning bond orders, adding hydrogens, creating disulfide bonds, optimization of the H-bond network and finally a restrained minimization of the complex.

### 2.2. Molecular dynamics simulations and ensemble preparation

The details of molecular dynamics simulations were described elsewhere [18]. Briefly, all-atom POPC membrane-embedded MD simulations were run starting from the homology model of the histamine H4 receptor JNJ7777120 complex and the crystal structure of the dopamine D3 receptor eticlopride complex using ff99SB force field for protein and GAFF force field for lipid and ligand atoms in the NAMD 2.7 [23] software. The systems were equilibrated with subsequent steps of i) 3200 steps minimization with restrained protein and ligand atoms ii) 3200 steps unrestrained minimization iii) heating in NVT ensemble to 310 K in 40 ps with restrained protein and ligand atoms iv) 1 ns MD simulation in Np<sub>z</sub>γT ensemble with restrained protein and ligand atoms v) 1 ns MD simulation in

Np<sub>z</sub>γT ensemble with gradual removal of the restraints. 20 ns production runs in Np<sub>z</sub>γT ensemble were conducted for both systems. Receptor conformations of the two trajectories were clustered using the average linkage method in the ptraj program from the AmberTools package [24] based on the RMSD of the amino acid residues that made up 90% cumulative occurrence in the 5 Å environment of the ligand. This method provided 28 representative conformations for the histamine H4 receptor and 27 representative conformations for the dopamine D3 receptor. All representatives were subjected to Impref restrained minimization in the Protein Preparation Wizard.

### 2.3. Single structure and ensemble docking methodologies

We collected 12,905 fragment-like compounds from our in-house collection complying with an extended version of the Rule of Three: having an MW ≤ 300 Da, logP ≤ 3, number of H-bond donors and acceptors ≤ 3, number of rotatable bonds ≤ 6, PSA < 130 Å<sup>2</sup>, containing 1–3 rings and no reactive functionalities (see [Property distributions and diversity assessment in the Supporting Information](#)). The structures of these fragments were prepared using LigPrep 2.5 [25]. The dominant protonation and tautomeric state at pH 7.4 was calculated using Epik 2.2 [26]. Their logP was calculated using the ChemAxon cxcalc utility [27]. In the single structure investigation the 12,905 fragments were docked into the binding site of the dopamine D3 X-ray structure and the histamine H4 homology model. Then in the ensemble docking approach the fragment set was docked into the binding sites of all representatives from the D3 and H4 MD trajectories. Glide 5.7 [28–31] software was used for docking. Grids for the initial homology model and crystal structure, as well as for the representatives from the MD trajectories were centered on the ligand centroids, and had dimensions of 14 × 14 × 14 Å for the inner box (which contains the ligand centroid during docking) and 44 × 44 × 44 Å for the outer box (which contains all ligand atoms during docking) to ensure that sampling of the binding mode was not biased by the grid size. Docking calculations were conducted using the single precision (SP) mode [5], with post-dock minimization performed for 15 poses. Only the top pose for each fragment by the Emodel scoring function was saved, which were ranked by the GlideScore scoring function for each individual receptor conformation. For single structure docking to the D3 X-ray structure and the H4 homology model, the top 50 compounds from the GlideScore ranked list were chosen for biological testing. In the ensemble docking approach mean ranks and their standard deviations calculated over the ensemble were used for evaluating each individual compound. Compounds having a mean rank lower than 500 were selected for biological testing. This cutoff gave a similar number of compounds to be tested as for the single structure case: 56 for the dopamine D3 receptor and 50 for the histamine H4 receptor.

## 3. Results and discussion

### 3.1. Receptor binding sites

While the histamine H1 and H4 receptors share 40% amino acid identity in the transmembrane region and they recognize the same endogenous ligand, there are substantial differences in their binding sites. For example Asn147<sup>4.57</sup> in H4 is equivalent to Trp158<sup>4.56</sup> in H1, Leu175<sup>5.39</sup> to Lys191<sup>5.39</sup>, Glu182<sup>5.46</sup> to Asn198<sup>5.46</sup> and Gln347<sup>7.42</sup> to Gly457<sup>7.42</sup>. Also, mutation of Asn147<sup>4.57</sup> and Glu182<sup>5.46</sup> showed significant alteration to JNJ7777120 inhibition constants [32]. Thus the initial homology model featured two specific H-bonds of JNJ7777120 to Asp94<sup>3.32</sup> and Glu182<sup>5.46</sup> as shown in Fig. 1A. In the course of the molecular dynamics

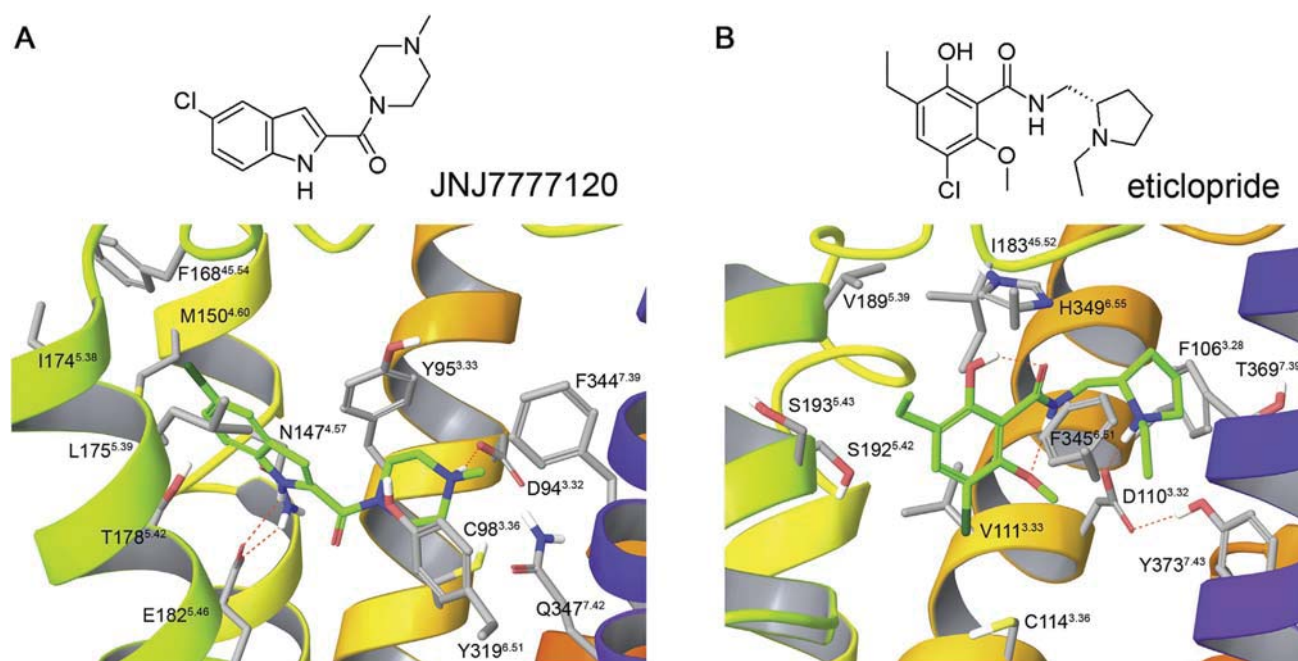


**Fig. 1.** Ligand structures and binding pockets of the initial receptor structures. A) Homology model of the human histamine H4 receptor in complex with JNJ7777120; B) X-ray structure of the human dopamine D3 receptor in complex with eticlopride. Receptors are represented as ribbons (helix 6 omitted for clarity) with interacting amino acids and ligands in gray and green skeletons, respectively and H-bonds in orange dash line. (For interpretation of the references to color in this figure legend, the reader is referred to the web version of this article.)

simulation the H4 receptor binding site appears to be relatively rigid based on side chain  $\chi_1$  and  $\chi_2$  angles of the interacting residues (Fig. 2A). Met150<sup>4.60</sup> is quite flexible and Leu175<sup>5.39</sup> assumes two different rotamer states, but these variations don't alter the

binding pattern of the ligand. However Glu182<sup>5.46</sup> also adopts two main rotamer states, which causes some variability in the ligand position within the binding site. The ionic interaction to Asp94<sup>3.32</sup> is mostly uninterrupted and surprisingly Gln347<sup>7.42</sup> also formed an H-

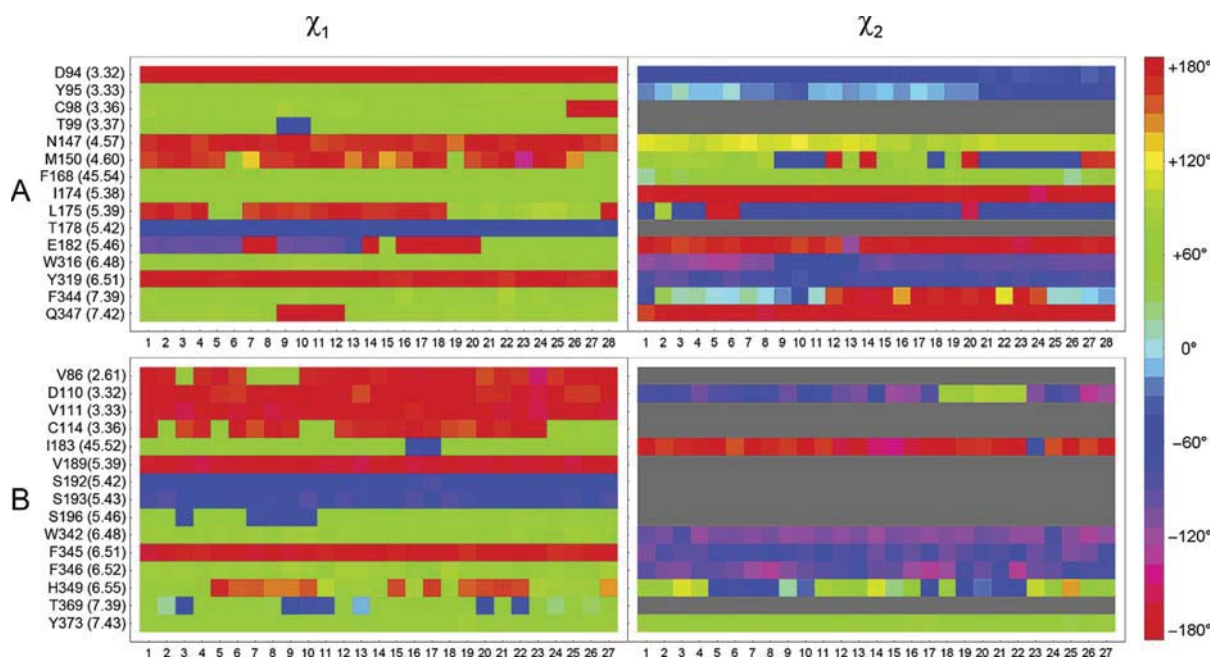


**Fig. 2.** Conformational variability of the binding sites:  $\chi_1$  and  $\chi_2$  side chain angles of binding site amino acids for each representative molecular dynamics frame in A) the H4 receptor and B) the D3 receptor. Angles are color coded according to the legend. (For interpretation of the references to color in this figure legend, the reader is referred to the web version of this article.)

bond with the carbonyl group of JNJ777120 in some of the representative frames. The D3 receptor binding site is also quite rigid, only Cys114<sup>3,36</sup>, Ser196<sup>5,46</sup> and Thr369<sup>7,39</sup> assume an alternative rotamer state featuring alternative H-bonds in a few representative structures (Fig. 2B). Interestingly, His349<sup>6,55</sup> was quite flexible, which seems to be in a tight H-bond network in the crystal structure. The ligand interaction pattern changed little; the highest RMSD from the crystal binding mode was 2.4 Å after superposition of the proteins, the ethylpyrrolidine part of eticlopride was able to move somewhat without losing the ionic interaction with Asp110<sup>3,32</sup> (shown in Fig. 1B).

### 3.2. Single structure and ensemble docking results

In the case of the H4 receptor the fragment library was docked to the homology model and to the 28 representative conformations collected from the molecular dynamics simulation, while for the D3 receptor docking has been carried out to the prepared X-ray structure and the 27 representative conformations from simulation. In both cases individual structural models provided a wide range of docking scores (GlideScore) but the single starting structure provided lower scores overall than the selected frames from MD. For example the docking scores of the top scoring fragments in each of the H4 frames ranged from  $-8.093$  to  $-9.920$  but it was  $-10.686$  for the homology model. Similarly for the D3 receptor top scores ranged from  $-8.063$  to  $-9.514$  but it was  $-9.796$  for the X-ray structure. Since binding sites appeared to be quite rigid during the MD simulation, these differences in the docking scores can be attributed to little variations in side chain geometries, indicating that specific interactions in the X-ray structure and homology model are in the optimal geometry with their respective ligands, while they loosen up during MD. Thus the distribution of the top scores indicate that X-ray structures and homology models have optimized protein-ligand interaction patterns while MD snapshots represent more diverse conformations, which in turn might be able to select more chemotypes than those optimized structures. For the single structures it was straightforward to select the top 50 fragments by GlideScore ranking for biological testing. For ensemble docking two different data fusion methods were considered. The rank-by-rank and rank-by-number consensus scoring schemes were investigated; the rank-by-vote method was shown to provide poorer results [33]. In the rank-by-rank scheme ligands are finally ranked by the mean of their rank numbers in each docking run to the representative structures. It was also investigated whether low standard deviation of ranks accompanies low mean ranks and we confirmed a strong correlation between

**Table 1**

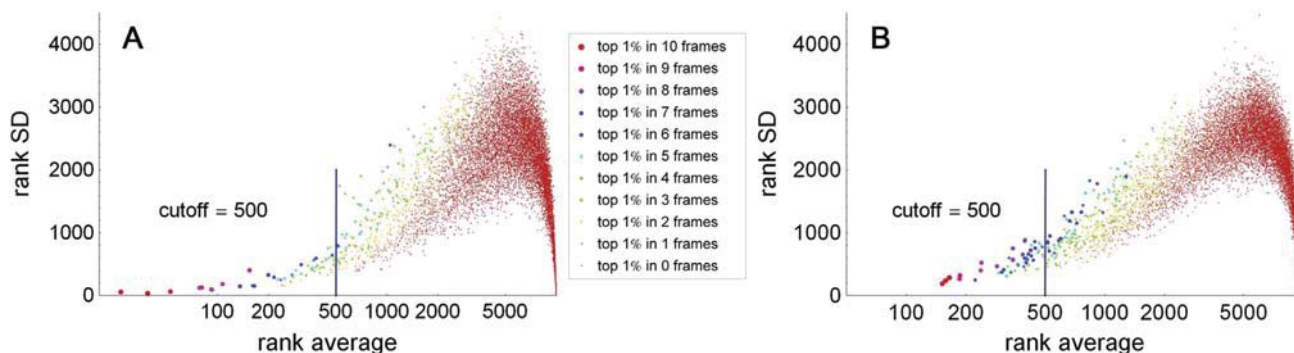
Hit rate statistics for the two receptors considered in this study. Hits are defined as showing higher than 20% inhibition in the D3 and H4 radioligand binding assays.

	D3	H4
Combined hit rate	25/92 (27%)	15/85 (18%)
Single structure hit rate	9/50 (18%)	11/50 (22%)
Ensemble docking hit rate	18/56 (32%)	8/50 (16%)
Overlap between hit sets	2/25 (8%)	4/15 (27%)

average rank and its standard deviation for fragments having mean rank lower than 500 (see Fig. 3). These fragments also fell in the top 1% of the ranked database in more than 3 representative frames both for the D3 and the H4 receptor. The correlation becomes less pronounced for higher mean ranks and eventually turns around for compounds ranked high by all MD frames. In the rank-by-number scheme ligands are finally ranked by the mean of their docking scores. It has been shown that using the mean of standardized Z-scores outperforms the average of the original scores; hence in this study the standardized GlideScores were evaluated. However, non-normal distribution of the GlideScores was observed for the fragment library and since there was two-thirds overlap between the top 50 selected by the rank-by-rank and rank-by-number schemes, the first one was finally used to select fragments for biological testing.

### 3.3. Pharmacological activities

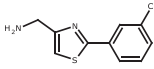
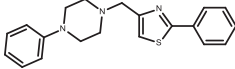
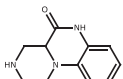
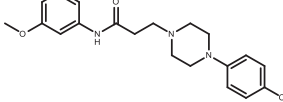
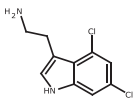
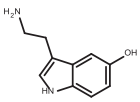
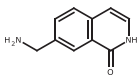
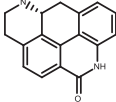
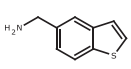
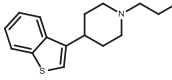
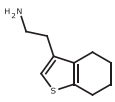
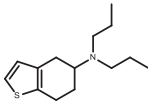
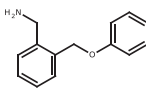
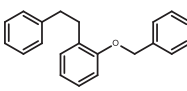
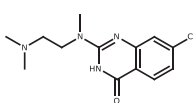
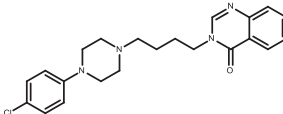
In the case of the D3 receptor 50 fragments from the X-ray structure docking run and 56 fragments from the ensemble docking run were selected for biological testing. These lists had 14 compounds in common, thus altogether 92 fragments were tested for D3 binding affinity in  $10 \mu\text{M}$  concentration. In the case of the H4 receptor 50 fragments from the initial homology model docking run and also 50 fragments from the ensemble docking run were selected for biological testing. These lists had 15 compounds in common, thus altogether 85 fragments were tested for H4 binding affinity in  $10 \mu\text{M}$  concentration. The only 30% overlap between the different methods is not altogether surprising since the crystal structure and the homology model select compounds that bind to a specific receptor conformation while ensemble docking selects compounds that have reasonably good interaction patterns with multiple receptor conformations. It has also been shown that the overlap of hits picked up by different screening paradigms likewise might be very low [34]. In the case of D3 25 virtual hits provided higher than 20% inhibition in the biological assay, corresponding to



**Fig. 3.** Log-linear plot of fragment rank averages and standard deviations of ranks in the ensemble docking approach for A) the D3 receptor and B) for the H4 receptor. Rank standard deviation is plotted against rank average calculated from the ranks obtained in the representative receptor structures for the 12,905 fragments. Markers are size and color coded by the number of receptor frames in which the fragment fell within the top 1% of the ranked library. (For interpretation of the references to color in this figure legend, the reader is referred to the web version of this article.)

**Table 2**

Experimental binding affinities of selected fragment hits of the D3 receptor and their LE and LELP values. The origin of the hit is indicated in the XRD and MD columns with + meaning the fragment was a virtual hit in the crystal structure docking or in the ensemble docking, respectively. Closest structural analogs from ChEMBL with measured binding affinity or functional activity against any of the five dopamine receptors are also indicated.

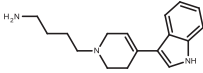
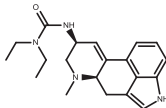
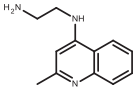
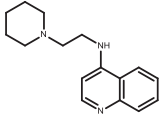
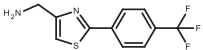
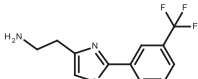
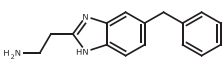
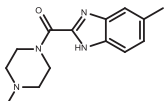
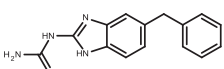
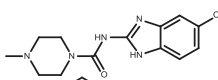
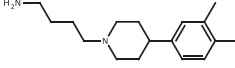
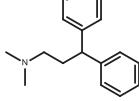
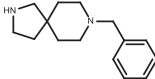
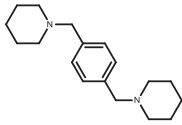
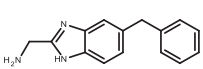
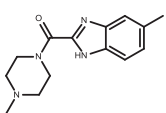
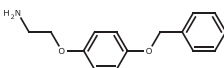
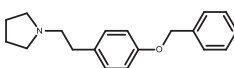
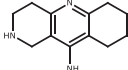
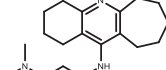
cpd	Structure	hD3 $K_i/\mu\text{M}$	LE	LELP	XRD	MD	Closest known D <sub>1–5</sub> R ligand
1		0.17	0.66	3.7		+	
2		0.50	0.57	1.2	+	+	
3		0.59	0.61	4.4		+	
4		1.1	0.63	0.7		+	
5		1.1	0.74	2.7	+		
6		1.6	0.66	4.2		+	
7		2.8	0.47	5.6	+		
8		2.8	0.40	4.2		+	

a combined hit rate of 27% (hit rates are summarized in Table 1). Out of these 9 came from the crystal structure docking run (18% hit rate) and 18 from the ensemble docking run (32% hit rate) with only 2 overlapping compounds. Binding affinity was determined for the 8 best compounds exhibiting higher than 75% inhibition at 10  $\mu\text{M}$  concentration (Table 2).  $K_i$  values were in the range of 0.17–2.8  $\mu\text{M}$ . Besides binding affinity various ligand efficiency metrics are applied in fragment-based lead discovery in order to prioritize fragment hits. These metrics incorporate molecule size either in terms of molecular mass or heavy atom count and lipophilicity usually represented with the octanol–water partition coefficient  $\log P$ . In this study ligand efficiency ( $\text{LE} = -RT \ln K_i/N_{\text{heavy}}$ ) and lipophilic ligand efficiency ( $\text{LELP} = \log P/\text{LE}$ ) [2] were considered. Since the D3 ligands identified here are very tight binders, LE values much higher than the usually accepted lower limit of 0.3 were obtained. As they are also on the lower side of lipophilicity, LELP values mostly below 5 were found, compounds 2 and 4 being the most favorable. In the case of H4 somewhat fewer, 15 virtual hits provided higher than 20% inhibition in the biological assay, corresponding to a combined hit rate of 18%. Out of these 11 came from the homology model docking run (22% hit rate) and 8 from the ensemble docking run (16% hit rate) with 4 overlapping compounds. Five of them were unavailable in the compound collection

in sufficient quantity for binding affinity measurement but  $K_i$  values were determined for the remaining 10 compounds (Table 3). These were in the range of 8.4–75  $\mu\text{M}$ , an order of magnitude higher than the hits for the D3 receptor. The lower hit rate and the lower binding affinities indicate a difference in the chemical tractability of the two receptors. LE values of the H4 ligands were correspondingly not as high as for D3 but still above the 0.3 limit up to 0.45. Also, the H4 ligands were somewhat more lipophilic resulting in higher LELP values, though still below 10. Especially fragments 10 and 18 showed favorable LE and LELP values. Taken together, these fragments would be suitable starting points for medicinal chemistry optimization; however, the scope of this study was to analyze the impact of different virtual fragment screening methodologies on hit finding. When hit-to-lead programs are initiated, novelty of the hits is also a crucial point. To assess this, substructure and similarity searches were conducted in the ChEMBL bioactivity database (<https://www.ebi.ac.uk/chembl/db/> accessed 21 January 2014). D3 hits were checked against all compounds with bioactivity data measured on the five dopamine receptors, while H4 hits against compounds with bioactivity data measured on the four histamine receptors. Exact substructure searches provided hits for 10 and 17, and similarity searches revealed additional similar known structures (see Tables 2 and 3). Compounds 2, 4, 8, 15 and 18 proved to be

**Table 3**

Experimental binding affinities of selected fragment hits of the H4 receptor and their LE and LELP values. The origin of the hit is indicated in the HM and MD columns with + meaning the fragment was a virtual hit in the homology model docking or in the ensemble docking, respectively. Closest structural analogs from ChEMBL with measured binding affinity or functional activity against any of the four histamine receptors are also indicated.

cpd	Structure	hH4 $K_i/\mu\text{M}$	LE	LELP	HM	MD	Closest known H <sub>1-4</sub> R ligand
9		8.4	0.35	6.4	+	+	
10		12.6	0.45	2.1	+		
11		14.3	0.39	7.1	+		
12		20.6	0.34	8.3	+		
13		21.9	0.32	9.3	+		
14		32.0	0.31	7.4	+		
15		32.9	0.36	5.4	+	+	
16		58.4	0.32	8.0	+	+	
17		58.7	0.32	8.1	+		
18		75.1	0.37	2.3		+	

truly novel ones, and others might also suggest potential unexplored growing vectors. Comparing the hit rates it can be seen that both X-ray structure and homology model were capable of providing useful hits in virtual screening, and in this particular case the homology model performed even better than the crystal structure. The superiority of the ensemble docking approach is not witnessed in this study. While for the D3 receptor the latter provided a substantially higher hit rate, the homology model performed best for the H4 receptor even though it was not preliminarily optimized in retrospective enrichment studies. Based on these results we conclude that both single structure and ensemble docking is useful for virtual fragment screening and seem to be complementary as the overlap between hit sets was low.

Consequently a combined approach would maximize the outcome of hit finding efforts.

### 3.4. Binding modes

While no H-bond or pharmacophoric constraints were applied during docking the majority of the virtual hits in all four hit lists were basic amines forming ionic or H-bond interactions with the conserved Asp110<sup>3,32</sup> in D3 and the homologous Asp94<sup>3,32</sup> in H4 or the other acidic residue Glu182<sup>5,46</sup> also known to play an important role in the recognition of histamine in H4. In the case of the D3 receptor it was found that docked poses of the *in vitro* active fragments provided very similar binding modes in multiple

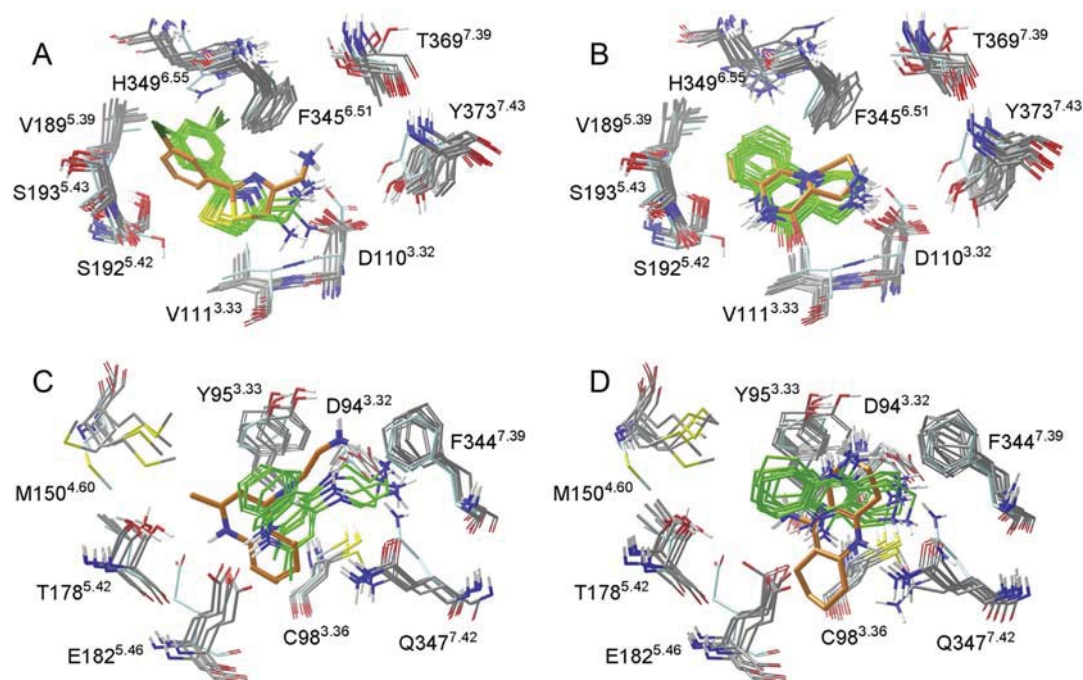


**Fig. 4.** Interaction modes of selected fragment hits obtained by single structure and ensemble docking. A) **1** in the D3 binding pocket; B) **2** in the D3 binding pocket; C) **10** in the H4 binding pocket; D) **18** in the H4 binding pocket. Selected interacting amino acids of the crystal structure and the homology model are shown in light blue skeleton, those of the representative MD frames in gray, single structure docked fragment poses in orange and ensemble docked poses in green skeletons. In A) and B) Phe346<sup>6.52</sup>, Val350<sup>6.56</sup> and Ser196<sup>5.46</sup> are omitted for clarity. In C) and D) Tyr319<sup>6.51</sup> and Leu175<sup>5.39</sup> are omitted for clarity. (For interpretation of the references to color in this figure legend, the reader is referred to the web version of this article.)

representative receptor conformations obtained by molecular dynamics simulation. Also the fragment binding modes from the X-ray structure docking were pretty much similar to the ensemble binding modes further strengthening the probability of their biological significance [35]. For example the thiazolemethanamine **1** produced nine very similar binding modes in ensemble docking with the basic amine interacting with Asp110<sup>3.32</sup>, the thiazole ring encased between Phe346<sup>6.52</sup> and Val111<sup>3.33</sup> and the chlorophenyl moiety facing His349<sup>6.55</sup> and Val350<sup>6.56</sup> with the chlorine substituent preferably pointing to the former, though in three poses pointing to the latter. The docked pose for the crystal structure is similar, though a bit shifted towards Asp110<sup>3.32</sup> and the chlorophenyl moiety rotated by 90° and the chlorine pointing to Val350<sup>6.56</sup> (Fig. 4A). The tricyclic D3 fragment **2** is quite rigid and produced eleven very similar binding modes and also the binding mode in the crystal structure was almost identical. The basic amine group again forms an ionic H-bond to Asp110<sup>3.32</sup> and the aromatic ring almost overlaps with the chlorophenyl moiety of fragment **1**. In a few structures an H-bond between the fragment amide N–H and the hydroxyl group of Ser196<sup>5.46</sup> or the backbone carbonyl of Ser192<sup>5.42</sup> is perceived (Fig. 4B). In the case of the H4 receptor the picture was not as clear as for D3. There was substantially higher variability among docked poses in the ensemble approach and binding modes from docking to the homology model produced different results in more cases. The major cause for this was probably the different rotamer state of Glu182<sup>5.46</sup> in the homology model and in most of the representative frames from MD. Compound **9** for example produced a variety of binding modes probably because of its multiple H-bond donor sites, though it got good docking scores both in the homology model and in the representative receptor conformations. Several similar poses were obtained for aminoquinoline **10**, in which the primary amine forms an ionic H-bond to Asp94<sup>3.32</sup>, a cation- $\pi$  interaction with Phe344<sup>7.39</sup> and the

protonated quinoline nitrogen forms another ionic H-bond to Glu182<sup>5.46</sup>. In the homology model the fragment is shifted towards the extracellular side of the pocket because of the greater distance between the two acidic sites, the quinoline ring is flipped and the anilinic N–H forms an additional H-bond to the phenolic OH of Tyr319<sup>6.51</sup> (Fig. 4C). Since this fragment was in the hit list from the homology model docking, the latter binding mode appears to be more feasible. For the tricyclic **18** seven similar poses were found in which the aliphatic amine group interacts with Asp94<sup>3.32</sup> and the carboaliphatic ring is encased between Tyr95<sup>3.33</sup>, Met150<sup>4.60</sup> and Leu175<sup>5.39</sup>. However, in four of these poses the protonated pyridine, while in three poses the anilinic N–H forms an H-bond with Glu182<sup>5.46</sup>. The pose found in the homology model differs from both of them: it is rotated by 90° with the aliphatic amine again interacting with Asp94<sup>3.32</sup>, the anilinic N–H with Glu182<sup>5.46</sup> the protonated pyridine with Gln347<sup>7.42</sup> and the carboaliphatic ring pointing towards the intracellular cavity of the binding site (Fig. 4D). Since this fragment was in the hit list from ensemble docking, the former binding mode appears to be more feasible. These findings underpin the superior hit rate for D3 and the inferior hit rate for H4 of the ensemble approach against the single structure hit rates. Also the higher binding affinities of D3 fragments correspond to the lower variability of their predicted binding modes [35].

#### 4. Conclusions

*In silico* methods of fragment-based lead discovery have not yet been widely investigated for GPCR targets. In the present study we have evaluated prospective structure based virtual screening methodologies on two GPCR targets namely the dopamine D3 and the histamine H4 receptors and a fragment library of 12,905 compounds. For both targets single structure and ensemble docking screens were

performed. For the D3 receptor the X-ray structure with eticlopride was available for the single structure screen, while a previously constructed H1 receptor based homology model of H4 was utilized. Representative receptor conformations for ensemble docking were generated by molecular dynamics simulations. Around 50 virtual hits from both methodologies for both receptors were measured *in vitro* and with a greater than 20% inhibition at 10  $\mu$ M criterion confirmed hit rates ranged from 16% to 32%. The reported hits provided high LE and low LELP values and are suitable starting points for hit-to-lead optimization. Analysis of the obtained binding modes provided insight to the variation in hit rates of the different methodologies. It was found that the X-ray structure, the homology model and structural ensembles are all suitable for docking based virtual screening of fragments against these GPCRs. However, there was little overlap among their hit sets and were thus complementary to each other. Combined approaches should provide valuable starting points for fragment-based lead discovery for other GPCRs as well if an X-ray structure or a good quality homology model is available.

## 5. Experimental

### 5.1. Human recombinant D3 binding assay

Cell cultures (CHO–K1) expressing human D3 receptors (purchased from HD Euroscreen Fast, Belgium) were homogenized in buffer solution (composition: 15 mM Tris, 2 mM MgCl<sub>2</sub>, 0.3 mM EDTA, 1 mM EGTA, pH = 7.4 at 25 °C) in 4× v/w with a Dounce tissue grinder and centrifuged at 40,000 g at 4 °C for 25 min. The supernatant was removed and the pellet was resuspended in 4× v/w buffer and re-centrifuged. This process was repeated twice more and the pellet was resuspended in buffer (composition: 75 mM Tris, 12.5 mM MgCl<sub>2</sub>, 0.3 mM EDTA, 1 mM EGTA, 250 mM Sucrose, pH = 7.4 at 25 °C) at a volume of 12.5 mL/g original weight. The preparations were then aliquoted and stored at –70 °C.

The aliquoted membrane was thawed and washed once in binding buffer containing 50 mM Tris–HCl; 5 mM MgCl<sub>2</sub>, 5 mM KCl; 1 mM CaCl<sub>2</sub>, 120 mM NaCl, 1 mM EDTA. In the same buffer 3.3  $\mu$ g protein/assay was incubated with 2 nM [<sup>3</sup>H]raclopride in the presence or absence of test compound (to determine the binding inhibition of the test compound or the total binding, respectively) for 120 min at 25 °C at a volume of 250  $\mu$ L in 96 Deep Well plate. Non-specific binding was determined in the presence of 10  $\mu$ M haloperidol. After incubation, samples were filtered over UniFilter GF/B™ using PerkinElmer Harvester and washed with 4 × 1 mL ice-cold binding buffer. The plate was dried at 40 °C for an hour and 40  $\mu$ L Microscint scintillation cocktail (PerkinElmer) was added to each well. The radioactivity was determined in MicroBeta 2450 microplate counter (PerkinElmer).

SEM was lower than 15% for single concentration measurements and lower than 7% for the hits. The ligand displacement experiments were repeated at least two times. The specific radioligand binding is defined as the difference between total binding and the non-specific binding determined in the presence of an excess amount of haloperidol. IC<sub>50</sub> values (i.e. concentration of compound giving 50% inhibition of specific binding) were determined from concentration–displacement curves by sigmoidal fitting. The inhibition constants ( $K_i$ ) were calculated using the Cheng–Prusoff equation:  $K_i = IC_{50}/[1 + (L/K_D)]$ , where  $[L]$  is the free radioligand concentration and  $K_D$  the affinity of the labeled ligand for receptor.  $K_D$  was determined from the Scatchard plot. GraFit 6.0 (Erithracus Software, Horley, UK) software was used for curve fittings.

### 5.2. Human recombinant H4 binding assay

Membranes from CHO–K1 cells expressing human histamine H4 receptors were purchased from PerkinElmer Life and Analytical

Sciences (Cat. No. ES-393-M400UA). Frozen membrane aliquots were thawed at room temperature and diluted to 200-fold (15  $\mu$ g protein/500  $\mu$ L diluted membrane/well) with binding buffer (50 mM TRIS–HCl pH 7.4, 5 mM EDTA).

The assay was performed according to the PerkinElmer assay protocol for human H4 receptor: 500  $\mu$ L diluted membrane suspension (15  $\mu$ g protein/assay) was incubated with [<sup>3</sup>H]histamine as radioligand. Final reaction volume was 550  $\mu$ L and final radioligand concentration was 4–7 nM. 10  $\mu$ M histamine was used for determination of non-specific binding. The samples were incubated at 27 °C for 30 min and binding was terminated by vacuum filtration through Whatman GF/B glass fiber filters, pre-soaked in 0.5% PEI. The filters were washed 3-times with 4 mL ice cold binding buffer. Filters were transferred to vials, 4 mL Optiphase HiSafe scintillation cocktail (PerkinElmer) was added and radioactivity was determined by Packard TriCarb 2900 TR (PerkinElmer) liquid scintillation counter.

SEM was lower than 15% for single concentration measurements and lower than 7% for the hits. The ligand displacement by the compounds was determined using a minimum of six concentrations in duplicate or triplicate, and experiments were repeated at least two times. The specific radioligand binding is defined as the difference between total binding and the non-specific binding determined in the presence of an excess of unlabeled ligand. IC<sub>50</sub> values (i.e. concentration of compound giving 50% inhibition of specific binding) were determined from concentration–displacement curves by sigmoidal fitting using Prism Software 4.0 (GraphPad, San Diego, CA, U.S.A.).  $K_i$  values (i.e. inhibition constants) were calculated using the Cheng–Prusoff equation:  $K_i = IC_{50}/[1 + (L/K_D)]$ , where  $[L]$  is the free radioligand concentration and  $K_D$  the affinity of the labeled ligand for receptor.  $K_D$  was determined from the Scatchard plot.

## Acknowledgments

The authors are thankful to Ákos Tarcsay for valuable discussions, Balázs Jójárt, Gábor Paragi and Ferenc Bogár for the MD simulation and subsequent clustering. This work was supported by COST Action CM1207.

## Appendix A. Supplementary data

Supplementary data related to this article can be found at <http://dx.doi.org/10.1016/j.ejmech.2014.02.034>.

## References

- [1] M. Baker, Fragment-based lead discovery grows up, *Nature Reviews Drug Discovery* 12 (2013) 5–7.
- [2] G.G. Ferenczy, G.M. Keser&Sudblac, How are fragments optimized? A retrospective analysis of 145 fragment optimizations, *Journal of Medicinal Chemistry* 56 (2013) 2478–2486.
- [3] A. Stamford, C. Strickland, Inhibitors of BACE for treating Alzheimer's disease: a fragment-based drug discovery story, *Current Opinion in Chemical Biology* 17 (2013) 320–328.
- [4] J. Tsai, J.T. Lee, W. Wang, J. Zhang, H. Cho, S. Mamo, R. Bremer, S. Gillette, J. Kong, N.K. Haass, K. Sproesser, L. Li, K.S. Smalley, D. Fong, Y.L. Zhu, A. Marimuthu, H. Nguyen, B. Lam, J. Liu, I. Cheung, J. Rice, Y. Suzuki, C. Luu, C. Settachatgul, R. Shellooe, J. Cantwell, S.H. Kim, J. Schlessinger, K.Y. Zhang, B.L. West, B. Powell, G. Habets, C. Zhang, P.N. Ibrahim, P. Hirth, D.R. Artis, M. Herlyn, G. Bollag, Discovery of a selective inhibitor of oncogenic B-Raf kinase with potent antimelanoma activity, *Proceedings of the National Academy of Sciences of the United States of America* 105 (2008) 3041–3046.
- [5] M. Sándor, R. Kiss, G.M. Keser&Sudblac, Virtual fragment docking by Glide: a validation study on 190 protein–fragment complexes, *Journal of Chemical Information and Modeling* 50 (2010) 1165–1172.
- [6] M.L. Verdonk, I. Giangreco, R.J. Hall, O. Korb, P.N. Mortenson, C.W. Murray, Docking performance of fragments and druglike compounds, *Journal of Medicinal Chemistry* 54 (2011) 5422–5431.
- [7] M. Vass, G.M. Keser&Sudblac, Fragments to link. A multiple docking strategy for second site binders, *Medicinal Chemistry Communications* 4 (2013) 510–514.

- [8] G.G. Ferenczy, G.M. Keser & Udblac, Thermodynamics of fragment binding, *Journal of Chemical Information and Modeling* 52 (2012) 1039–1045.
- [9] S. Kawatkar, H. Wang, R. Czerminski, D. Joseph-McCarthy, Virtual fragment screening: an exploration of various docking and scoring protocols for fragments using Glide, *Journal of Computer-Aided Molecular Design* 23 (2009) 527–539.
- [10] A. Kumar, K.Y. Zhang, Computational fragment-based screening using RosettaLigand: the SAMPL3 challenge, *Journal of Computer-Aided Molecular Design* 26 (2012) 603–616.
- [11] S. Kawatkar, D. Moustakas, M. Miller, D. Joseph-McCarthy, Virtual fragment screening: exploration of MM-PBSA re-scoring, *Journal of Computer-Aided Molecular Design* 26 (2012) 921–934.
- [12] T. Zhu, H. Lee, H. Lei, C. Jones, K. Patel, M.E. Johnson, K.E. Hevener, Fragment-based drug discovery using a multidomain, parallel MD-MM/PBSA screening protocol, *Journal of Chemical Information and Modeling* 53 (2013) 560–572.
- [13] C.B. Rao, J. Subramanian, S.D. Sharma, Managing protein flexibility in docking and its applications, *Drug. Discovery Today* 14 (2009) 394–400.
- [14] W. Sherman, T. Day, M.P. Jacobson, R.A. Friesner, R. Farid, Novel procedure for modeling ligand/receptor induced fit effects, *Journal of Medicinal Chemistry* 49 (2006) 534–553.
- [15] D.J. Osguthorpe, W. Sherman, A.T. Hagler, Exploring protein flexibility: incorporating structural ensembles from crystal structures and simulation into virtual screening protocols, *Journal of Physical Chemistry B* 116 (2012) 6952–6959.
- [16] C.N. Cavasotto, J.A. Kovacs, R.A. Abagyan, Representing receptor flexibility in ligand docking through relevant normal modes, *Journal of the American Chemical Society* 127 (2005) 9632–9640.
- [17] F. Sirci, E.P. Istyastono, H.F. Vischer, A.J. Kooistra, S. Nijmeijer, M. Kuijter, M. Wiltmans, R. Mannhold, R. Leurs, I.J. de Esch, C. de Graaf, Virtual fragment screening: discovery of histamine H3 receptor ligands using ligand-based and protein-based molecular fingerprints, *Journal of Chemical Information and Modeling* 52 (2012) 3308–3324.
- [18] A. Tarcsay, G. Paragi, M. Vass, B. Jójárt, F. Bogár, G.M. Keser & Udblac, The impact of molecular dynamics sampling on the performance of virtual screening against GPCRs, *Journal of Chemical Information and Modeling* 53 (2013) 2990–2999.
- [19] Prime, Version 3.0, Schrödinger, LLC, New York, NY, 2012.
- [20] MacroModel, Version 9.9, Schrödinger, LLC, New York, NY, 2012.
- [21] Schrödinger Suite 2011 Induced Fit Docking Protocol; Glide Version 5.7, Schrödinger, LLC, New York, NY, 2011. Prime version 3.0, Schrödinger, LLC, New York, NY, 2011.
- [22] Schrödinger Suite 2011 Schrödinger Suite; Epik Version 2.2, Schrödinger, LLC, New York, NY, 2011. Impact version 5.7, Schrödinger, LLC, New York, NY, 2011; Prime version 2.3, Schrödinger, LLC, New York, NY, 2011.
- [23] J.C. Phillips, R. Braun, W. Wang, J. Gumbart, E. Tajkhorshid, E. Villa, C. Chipot, R.D. Skeel, L. Kalé, K. Schulten, Scalable molecular dynamics with NAMM, *Journal of Computational Chemistry* 26 (2005) 1781–1802.
- [24] D.A. Case, T.E. Cheatham, T. Darden, H. Gohlke, R. Luo, K.M. Merz, A. Onufriev, C. Simmerling, B. Wang, R.J. Woods, The Amber biomolecular simulation programs, *Journal of Computational Chemistry* 26 (2005) 1668–1688.
- [25] LigPrep, Version 2.5, Schrödinger, LLC, New York, NY, 2011.
- [26] Epik, Version 2.2, Schrödinger, LLC, New York, NY, 2011.
- [27] Calculator, Version 5.10.2, ©, ChemAxon Ltd, 1998–2012.
- [28] Glide, Version 5.7, Schrödinger, LLC, New York, NY, 2011.
- [29] R.A. Friesner, J.L. Banks, R.B. Murphy, T.A. Halgren, J.J. Klicic, D.T. Mainz, M.P. Repasky, E.H. Knoll, D.E. Shaw, M. Shelley, J.K. Perry, P. Francis, P.S. Shenkin, Glide: a new approach for rapid, accurate docking and scoring. 1. Method and assessment of docking accuracy, *Journal of Medicinal Chemistry* 47 (2004) 1739–1749.
- [30] T.A. Halgren, R.B. Murphy, R.A. Friesner, H.S. Beard, L.L. Frye, W.T. Pollard, J.L. Banks, Glide: a new approach for rapid, accurate docking and scoring. 2. enrichment factors in database screening, *Journal of Medicinal Chemistry* 47 (2004) 1750–1759.
- [31] R.A. Friesner, R.B. Murphy, M.P. Repasky, L.L. Frye, J.R. Greenwood, T.A. Halgren, P.C. Sanschagrin, D.T. Mainz, Extra precision Glide: docking and scoring incorporating a model of hydrophobic enclosure for protein-ligand complexes, *Journal of Medicinal Chemistry* 49 (2006) 6177–6196.
- [32] H.D. Lim, C. de Graaf, W. Jiang, P. Sadek, P.M. McGovern, E.P. Istyastono, R.A. Bakker, I.J. de Esch, R.L. Thurmond, R. Leurs, Molecular determinants of ligand binding to H4R species variants, *Molecular Pharmacology* 77 (2010) 734–743.
- [33] R. Wang, S. Wang, How does consensus scoring work for virtual library screening? An idealized computer experiment, *Journal of Chemical Information and Computer Science* 41 (2001) 1422–1426.
- [34] J. Wielens, S.J. Headley, D.I. Rhodes, R.J. Mulder, O. Dolezal, J.J. Deadman, J. Newman, D.K. Chalmers, M.W. Parker, T.S. Peat, M.J. Scanlon, Parallel screening of low molecular weight fragment libraries: do differences in methodology affect hit identification? *Journal of Biomolecular Screening* 18 (2013) 147–159.
- [35] M. Orita, K. Ohno, M. Warizaya, Y. Amano, T. Niimi, Lead generation and examples opinion regarding how to follow up hits, *Methods in Enzymology* 493 (2011) 383–419.

# Multiple fragment docking and linking in primary and secondary pockets of dopamine receptors

Márton Vass,<sup>†</sup> Éva Ágai-Csongor,<sup>†</sup> Ferenc Horti,<sup>†</sup> and György M. Keserű<sup>\*,‡</sup>

<sup>†</sup>Gedeon Richter Plc, Gyömrői út 19-21, H-1103 Budapest, Hungary

<sup>‡</sup>Research Centre for Natural Sciences, Hungarian Academy of Sciences, Magyar tudósok körútja 2, H-1117 Budapest, Hungary

**KEYWORDS:** *fragment docking, fragment linking, dopamine receptors, G protein-coupled receptors, selective antagonists*

**ABSTRACT:** A sequential docking methodology was applied to computationally predict starting points for fragment linking using the human dopamine D<sub>3</sub> receptor crystal structure and a human dopamine D<sub>2</sub> receptor homology model. Two focused fragment libraries were docked in the primary and secondary binding sites and best fragment combinations were enumerated. Similar top scoring fragments were found for the primary site, while secondary site fragments were predicted to convey selectivity. Three linked compounds were synthesized that had subnanomolar affinity on D<sub>3</sub> receptors and 9, 39 and 55-fold selectivity in favor of D<sub>3</sub> over D<sub>2</sub> receptors. The observed subtype selectivity of the compounds was assessed on a structural basis.

Fragment-based drug discovery (FBDD) has recently proved to have significant utility in early phase drug research.<sup>1</sup> Fragments are polar compounds of low molecular weight and low complexity enabling more efficient sampling of chemical space and exploring enthalpy dominated targeting of protein hot spots resulting in better physico-chemical and ADMET profiles of fragment derived leads and clinical candidates.<sup>2</sup> The two main strategies of fragment hit elaboration are growing and linking.<sup>3</sup> In the first one a single fragment is decorated with additional functionalities while in the second two (or more) fragments are identified that bind to the target simultaneously and in close proximity and are subsequently incorporated in a single molecule using a suitable linker moiety.

Although FBDD in the last decade has shown remarkable efficiency on enzyme targets, its applicability for membrane proteins has been limited by difficulties in obtaining structural information on membrane proteins and application of sensitive biophysical screening methods frequently used for fragment screening such as high-throughput X-ray screening, surface plasmon resonance (SPR) and nuclear magnetic resonance (NMR). Recent advances in G protein-coupled receptor stabilization and structural investigation made it possible to develop biophysical assays for GPCRs and to utilize structural information in structure-based drug design. Several recent reports described experimental<sup>4</sup> and virtual fragment screening<sup>5,6</sup> as well as structure-guided optimization efforts<sup>7</sup> on GPCRs. It is expected that FBDD applied to GPCRs can provide novel and high quality compounds for this target family.

Recent clinical evidence supports the effectiveness of dual dopamine D<sub>2</sub> and D<sub>3</sub> antagonists or partial agonists in schizophrenia, depression and bipolar mania.<sup>8</sup> Finding the balance between D<sub>3</sub> and D<sub>2</sub> affinities is essential for a beneficial therapeutic effect and safety profile. Dual acting compounds should show higher affinity to the D<sub>3</sub> than to the D<sub>2</sub> receptors due to different expression levels of the two receptors in specific brain areas. Since the elucidation of the dopamine D<sub>3</sub> crystal structure in complex with eticlopride in 2010,<sup>9</sup> much attention has been directed towards the structure-based screening and design of D<sub>3</sub> ligands. We have recently evaluated the performance of a sequential docking methodology to computationally predict starting points for fragment linking.<sup>10</sup> In the present study we apply this methodology for fragment docking and linking to the D<sub>3</sub> crystal structure and a D<sub>2</sub> homology model and assess the subtype selectivity of the compounds on a structural basis. A similar methodology was also used by Abagyan et al. with dopamine as the fixed primary site ligand and no subsequent linking of the identified fragments.<sup>11</sup>

**Homology modeling and protein structure preparation.** The human dopamine D<sub>2</sub> receptor amino acid sequence from the UniProt server<sup>12</sup> was aligned to the sequence of the template, chain A of the 2.89 Å resolution X-ray structure of the human dopamine D<sub>3</sub> receptor crystallized with the D<sub>2</sub>-D<sub>3</sub> dual antagonist eticlopride (PDB code: 3PBL) using Prime 3.2.<sup>13</sup> The third intracellular loop was not modeled and the eticlopride ligand was included in homology model building to prevent collapse of the binding site. Finally the whole structure was subjected to Impref restrained minimization in the Protein Prepara-

tion Wizard in the Schrödinger Suite 2013.<sup>14</sup> Chain A of the dopamine D<sub>3</sub> crystal structure was subjected to the full Protein Preparation Wizard workflow with default settings.

**Ligand preparation and docking.** An in-house focused library of 196 fragments was collected containing a basic amine moiety in an aliphatic ring connected directly or through a short linker to a substituted aryl or hetaryl moiety (see general formula in the Supporting Information). Such compounds were believed to function as primary binding site ligands of the D<sub>2</sub> and D<sub>3</sub> receptors. It has been shown that the primary binding sites of the two receptors are nearly identical and selectivity can be achieved by modulation in the secondary binding pocket.<sup>15</sup> Another in-house focused library of 266 fragments were collected containing a cyclohexyl or piperidine ring (see general formula in the Supporting Information) as these fragments were believed to function as secondary binding site ligands based on known D<sub>3</sub> antagonists such as SB-277011<sup>16</sup> suitable for modulating selectivity. The two libraries were prepared for docking using LigPrep 2.6.<sup>17</sup> Protonation and tautomeric states at pH 7±2 were enumerated using Epik 2.4.<sup>18</sup> The Glide 5.9<sup>19</sup> software was used for sequential docking the two libraries to the two receptor structures according to the protocol described in ref. 10, briefly: the first library was docked to the apo receptor structures, then the docking poses were merged with the receptor, new grids were constructed including the merged ligands and the second fragment library was docked to the partially occupied binding sites. Top scoring fragment combinations were visually inspected; linked compounds were synthesized and tested in radioligand binding assays.

**Primary site docking results.** Docking of the first focused library of basic fragments produced results similar binding modes as in ref. 15. All of the 196 fragments could be docked into the inner binding site of the D<sub>3</sub> receptor, of which 145 produced an ionic hydrogen bond to the characteristic Asp110<sup>3-32</sup> in the D<sub>3</sub> crystal structure and the aromatic moiety encased between hydrophobic residues Phe345<sup>6,51</sup>, Phe346<sup>6,52</sup>, Val111<sup>3-33</sup> and Ile183<sup>45-52</sup>. The top 15 fragments in D<sub>3</sub> docking also achieved high ranks when the same library was docked to the D<sub>2</sub> crystal structure, particularly the highest scoring 1-(3-cyano-5-trifluoromethylphenyl)piperazine was identical in both receptors providing good docking scores (-8.576 for D<sub>3</sub> and -8.745 for D<sub>2</sub>) and identical binding modes. This is in line with the highly conserved nature of the primary binding site. Docking seemed to favor a *meta*-trifluoromethyl substituent in further high ranking fragments as well. Binding modes of the four top ranked compounds are depicted in Figure 1.

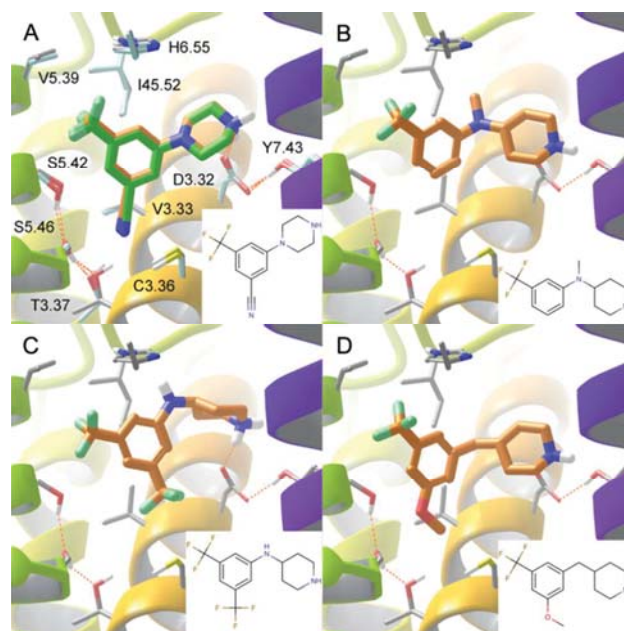


**Figure 1.** Binding modes of the top four fragments (from A to D) in D<sub>3</sub> primary site docking. In A) the D<sub>3</sub> and D<sub>2</sub> binding sites are overlaid in grey and light blue carbons respectively, as well as docked poses of the ligand in orange and green carbons respectively. From B) to D) only D<sub>3</sub> results are shown. Helix 6 is omitted for clarity. Compound structures are shown as insets.

**Secondary site docking results.** The 145 well-docked fragments were merged with the apo D<sub>3</sub> structure allowing for 145 new grids to be constructed and the second focused fragment library was docked to all of these new grids of partially occupied binding site. Docking scores of the 266 fragments in all 145 D<sub>3</sub> grids were averaged and ranked by this mean docking score. The single best primary site ligand was also merged with the apo D<sub>2</sub> homology model and the second library was docked into this partially occupied structure to assess structural determinants of selectivity. Top ranking secondary site binders in the D<sub>3</sub> receptor and their binding modes in the D<sub>2</sub> receptor were visually inspected. The binding modes of the top three fragments by mean D<sub>3</sub> docking score in ten D<sub>3</sub> grids and the single D<sub>2</sub> grid are shown in Figure 2. It can be seen that these fragments produce extensive H-bonding patterns in the secondary binding site of the D<sub>3</sub> crystal structure. Carbonyl groups of the cyclohexylurea (mean docking score: -6.574) and the cyclohexylglycinamide (mean docking score: -6.230) and one of the S=O groups of the cyclohexylaminosulfonamide (mean docking score: -6.087) act as acceptors for Thr369<sup>7-39</sup> in D<sub>3</sub> and the homologous Thr412<sup>7-39</sup> in D<sub>2</sub>. Two NH groups of all three ligands interact as donors to Glu90<sup>2-65</sup> and Ser366<sup>7-36</sup> in D<sub>3</sub> as well as the same Glu95<sup>2-65</sup> and Ser409<sup>7-36</sup> amino acids in D<sub>2</sub>. The only interaction different between the two receptor subtypes is the second S=O group of the cyclohexylaminosulfonamide fragment, which acts as an acceptor for Tyr36<sup>1-39</sup> in D<sub>3</sub>, while in the homologous position of D<sub>2</sub> Leu41<sup>1-39</sup> can be found incapable of forming a hydrogen bond with the ligand.

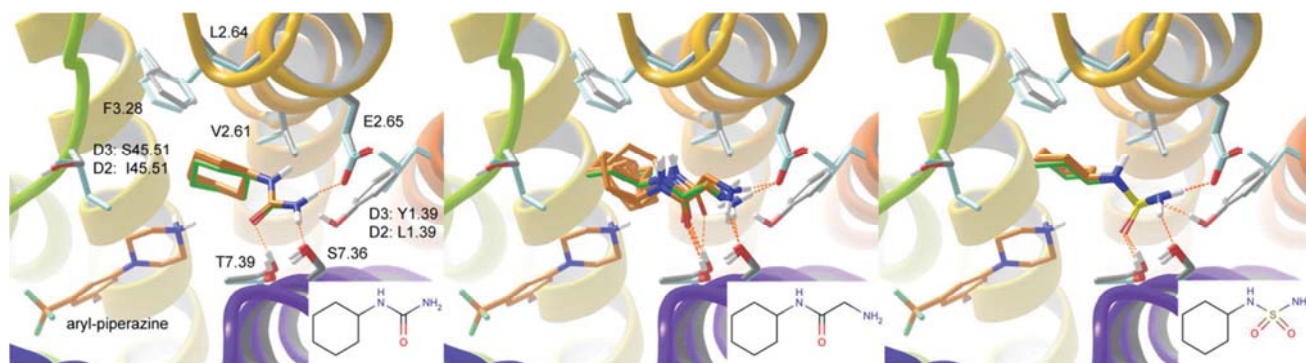


**Figure 2.** Binding modes of the top three fragments in D<sub>3</sub> and D<sub>2</sub> secondary site docking. The D<sub>3</sub> and D<sub>2</sub> binding sites are overlaid in grey and light blue carbons respectively, as well as an ensemble of 10 docked poses of the ligand in D<sub>3</sub> in orange carbons and a single docked pose of the ligand in D<sub>2</sub> in green carbons. Only the top ranked primary site ligand is included for clarity. Compound structures are shown as insets.

**Table 1. Experimental and docking data of linked compounds.**

Entry	Compound structure	hD <sub>3</sub> R K <sub>i</sub> (nM) <sup>a</sup>	hD <sub>3</sub> R docking score	hD <sub>2</sub> R K <sub>i</sub> (nM) <sup>a</sup>	hD <sub>2</sub> R docking score	Selectivity
1		0.75 ± 0.10	-10.393	30 ± 11	-10.664	39
2		0.62 ± 0.23	-10.488	5.4 ± 0.2	-11.210	9
3		0.67 ± 0.15	-10.514	37 ± 9	-10.833	55

<sup>a</sup>Inhibition constants from binding experiments on recombinant human D<sub>2</sub> and D<sub>3</sub> receptors. For details on the assays, see the Supporting Information. The data are derived from at least three independent experiments; the standard error of the mean is indicated.

Furthermore, these ligands were found to produce robust binding modes in most of the 145 D<sub>3</sub> grids. As can be seen from Figure 2 the predicted binding modes of the second-site ligands in the grids containing the top ten primary site ligands are almost identical in the case of the urea and the sulfonamide fragment and show little variability for the glycine derivative. Robust ensembles of docking poses have been associated with higher fidelity of the predicted binding mode<sup>20</sup> and a higher entropy change upon binding.<sup>21</sup> Further fragments produced less robust binding modes. Therefore these top three fragments predicted to bind the secondary site were selected

for linking with the top primary aryl-piperazine fragment. Docking suggested possible linking of the basic aryl-piperazine nitrogen with either the para or the meta position of the cyclohexyl rings of the secondary fragments. The distance of the para positions in the various docking poses ranged from 3.8 to 4.5 Å while the distance of the meta positions ranged from 3.4 to 3.6 Å, thus both seemed to be suitable linking points. Because of synthetic accessibility and fewer possible stereoisomers, linking was carried out at the symmetric para position.

**Biological activities.** Linked compounds 1-3 were synthesized and tested in *in vitro* [<sup>3</sup>H]raclopride binding

experiments against recombinant human D<sub>2</sub> and D<sub>3</sub> receptors. See Supporting Information for synthetic routes and experimental details. The ligand displacement experiments were repeated at least three times. K<sub>i</sub> values and derived selectivities of the compounds are shown in Table 1. The linked compounds possessed subnanomolar activities against the D<sub>3</sub> receptor and low- to mid-nanomolar activity against the D<sub>2</sub> receptor. The selectivity of compound 2 was lowest, only 9 times higher K<sub>i</sub> was measured for D<sub>2</sub> than for D<sub>3</sub>, which is in line with the higher flexibility and less robust predicted binding mode of the secondary site fragment. On the other hand, compound 3 showed a 55 times higher K<sub>i</sub> for D<sub>2</sub> than to D<sub>3</sub>, which is also supported by the docking results. This was the only compound featuring an extra D<sub>3</sub> specific interaction, namely the H-bond with Tyr36<sup>1,39</sup>, which is not present in D<sub>2</sub>. Docking of the linked compounds to the apo structures provided similar binding modes and the same H-bonding pattern as the original unlinked fragments (data not shown). Only a small upward shift of the aryl-piperazine fragment was evident in the primary binding site (RMSD: 1.7 Å) and very small deviations were seen in the secondary fragment binding modes (RMSD: 0.57 Å for the urea, 1.06 Å for the glycinamide and 0.84 Å for the sulfonamide fragment). The docking scores of the linked compounds were very high, and although we could not predict the selectivity, in this particular case the relative values of compounds at both receptors were in accordance with the experimental data (see Table 1).

In conclusion we have applied our sequential fragment docking methodology to identify fragments to link in a GPCR target, namely the dopamine D<sub>3</sub> receptor binding site. A homology model was also built for the D<sub>2</sub> receptor subtype and docking of the fragments as well as the full linked compounds was carried out to both receptors in order to assess the structural basis of subtype selectivity of the predicted binders. Three linked compounds were synthesized and experimental results were in line with docking predictions. Thus it has been shown that multiple fragment docking can provide starting points for linking for GPCR targets with elucidated 3D structures, and subtype selectivity has been achieved by virtual secondary site fragment screening and fragment linking.

## ASSOCIATED CONTENT

**Supporting Information.** General formulae of the focused fragment libraries, synthetic and experimental details. This material is available free of charge via the Internet at <http://pubs.acs.org>.

## AUTHOR INFORMATION

### Corresponding Author

\*(G.M.K.) Tel: +36-1-438-1155; Fax: +36-1-438-1143; E-mail: [keseru.gyorgy@ttk.mta.hu](mailto:keseru.gyorgy@ttk.mta.hu).

### Funding Sources

This research was supported in part by COST Action CM1207.

### Notes

The authors declare no competing financial interest.

## ACKNOWLEDGMENTS

We thank Árpád Könczöl and Zoltán Szakács for compound analytics and Ákos Tarcsay for valuable discussions.

## ABBREVIATIONS

FBDD, Fragment-based drug discovery; ADMET, absorption – distribution – metabolism – excretion – toxicity; GPCR, G protein-coupled receptor.

## REFERENCES

- (1) Murray, C. W.; Verdonk, M. L.; Rees, D. C. Experiences in fragment-based drug discovery. *Trends Pharmacol. Sci.* **2012**, *33*, 224-232.
- (2) Ferenczy, G. G.; Keserű, G. M. Thermodynamics of fragment binding. *J. Chem. Inf. Model.* **2012**, *52*, 1039-1045.
- (3) de Kloe, G. E.; Bailey, D.; Leurs, R.; de Esch, I. J. Transforming fragments into candidates: small becomes big in medicinal chemistry. *Drug Discov. Today* **2009**, *14*, 630-646.
- (4) Visegrády, A.; Keserű, G. M. Fragment-based lead discovery on G-protein-coupled receptors. *Expert. Opin. Drug. Discov.* **2013**, *8*, 811-820.
- (5) de Graaf, C.; Kooistra, A. J.; Vischer, H. F.; Katritch, V.; Kuijter, M.; Shiroishi, M.; Iwata, S.; Shimamura, T.; Stevens, R. C.; de Esch, I. J.; Leurs, R. Crystal structure-based virtual screening for fragment-like ligands of the human histamine H<sub>1</sub> receptor. *J. Med. Chem.* **2011**, *54*, 8195-8206.
- (6) Sirci, F.; Istyastono, E. P.; Vischer, H. F.; Kooistra, A. J.; Nijmeijer, S.; Kuijter, M.; Wijtmans, M.; Mannhold, R.; Leurs, R.; de Esch, I. J.; de Graaf, C. Virtual fragment screening: discovery of histamine H<sub>3</sub> receptor ligands using ligand-based and protein-based molecular fingerprints. *J. Chem. Inf. Model.* **2012**, *52*, 3308-3324.
- (7) Chen, D.; Ranganathan, A.; Ijzerman, A. P.; Siegal, G.; Carlsson, J. Complementarity between in silico and biophysical screening approaches in fragment-based lead discovery against the A<sub>2A</sub> adenosine receptor. *J. Chem. Inf. Model.* **2013**, *53*, 2701-2714.
- (8) Ágai-Csongor, É.; Domány, G.; Nógrádi, K.; Galambos, J.; Vágó, I.; Keserű, G. M.; Greiner, I.; Laszlovszky, I.; Gere, A.; Schmidt, É.; Kiss, B.; Vastag, M.; Tihanyi, K.; Sággy, K.; Laszy, J.; Gyertyán, I.; Zájer-Balázs, M.; Gémesi, L.; Kapás, M.; Szombat-helyi, Z. Discovery of cariprazine (RGH-188): a novel antipsychotic acting on dopamine D<sub>3</sub>/D<sub>2</sub> receptors. *Bioorg. Med. Chem. Lett.* **2012**, *22*, 3437-3440.
- (9) Chien, E. Y.; Liu, W.; Zhao, Q.; Katritch, V.; Han, G. W.; Hanson, M. A.; Shi, L.; Newman, A. H.; Javitch, J. A.; Cherezov, V.; Stevens, R. C. Structure of the human dopamine D<sub>3</sub> receptor in complex with a D<sub>2</sub>/D<sub>3</sub> selective antagonist. *Science* **2010**, *330*, 1091-1095.
- (10) Vass, M.; Keserű, G. M. Fragments to link. A multiple docking strategy for second site binders. *MedChemComm* **2013**, *4*, 510-514.
- (11) Lane, J. R.; Chubukov, P.; Liu, W.; Canals, M.; Cherezov, V.; Abagyan, R.; Stevens, R. C.; Katritch, V. Structure-based ligand and discovery targeting orthosteric and allosteric pockets of dopamine receptors. *Mol. Pharmacol.* **2013**, *84*, 794-807.
- (12) <http://www.uniprot.org/>
- (13) Prime, version 3.2; Schrödinger, LLC: New York, NY, 2013.
- (14) Schrödinger Suite 2013, Protein Preparation Wizard, Epik version 2.3, Impact version 5.8, Prime version 3.1; Schrödinger, LLC: New York, NY, 2013.
- (15) Newman, A. H.; Beuming, T.; Banala, A. K.; Donthamsetti, P.; Pongetti, K.; LaBounty, A.; Levy, B.; Cao, J.; Michino, M.; Luedtke, R. R.; Javitch, J. A.; Shi, L. Molecular determinants of

1 selectivity and efficacy at the dopamine D<sub>3</sub> Receptor. *J. Med.*  
2 *Chem.* **2012**, 55, 6689-6699.

3 (16) Reavill, C.; Taylor, S. G.; Wood, M. D.; Ashmeade, T.; Aus-  
4 tin, N. E.; Avenell, K. Y.; Boyfield, I.; Branch, C. L.; Cilia, J.;  
5 Coldwell, M. C.; Hadley, M. S.; Hunter, A. J.; Jeffrey, P.; Jewitt, F.;  
6 Johnson, C. N.; Jones, D. N.; Medhurst, A. D.; Middlemiss, D. N.;  
7 Nash, D. J.; Riley, G. J.; Routledge, C.; Stemp, G.; Thewlis, K. M.;  
8 Trail, B.; Vong, A. K.; Hagan, J. J. Pharmacological actions of a  
9 novel, high-affinity, and selective human dopamine D<sub>3</sub> receptor  
10 antagonist, SB-277011-A. *J. Pharmacol. Exp. Ther.* **2000**, 294, 1154-  
11 1165.

11 (17) LigPrep, version 2.6; Schrödinger, LLC: New York, NY,  
12 2013.

13 (18) Epik, version 2.4; Schrödinger, LLC, New York, NY, 2013.

14 (19) Glide, version 5.9; Schrödinger, LLC: New York, NY, 2013.

15 (20) Gorelik, B.; Goldblum, A. High quality binding modes in  
16 docking ligands to proteins. *Proteins* **2008**, 71, 1373-1386.

17 (21) Purisima, E. O.; Hogues, H. Protein-ligand binding free  
18 energies from exhaustive docking. *J. Phys. Chem. B* **2012**, 116,  
19 6872-6879.